

**REGULATION OF THE ACTIN CYTOSKELETON BY  
STE20-LIKE KINASES AND THE ARGINYL  
TRANSFERASE 1 IN *DICTYOSTELIUM DISCOIDEUM***

**Dissertation der Fakultät für Biologie der  
Ludwig-Maximilian-Universität  
München**

**vorgelegt von**

**PETROS BATSIOS**

**aus München**

**September, 2009**

---

The experimental part of the work was carried out in the laboratory of Prof. Dr. Michael Schleicher from October 2005 to March 2009 at the Institute for Cell Biology, Ludwig-Maximilian-Universität München.

Ehrenwörtliche Versicherung

Diese Dissertation wurde selbstständig und ohne unerlaubte Hilfsmittel angefertigt.

München, September 2009

Petros Batsios

1. Gutachter: **Prof. Dr. Michael Schleicher**

2. Gutachter: **Prof. Dr. Angelika Boettger**

**Rigorosum am 22.01.2010**

Papers:

2007

Rohlf, M., Arasada, R., Batsios, P., Janzen, J., Schleicher, M. (2007). The Ste20-like kinase SvkA of *Dictyostelium discoideum* is essential for late stages of cytokinesis. *J Cell Sci.* **120:4345-4354.**

Talks:

2008

Batsios, P. (2008). The Ste20-like kinase Krs2 is required for cell migration during chemotaxis. *33rd FEBS Congress - 11th IUBMB conference*. Athens, Greece. FEBS J, Vol. 275, Issue s1, Abstract: **OP4D-1.**

Meeting abstracts:

2008

Batsios, P., Schleicher, M., and Müller-Taubenberger, A. (2008). The role of arginylation for actin dynamics in *Dictyostelium discoideum*. *ASCB Annual meeting*. San Francisco, USA. Mol. Biol. Cell **19 (suppl), 369 B313.**

2007

Batsios, P., Arasada, R., Schleicher, M., and Rohlf, M. (2007). The STE20-like Severin kinase of *Dictyostelium discodeum* is essential for late stages of cytokinesis. *ASCB & ECF, Summer meeting*. Dijon, France. Abstract: **35.**

2006

Batsios, P., Arasada, R., Rohlf, M., und Schleicher, M. (2006). The STE20-like kinase DST10 is involved in phagocytosis and late development of *Dictyostelium discoideum*. *Deutsche Gesellschaft für Zellbiologie, Jahrestagung*. Braunschweig, Germany. Eur. J. Cell Biol, 85S1 (supp. 56), **O-23.**

# TABLE OF CONTENTS

SUMMARY .....	1
ZUSAMMENFASSUNG .....	3
1. Introduction.....	5
1.1 Ste20-like kinases .....	5
1.2 Actin and actin regulation.....	10
1.3 Post-translational modifications of actin .....	12
1.4 <i>Dictyostelium discoideum</i> as model organism.....	15
1.5 Goals of the project.....	16
2. Materials and Methods.....	18
2.1 Materials .....	18
2.1.1 Computer programs .....	19
2.1.2 Reagents.....	19
2.1.3 Media .....	20
2.1.4 Buffers.....	20
2.1.5 Instruments and centrifuges .....	20
2.1.6 Bacteria strains.....	22
2.1.7 <i>D. discoideum</i> strains .....	22
2.1.8 Vectors .....	23
2.2 Methods.....	24
2.2.1 Molecular Biological Methods .....	24
2.2.2 Biochemical Methods .....	24
2.2.2.1 SDS-Polyacrylamide Gel Electrophoresis and Western blotting.....	24
2.2.2.2 GST-tagged protein expression.....	25
2.2.2.3 Immunoprecipitation and Nanotrap .....	26
2.2.2.4 Two-dimensional gel electrophoresis .....	26
2.2.3 Cell Biological Methods .....	27
2.2.3.1 <i>D. discoideum</i> growth in liquid medium and on agar plates.....	27
2.2.3.2 Analysis of cell shape and cell migration .....	28
2.2.3.3 Chemotaxis .....	28
2.2.3.4 Phagocytosis and pinocytosis assay.....	28
2.2.3.5 Phototaxis.....	29
2.2.3.6 Indirect immunofluorescence.....	29

---

2.2.3.7	Reflection Interference Contrast Microscopy .....	30
2.2.3.8	Total Internal Reflection Fluorescence Microscopy .....	30
3.	Results .....	31
3.1	Ste20-like kinases in <i>D. discoideum</i> .....	31
3.1.1	The Ste20-like kinase DstA in <i>D. discoideum</i> .....	31
3.1.1.1	DstA antibodies .....	34
3.1.1.2	Subcellular localization of DstA .....	37
3.1.1.3	Isolation of <i>dst1</i> knockouts .....	41
3.1.1.4	Phenotype characterization of the <i>dst1</i> null .....	42
3.1.1.5	Interactors for DstA .....	50
3.1.2	The Ste20-like kinase Krs2 in <i>D. discoideum</i> .....	55
3.1.2.1	Sequence analysis of Krs2 .....	55
3.1.2.2	Generation of Krs2 antibodies .....	62
3.1.2.3	Subcellular localization of Krs2 .....	63
3.1.2.4	Isolation of <i>krsB</i> knockouts .....	68
3.1.2.5	Characterization of the <i>krsB</i> null phenotype .....	69
3.1.2.6	Interactors for Krs2 .....	75
3.2	Actin isoforms and actin modifications in <i>D. discoideum</i> .....	77
3.2.1	Actin isoforms in <i>D. discoideum</i> .....	77
3.2.2	The Arg-tRNA transferase (Ate1) in <i>D. discoideum</i> .....	79
3.2.2.1	Sequence analysis of Ate1 .....	79
3.2.2.2	Subcellular localization .....	83
3.2.2.3	Characterization of the <i>ate1</i> null phenotype .....	84
4.	Discussion .....	91
4.1	The Ste20-like kinase DstA .....	91
4.2	The Ste20-like kinase Krs2 .....	94
4.3	Actin isoforms and post-translational modifications .....	95
5.	References .....	98
	List of Figures .....	108
	List of Tables .....	110
	Acknowledgements .....	111
	Curriculum Vitae .....	112

## SUMMARY

The regulation of actin by actin-binding proteins and salt conditions is very well studied. Though, little is known about regulation of the actin cytoskeleton by post-translational modifications like arginylation or phosphorylation. The social amoeba *Dictyostelium discoideum* contains 41 actins and actin-related proteins, among them 16 actin isoforms with differences mainly in the N-terminal region, the most suitable target for post-translational modifications. The main objectives of this work were the characterization of two Ste20-like kinases and studies on an Arg-tRNA-transferase null mutant.

DstA is a Ste20-like kinase with the GCK (germinal center kinase) subfamily domain architecture. It has in the N-terminal half high similarities to the human Ysk1 and Mst3 kinase domains, but no other conserved protein domains at the C-terminus. DstA is equally expressed during all stages of the developmental life cycle of *D. discoideum*. The GFP-DstA full length kinase is distributed throughout the cytoplasm. The disruption of the *dst1* gene revealed a growth defect in shaking cultures. In submerged cultures we observed the formation of starvation induced aggregates which usually does not happen in full medium. On bacterial lawns *dst1* null developed long and aberrant streams. Ectopic expression of GFP-DstA full length rescued this phenotype, but GFP-DstA which lacks the catalytic domain did not. This suggests an absolute requirement of the kinase activity. Interestingly, *dst1* null cells at the vegetative cell stage were able to migrate towards the chemoattractant cAMP. Expression of the cell cortex marker GFP-coronin in the knockout background and microscopic observation of phagocytosis revealed no alteration of the Coronin localization in the mutant. However, a delay in completing the process of yeast phagocytosis of *dst1* null cells was observed. Slug migration of *dst1* knockouts was inhibited. Also this phenotype was rescued by the ectopic expression of GFP-DstA in the knockout strain. Our findings, suggest a novel role for this family of kinases in development and phagocytosis.

Krs2, a related GCK in *D. discoideum*, has a conserved catalytic domain and a unique stretch of four calpain-III domains in its C-terminus. It has high similarity to the human Mst1 kinase. Krs2, as shown by protein and mRNA levels, was uniformly expressed during all stages of the development. GFP-Krs2 full length localized to the centrosome. The very C-terminal calpain-III domain is important for the localization to the centrosome. Knockout of the *krsB* gene decreased the size of the fruiting bodies due to an early separation of

streams. Indeed, *krsB* null cells had, at the stage of stream formation, a clear chemotaxis defect with poor cell polarity and a decreased motility. The *krsB* null cells did not react to folic acid as wild type cells do. Expression of GFP-tubulin in the knockout strain revealed that centrosomes were farther from the leading edge of a cell. Our data supports a role for this family of kinases in cell polarity and the suppression of lateral pseudopods.

*D. discoideum* contains only one gene coding for an Arg-tRNA-transferase (Ate1), the enzyme known to be responsible for arginylation. *D. discoideum* Ate1 is highly homologous to Ate1 enzymes from human, mouse and fly. The knockout of *ate1* in *D. discoideum* has no significant effect on development and cell growth but leads to a 20 % decrease in cell size. The F-actin content and localization is not disturbed in *ate1* null cells. The contact area of *ate1* null cells to a glass substrate is reduced, a phenotype which is rescued by the ectopic expression of GFP-Ate1 in the knockout strain. GFP-Ate1 full length expressed in the wild type and in the null mutant accumulates primarily in the cytosol. Expression of the F-actin marker GFP-LimE $\Delta$ coil in *ate1* null cells revealed a lack of adhesion points at the attachment area of the cell. The *ate1* null cells were able to form these spots under agar. Interestingly, *ate1* rescue cells form intensive actin structures at the surface area. Using 2D-PAGE we were able to visualize changes in the biochemical properties of actins in *ate1* null cells, but were so far unable to prove a direct actin arginylation. Our data suggest that Ate1 has a regulatory role on the actin cytoskeleton.



## ZUSAMMENFASSUNG

Die Regulierung von Aktin durch Aktin bindende Proteine und Salzbedingungen ist relativ gut verstanden. Weniger ist jedoch über die Regulierung des Aktin Zytoskeletts durch post-translationale Modifikationen wie Arginylierung oder Phosphorylierung bekannt. Die soziale Amöbe *Dictyostelium discoideum* enthält 41 Aktine und Aktin-verwandte Proteine, darunter 16 Aktin Isoformen mit ausgeprägten Sequenzunterschieden im N-terminalen Bereich, das bevorzugte Ziel post-translationaler Modifikationen. Die wichtigsten Ziele dieser Arbeit waren eine erste Charakterisierung der kürzlich isolierten Arg-tRNA-Transferase Null-Mutante, sowie Untersuchungen von zwei Ste20-ähnlichen Kinasen.

DstA ist eine Ste20-ähnliche Kinase mit der typischen Domänen-Architektur der GCK (germinal center kinase) Unterfamilie. Sie hat viele Ähnlichkeiten zu den humanen Ysk1 und Mst3 Kinasedomänen, aber keine Ähnlichkeiten in der C-terminalen Hälfte. DstA ist gleichmäßig in allen Entwicklungsstadien von *D. discoideum* exprimiert. GFP-DstA lokalisiert im Zytosol der Zellen. Die Disruption des *dst1* Gens führte zu einem Wachstumsdefekt in Schüttelkulturen und zur Ausbildung von Zell-Aggregaten auf Platten mit Flüssigmedium. Die Bildung von Aggregaten schon in Vollmedium ist äußerst ungewöhnlich für *D. discoideum*. Auf Bakterienrasen entwickelten *dst1* Null-Zellen sehr lange Ströme. Ektopische Expression des vollständigen GFP-DstA in der Null-Mutante behebt diesen aberranten Phänotyp. Die Expression von GFP-DstA, dem die katalytische Domäne fehlte, konnte das aber nicht. Das weist auf die Bedeutung der Kinase-Aktivität hin. Interessanterweise reagieren *dst1* Null-Zellen im vegetativen Zellstadium auf cAMP und wandern darauf zu. Die Expression des kortikalen Markers GFP-Coronin im Null-Hintergrund und die mikroskopische Auswertung phagozytischer Mutanten zeigte keine Veränderung der Coronin Lokalisierung, wohl aber eine Verlangsamung der Aufnahme von Hefe. Die Phototaxis der Slugs war in den *dst1* Null-Zellen inhibiert. Auch diese phänotypischen Veränderungen konnten durch die ektopische Expression von GFP-DstA wieder aufgehoben werden. Unsere Ergebnisse deuten auf eine neuartige Funktion für diese Familie von Kinasen in der Entwicklung und der Phagozytose.

Krs2, eine verwandte GCK in *D. discoideum*, enthält eine konservierte katalytische Domäne und einen einzigartigen C-terminalen Abschnitt, der aus vier aufeinanderfolgenden Calpain-III Domänen besteht. Dieses Enzym zeigt ausgeprägte Ähnlichkeiten zu der

humanen Kinase Mst1. Krs2 ist, wie über den mRNA- und Proteingehalt ermittelt werden konnte, gleichmäßig über alle Entwicklungsstadien von *D. discoideum* vorhanden. GFP-Krs2 ist am Zentrosom angereichert. Die am weitesten auf der C-terminalen Seite liegende Calpain III-Domäne ist wichtig für die Lokalisierung am Zentrosom. Die Disruption des *krsB* Gens führte zu kleineren Fruchtkörpern, was auf ein verfrühtes Auseinanderbrechen der Ströme in der fortgeschrittenen Entwicklungsphase zurückzuführen sein dürfte. In der Tat sind *krsB* Null-Zellen in diesem Entwicklungsstadium chemotaktisch weniger aktiv, nicht richtig elongiert, und weniger beweglich. *KrsB* Null-Zellen reagieren nicht auf Folsäure wie der Wildtyp. Die Expression von GFP-Tubulin im *krsB* Null-Hintergrund lässt im Vergleich zum Wildtyp einen größeren Abstand des Zentrosoms zur Frontlinie des Lamellipodiums vermuten. Unsere Ergebnisse unterstützen die Funktion dieser Familie von Kinasen bei der Zell polarität und der Unterdrückung von lateralen Pseudopodien.

*D. discoideum* hat nur ein Gen für das arginylierende Enzym Arg-tRNA transferase (*Ate1*). *D. discoideum* *Ate1* ist homolog zu den *Ate1* Enzymen vom Menschen, der Maus und der Fruchtfliege. Die Disruption des *ate1* Gens in *D. discoideum* hat keinen Effekt auf die Entwicklung und das Wachstum der Zellen, führt aber zu einer 20%-igen Reduzierung der Zellgröße. Der F-Aktin Gehalt und die F-Aktin Lokalisierung sind in den *ate1* Null-Zellen nicht beeinflusst. Allerdings ist die Kontaktfläche der *ate1* Null-Zellen auf einer Glasoberfläche reduziert. Dieser Phänotyp wird durch die ektopische Expression eines GFP-*Ate1* Konstrukts im Mutantenhintergrund behoben. GFP-*Ate1* in Wildtyp und Mutante akkumuliert primär im Zytosol. Die Expression des F-Aktin Markers GFP-LimE $\Delta$ coil in *ate1* Null-Zellen zeigte ein Fehlen von Adhäsionspunkten im Glas/Zelle Kontaktbereich. Allerdings konnten *ate1* Null-Zellen solche Adhäsionspunkte unter Agar ausbilden. Interessant war auch die Beobachtung, dass *ate1* rescue Zellen viel deutlichere Aktinstrukturen auf der Kontaktfläche ausbildeten. Über 2D Gelelektrophorese war es möglich, Unterschiede in den Laufeigenschaften von Aktin aus *ate1* Null-Zellen festzustellen, eine direkte Aktin Arginylierung konnte allerdings bisher noch nicht nachgewiesen werden. Unsere Ergebnisse deuten auf eine Funktion von *Ate1* als Regulator des Aktin Zytoskeletts.

## 1. Introduction

Proteins are synthesized during translation, following the instruction encoded in the genome. Proteins can be further modified by post-translational modifications. These modifications modulate the function or the stability of proteins and, thereby, achieve an even higher complexity as it is encoded by the genome alone. The post-translational modifications can remove or attach different functional groups, such as amino acids, acetate, phosphate, lipids or carbohydrates onto the polypeptide chain (Burnett and Kennedy, 1954; Sadoul et al., 2008). The resulting changes in the chemical nature of polypeptides can change, for example, protein-protein interactions or the lipophilicity of the protein.

N-terminal modifications are very common in the intracellular environment. The N-terminal methionine, for example, is usually cleaved off before the polypeptide is further processed by additional post-translational modification. Peptidases remove amino acids from the N-terminus of the proteins to achieve that following amino acids are available for modification and are processed for proteolysis (Meinzel et al., 2006). Another very frequent post-translational modification is protein phosphorylation, which can for example activate or inactivate enzymes.

### 1.1 Ste20-like kinases

Phosphorylation is an important post-translational modification discovered more than 50 years ago. Proteins that mediate phosphorylation are termed protein kinases and proteins that catalyze the reverse reaction are protein phosphatases. During phosphorylation a phosphoric group is added onto a serine, threonine or tyrosine residue of the target protein which might lead to conformational changes that can, for example, activate or deactivate the target. In some organisms also basic amino acids like histidine, arginine and lysine can be phosphorylated (Cozzone, 1988; Zinda and Singleton, 1998). Protein kinases are part of complex signaling networks that regulate, for example, cell cycle progression or homeostasis, which makes them important therapeutic targets. Protein kinases can be classified based on their phylogenetic relations. One of these phylogenetic groups are the Ste kinases, comprising nearly 10% or 15% of the human or amoeba kinome, respectively (Table 1). The Ste group is further subcategorized into Ste7, Ste11 and Ste20 kinases.

Ste20-like kinases are serine/threonine kinases that were first discovered in *S. cerevisiae* and are named for the sterile-phenotype of knockouts in yeast. They consist of kinases that are reported to be activators of MAPK signaling and are involved in regulation of the cytoskeleton. Ste20-like kinases can be subdivided into two families according to their domain architecture: (1) The p21-activated-kinases (PAKs) have a C-terminal kinase domain and a more N-terminal CDC42/Rac-interactive-binding (CRIB) domain that mediates binding to small GTPases. (2) The germinal center kinases (GCKs) have the kinase domain at the N-terminus and diverse C-termini that might regulate kinase activity or localization. All Ste20-like kinases have a characteristic amino acid motif (v/i)GTPyWMAPEv (small letters indicate weak conservation) in the activation segment of the catalytic domain.

**Table 1. Number of Ste kinases in various organisms.**

Organism	Kinases	Ste
<b>human</b>	<b>518</b>	<b>47</b>
fly	239	18
<b>sea urchin</b>	<b>353</b>	<b>21</b>
worm	411	25
<b>yeast</b>	<b>130</b>	<b>14</b>
amoeba	285	43

While the PAK kinase family has two distinct subfamilies and a total of six members in human that were reported to be involved in actin reorganization, transcription, apoptosis and hormone signaling (Jaffer and Chernoff, 2002), the GCK family is much larger and contains 27 members in humans. It has been shown that these kinases control key reactions in cell division, cell growth, cell polarity, apoptosis, morphogenesis and reorganization of the cytoskeleton. The GCK family was further divided into eight subfamilies based on conserved protein stretches within and outside the catalytic domain (Dan et al., 2001). Several of these GCK subfamilies play a role in MAP kinase signaling, for example, kinases belonging to the GCK-I, IV and V subfamily feed into the JNK pathway, whereas the GCKs from subfamily VI and VII regulate the p38 kinase cascade. Another important example for the role of GCKs are Mst3, Mst4 and Sok1 from the GCK-III subfamily which were shown to regulate apoptosis (Pombo et al., 2007).

Recently, crystal structures of the GCK kinase domains of Tao2 (Zhou et al., 2004), Osr1 (Lee et al., 2009) and Mst1 (Hwang et al., 2007) have been published. The kinase domains consist of  $\alpha$ -helices and  $\beta$ -sheets that form the conserved kinase fold with the ATP-binding cleft and the catalytic loop. The structure of Tao2 showed a phosphorylation site on Ser181 which brings the kinase domain into an active conformation. The switch from active to inactive form involves the characteristic signature sequence of Ste20-like kinases and might be a general mechanism to modulate kinase function (Zhou et al., 2004). Interestingly, Osr1 crystals were resolved in an inactive conformation where the activation loops of two monomers form a domain-swapped dimer (Figure 1). The domain-swapping is discussed as an indication for trans-autophosphorylation that might activate Osr1. On the other hand, the activation loops intercalated into a tight domain-swapped dimer might prevent Osr1 activation, until substrates or activators bind the unresolved regulatory domain of Osr1 (Lee et al., 2009).

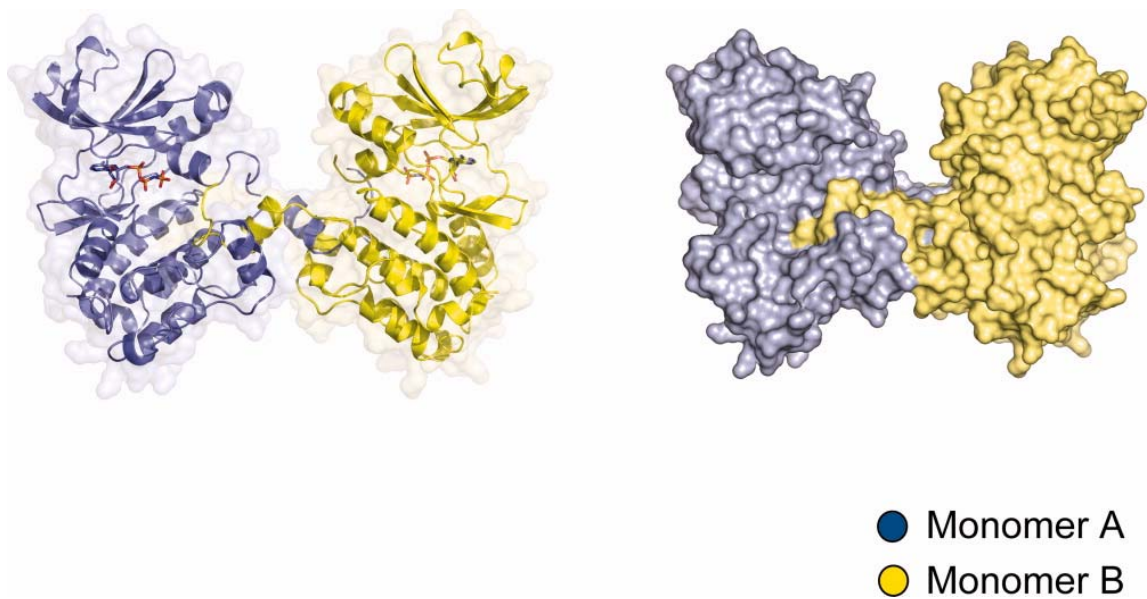


Figure 1. Osr1 crystal structure (Lee et al., 2009).

The two monomers of the catalytic domain of the Osr1 kinase are forming a domain-swapped dimer.

The genome of *D. discoideum* (Eichinger et al., 2005) contains four p21 activated kinases and thirteen highly homologous GCKs (Goldberg et al., 2006). The first *D. discoideum* GCK-III kinase was purified based on its *in vitro* ability to phosphorylate the F-actin fragmenting protein severin (Eichinger et al., 1998). Knockout of the severin kinase leads to a cytokinesis defect with huge multinucleated cells (Rohlfes et al., 2007). Krs1 is a GCK-II member was shown to phosphorylate severin *in vitro* as well. The Krs1 catalytic domain

together with a part of its regulatory domain is necessary to have a fully active kinase (Arasada et al., 2006). *Krs1* is required for normal development and cAMP relay (Muramoto et al., 2007).

Preliminary characterization of the kinase DST10/DstA and its knockout *dst1* null revealed defects during development and phagocytosis (Batsios, 2005). The more extensive characterization of the *dst1* null phenotype, generation of a rescue strain and an anti-DstA specific antibody are part of this work.

A second project about Ste20-like kinases in this thesis deals with the GCK-II kinase *Krs2*. *Krs2* contains an unusual stretch of four calpain III-like domains. *D. discoideum* has only one other ORF that shows homologies to domain III of the calpain family. This protein is CplA, and contains tandem calpain III-like domains and undergoes weak autoproteolytic cleavage but does not have a real calpain-like protease domain (Czerwinski, 2006; Huang et al., 2003). So far, it has been reported that mammalian calpain 10 and *Dictyostelium* CplA are the only proteins with tandem calpain III-like domains (Czerwinski, 2006). So far, no kinase with calpain III-like domains in its protein sequence has been documented. We found in *Entamoeba histolytica* a calpain III-like domain as part of a protein kinase. The calpain III-like domains as part of a kinase is interesting as a possible novel regulatory element for kinases.

Calpains, or calcium-dependent protease with papain-like activity, are cytoplasmic cysteine protease activated by calcium. They are highly conserved proteases with homologues present in invertebrates, plants, fungi, and mammals. These proteases are ubiquitous as well as tissue-specific in humans. The typical calpain isoform consists of an 80 kDa catalytic subunit and a 30 kDa regulatory subunit. The regulatory subunit possesses a hydrophobic, glycine-rich domain for membrane association. Each subunit contains an EF-hand domain, characteristic of most calcium-binding proteins (Goll et al., 2003).

There are two prototypical calpains,  $\mu$ -calpain, and m-calpain with different characteristics (Table 2). In most cases the  $\mu$ -calpains are affected by small changes of calcium concentrations, whereas the m-calpain are mainly activated by intracellular signaling via phosphorylation by protein kinase A (PKA) and other kinases (Shiraha et al., 2002). Following calcium stimulation, the 80 kDa subunit is autocatalytically processed to a 76 kDa fragment, and the 30 kDa regulatory subunit is processed to 18 kDa. The regulatory



subunit is critical for calpain activity; for example, it is necessary for embryonic development as genetic deletion of the subunit is lethal at E11.5 (Vosler et al., 2008). The requirement of m-calpain for development has also been demonstrated where it is necessary for embryo implantation (Vosler et al., 2008).

**Table 2. Characteristics of mammalian calpains.**

	$\mu$ -Calpain	m-Calpains
<b>Subcellular localization</b>	<b>in the cytosol</b>	<b>at the membrane</b>
Activation with $[Ca^{2+}]$ range	3-50 $\mu$ M	0.4-0.8 mM
<b>Large subunit</b>	<b>~80 kDa (Domain I, II, III, IV)</b>	<b>~80 kDa (Domain I, II, III, IV)</b>
Small subunit	~30 kDa (Domain V, VI)	~30 kDa (Domain V, VI)

The catalytic subunit of calpain is formed by domains I to IV (Figure 2, Table 3). Domain I facilitates the interaction with the small subunit. Domain II, with subdomains, IIa and IIb, carries the catalytic triad with residues of Cys105, His262, and the Asn286 responsible for protease activity. Domain III shows similarities to C2 sequences that bind phospholipids. Domain IV at the C-terminal end of the large subunit, consists of five consecutive EF-hand motifs. The smaller regulatory subunit contains domain V, which is a highly flexible, glycine-rich region, and domain VI, which contains a  $Ca^{2+}$  binding region, similar to domain IV of the catalytic subunit (Wu et al., 2007).

**Table 3. Function of Calpain Subdomains.**

Domain	I	II	III	IV	V	VI
<b>Function</b>	<b>Not clear</b>	<b>Cysteine protease</b>	<b>Not clear</b>	<b>Calmodulin-like domain, <math>Ca^{2+}</math>-binding</b>	<b>Glycine-cluster</b>	<b>Calmodulin-like domain, <math>Ca^{2+}</math>-binding</b>

There are diverse functions for calpains, for example, calpains have been reported to be involved in cytoskeleton regulation. Mammalian calpain 6 is involved in microtubule

stabilization mainly mediated by domain III. Knock down of calpain 6 induced actin reorganization, resulting in lamellipodium formation with membrane ruffling (Tonami et al., 2007). In addition, calpain proteases have been shown to contribute to the control of cell migration by regulating the dynamics of integrin-mediated adhesion and actin-based membrane protrusion (Perrin and Huttenlocher, 2002). Recently, it has been shown that calpains are involved in polarity of extending neuritis (Gartner and Dotti, 2009).

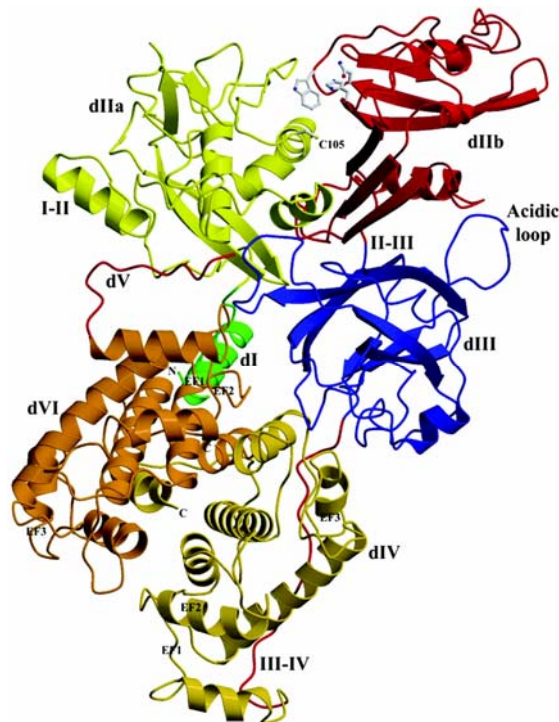


Figure 2. Crystallographic structure of human m-calpain [from (Goll et al., 2003)]. The domains are shown in different colors. Calpain III-like domain (blue) is thought to be important for microtubule and membrane interactions.

## 1.2 Actin and actin regulation

The following part focuses on actin and post-translational modifications. Actin is the most abundant protein, essential for many organisms and therefore a well studied component of a cell. Actin was first discovered in 1942 as part of the actomyosin complex in muscle cells and was later confirmed to be widely expressed in eukaryotic and prokaryotic cells. The bacterial MreB, for example, is reported to have a similar structure and function as eukaryotic G-actin (Egelman, 2003). Actin polymerizes to filaments which assemble into filamentous networks. Nevertheless its regulation *in vivo*, especially by post-translational modifications, is not completely understood.



Many fundamental cellular processes require dynamic changes in the F-actin cytoskeleton network. These processes include cell adhesion, cytokinesis, cell migration and phagocytosis. They are regulated by mechanisms that evolved by harnessing of the unique actin characteristics. Intracellular salts (KCl or MgCl<sub>2</sub>) or the intracellular ATP/ADP-actin concentrations control actin polymerization. A well studied chapter in the field of actin regulation describes actin-binding proteins. These proteins not only affect kinetics at any phase of actin polymerization, but can also affect the structures of the three dimensional network, e.g. by cross-linking and/or destabilizing F-actin filaments.

Most eukaryotic cells have a large number of actin-binding proteins with different functions, locations and concentrations. Some of these proteins react to changes of intracellular Ca<sup>2+</sup> levels, are activated by the interaction with lipids, or are regulated by post-translational modifications, such as phosphorylation. In the intracellular environment ion-concentrations (Mg<sup>2+</sup> or K<sup>+</sup>) are such that most of the actin would be polymerized, this would mean that cells could not move due to a high cytoplasmic viscosity and a lack of free G-actin. Actin-binding proteins can be grouped concerning their effect on G- and/or F-actin. Some examples are given below.

Several actin-binding proteins can depolymerize or sever actin filaments into shorter fragments, which lead to a weakening of the F-actin cortex. This type of actin severing proteins include the actin severing proteins of the gelsolin and severin type (Andre et al., 1988) and members of the ADF/cofilin family (Van Troys et al., 2008). G-actin sequestering proteins, like profilin and thymosin beta 4, bind to actin monomers and take approximately half the cellular actin out of the polymerization equilibrium until stimuli remove the interaction of actin with the sequestering proteins (Arasada et al., 2007; Czisch et al., 1993). Another type of actin-binding proteins are capping proteins, that inhibit actin filament elongation by capping the fast growing ends and consequently keeping cytoplasmic viscosity low (Haus et al., 1991). The removal of capping proteins, the uncapping, plays a critical role during cell motility and phagocytosis. A stimulus uncaps the filaments releasing a high number of free barbed ends that can immediately continue polymerization. This results in the rapid formation of cellular protrusions needed for cell motility or phagocytosis.

The class of actin nucleators has mainly two mechanistically different groups, the formins and the Arp2/3 complex. Formins nucleate and catalyze polymerization at the barbed end

and remain associated with the growing filament. This enables formins to form primary actin structures and actin cables in the cell and were also shown to be important for filopodia formation (Schirenbeck et al., 2005). On the other hand the Arp2/3 complex was identified as an actin nucleator with the ability to initiate branch formation. The Arp2/3 complex is important for pseudopodia and lamellipodia formation and has an important function in phagocytic cup formation (Goley and Welch, 2006).

Other actin-binding proteins regulate the three-dimensional architecture of actin filaments by bundling or cross-linking the filaments or by linking them to other cellular structures. This type of actin-binding proteins includes members like  $\alpha$ -actinin (Witke et al., 1993), cortexillin (Faix, 2002), filamin (Khaire et al., 2007), fimbrin (Prassler et al., 1997), myosin II (Kollmar, 2006) or VASP (Schirenbeck et al., 2006).

### **1.3 Post-translational modifications of actin**

The regulation of actin networks by actin-binding proteins is relatively well studied. The effect of post-translational modifications on different actin isoforms adds a big piece of complexity to the field of actin regulation and is less well characterized.

One of the mysteries about actin is the existence of multiple actin isoforms that have an extremely similar amino acid sequence. For example, humans have six actin isoforms with different amino acid sequences and expressed in different cell types (Rubenstein, 1990). The human isoforms have been shown in multiple studies to preferentially incorporate into different actin networks and are suggested to have different roles *in vivo* (Rubenstein, 1990). Another extreme example for the variability of actins is the model organism *Dictyostelium discoideum* we used in this study. The *D. discoideum* actinome (Joseph et al., 2008) comprises of 41 actins and actin-related proteins. The genome contains 17 genes that encode proteins identical to actin15. Actin15 comprises more than 95% of the total actin content in a *D. discoideum* cell (Vandekerckhove and Weber, 1980). The other actin content comes from 16 conventional actin isoforms that differ slightly in their protein sequences. Most of these actin isoforms in *D. discoideum* have changes at the second and/or third amino acid position of the N-terminus. It is thought that these differences might cause unique sensitivity of these isoforms for post-translational modifications at the N-terminus, which might indicate novel regulatory mechanisms for the actin meshwork.

Acetylation is one very well studied post-translational modification. Many proteins in the cytosol are acetylated at the N-terminus (e.g. tubulin) (Fukushima et al., 2009). As examined so far, all actins are acetylated at the N-terminus. It has been supposed that this kind of biological masking of N-termini protects a protein against attack from aminopeptidases, ubiquitination and other modifications and/or anchors the N-terminal part of the protein in an apolar environment. During acetylation the first methionine is usually removed and the new N-terminus is acetylated with a preference for small and neutral amino acids, such as alanine, glycine, serine or threonine in this position (Boissel et al., 1988). In proteins where the second amino acid is charged, the initiator methionine itself is more likely to be acetylated. In eukaryotes two different actin classes have been reported to be acetylated. In class I or non-muscle actins the primary sequence of Met-Asp-actin is processed to Ac-Asp-actin. In this context the acetylation of the initiator Met, followed by its removal and acetylation of the Asp residue (Rubenstein et al., 1981; Rubenstein and Martin, 1983) is required. In contrast, class II or skeletal muscle actins are processed from Met-Cys-X-actin (where X is usually Asp) to Ac-X-actin directly after N-terminal aminopeptidation. For *D. discoideum* it was shown that part of the total actin is acetylated following a mechanism similar to the one described for class I actins (Rubenstein et al., 1981).

Recently another puzzling N-terminal actin modification has been reported in mammals. Arginylation is a modification discovered more than 45 years ago (Kaji et al., 1963), but its cellular effects are hardly understood. During arginylation it is thought that the Arg-transfer RNA (tRNA) protein transferase (Ate1) (Balzi et al., 1990; Kaji, 1968) transfers arginine from tRNA onto the N-terminus of proteins. A peptide bond can be formed between the carboxy group with one of the three N-terminal residues, Asp, Glu or Cys, and the amino group of the transferred arginine. This arginylation requires, prior to post-translational modification, proteolysis or Met-aminopeptidation of the N-terminus. Interestingly, it has been reported that side chains of peptides can also be arginylated (Rai et al., 2008). As Kashina et al., 2006 recently showed  $\beta$ - but not  $\gamma$ -actin in cultured fibroblasts undergoes N-terminal arginylation, which regulates actin polymerization and lamellipodia formation in motile cells (Kashina, 2006) (Figure 3). Arginylation could be a general mechanism that regulates actin isoform segregation *in vivo* and participates in the formation of loose actin networks at the leading edge of the cell (Kashina, 2006; Rai et al., 2008).

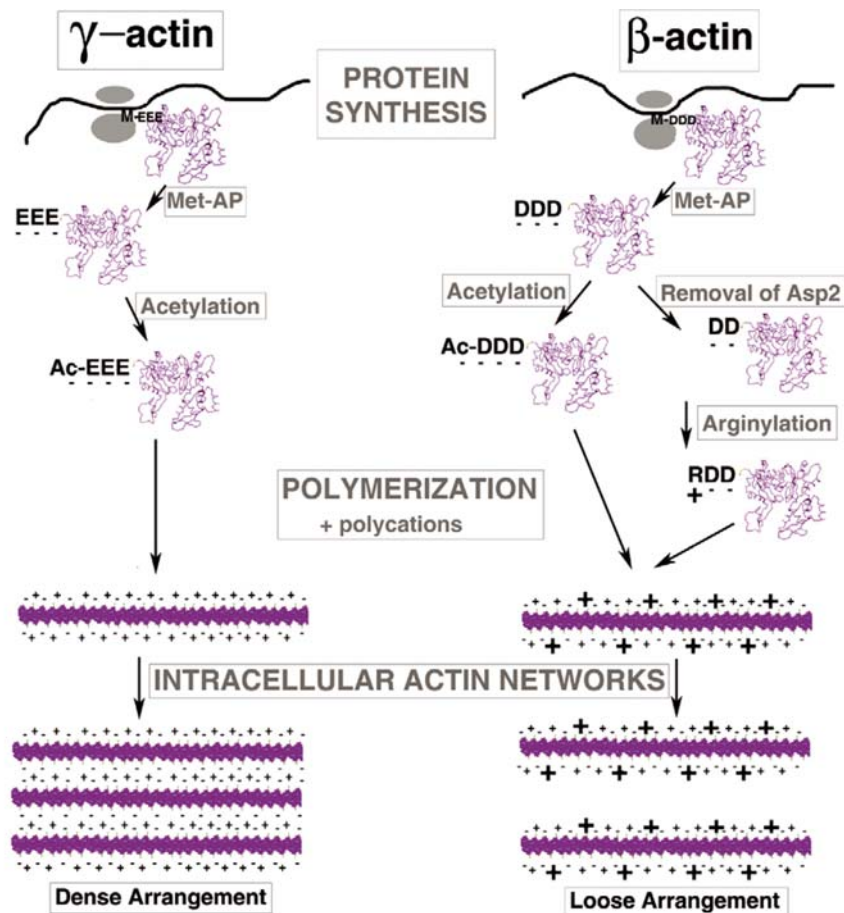


Figure 3. Arginylation of actin isoforms.

Kashina *et al.*, postulate a model to explain a function for beta-actin arginylation. Monomers of beta- as well as gamma-actin are acetylated, resulting in negative charges at the surface. These charges result in tight F-actin networks. In contrast, to achieve loose F-actin arrangements Ate1 arginylates beta-actin, resulting in positive charges, which are postulated to repel negative charges from the acetylated actin filaments. [Figure from (Kashina, 2006)]

The Arg-transferRNA protein transferase, Ate1, is an evolutionarily conserved enzyme that was shown to be essential for embryonic development in mammals (Rai et al., 2008). Mice that lack arginyltransferase have a defect in cardiovascular development and angiogenesis. Alpha cardiac actin function, myofibril formation and contractility during heart development are also affected (Rai et al., 2008). The arginylation of alpha cardiac actin occurs at four sites of the molecule (Rai et al., 2008). The four additional arginines possibly modulate actin polymerization and co-assembly with other myofibril proteins (Wong et al., 2007).

In addition to acetylation and arginylation, another, more common, type of post-translational modification has been documented for actin. Phosphorylation of actin,

mediated by protein kinases, occurs in all organisms from mammals to lower eukaryotes. Actin can be phosphorylated on serine (Carrascosa and Wieland, 1986), threonine (De Corte et al., 1996; Furuhashi et al., 1998) and tyrosine (Schweiger et al., 1992) residues. Serine phosphorylation of actin is stimulated by insulin and is probably mediated by PKC (Carrascosa and Wieland, 1986). Actin in the actin-fragmin complex of *Physarum polycephalum* is phosphorylated by the actin-fragmin kinase (AFK) at the residues Thr203 and Thr202 (De Corte et al., 1996). Upon stress, actin in *D. discoideum* is phosphorylated at Tyr53 by an unknown kinase (Schweiger et al., 1992). This phosphorylation can regulate actin polymerization or depolymerization as shown (Waelkens et al., 1995). In addition they might influence the interaction with actin-binding proteins and thereby, the formation of the 3D actin-networks.

The identification of actin isoforms in *D. discoideum*, their post-translational modifications (especially arginylation and phosphorylation), as well as the characterization of the single Ate1 ortholog in this amoeba are one focus of the present work.

### **1.4 *Dictyostelium discoideum* as model organism**

*D. discoideum* was first described in 1935 and classified as myxomycete (Linnell and Raper, 1935). In its natural habitat this eukaryotic microorganism, lives in forest soil and on decaying leaves, using actin-based phagocytosis to feed on bacteria. In contrast, the lab-strains, used in this work can grow in liquid cultures taking up culture medium by macropinocytosis.

The amoebae grow as independent, single cells until the nutrients in the surrounding are exhausted. This initiates a developmental program, in which up to  $10^5$  cells aggregate by cAMP-mediated chemotaxis to form a fruiting body with robust spores (Gerisch, 1987; Loomis, 1996). During this developmental cycle, single amoebae migrate towards a centre, forming aggregates and mounds. The intermediate slug or pseudoplasmodium can positively migrate towards a light source to find favorable conditions to continue the development. The cells in the mounds or slugs undergo differentiation into two major cell types, the prespore and prestalk cells that further develop into a mature fruiting body composed of spore cells that are supported by a thin long stalk made of dead cells. The spores are oval shaped, extremely resistant and germinate into amoebae under favorable

conditions. Under laboratory conditions, the entire developmental cycle can be completed within 24 hours (Chisholm and Firtel, 2004).

As the developmental cycle relies on cell motility, chemotaxis and signal transduction in this microorganism provide a convenient system to study these processes. In addition, *D. discoideum* can be manipulated conveniently using a variety of molecular genetics, biochemical and cell biological tools (Noegel and Schleicher, 2000), and is therefore widely used to study fundamental cellular processes like cytokinesis, phagocytosis, endocytosis, osmoregulation and infection (Skriwan et al., 2002).

*D. discoideum*, as a highly motile organism, is especially useful to study actin based processes. The recent completion of the genome sequencing project (Eichinger et al., 2005) confirmed for example the representation of almost all classes of metazoan actin-binding proteins, underscoring that *D. discoideum* is a suitable model system for studies of the actin cytoskeleton.

### **1.5 Goals of the project**

Post-translational modifications, Ste20-like kinases and calpains have been documented to be involved in human diseases. Abnormal actin regulation has been documented to lead to disease. In muscle an accumulation of alpha-actinin at the Z bands characterizes myopathy (Dustin and Brion, 1988). In several forms of hemolytic anemias, alterations of the membranous cytoskeletal components of the red blood cells — spectrin, ankyrin, actin — may explain their abnormal shape and excessive fragility (Dustin and Brion, 1988). In the nervous system, many pathological conditions are related to abnormal cytoskeletal components (Dustin and Brion, 1988). Ste20-like kinases have a role in inflammatory bowel diseases (IBD), primarily ulcerative colitis (UC) and Crohn's disease (CD) as well as prostate cancer (Moore et al., 2000; Yan and Merlin, 2008). Tissue-specific calpains have been implicated in diabetes, cataracts, multiple sclerosis, cancer, Duchenne's muscular dystrophy, and Alzheimer's disease and are known to cause autosomal recessive limb-girdle muscular dystrophy type 2A (Zatz and Starling, 2005). Any novel regulatory process could add knowledge combating diseases caused by the investigated molecules or regulatory processes.



In the present work the following two topics are addressed to characterize signal transduction pathways that target the actin cytoskeleton:

(1) Ste20-like kinases as members of signaling cascades and their effect on the actin cytoskeleton.

Members of the Ste20-like kinases in *D. discoideum* were shown to phosphorylate the F-actin fragmenting protein severin *in vitro* (Arasada et al., 2006; Eichinger et al., 1998). This makes these kinases interesting as possible candidates for the actin cytoskeleton regulation. Therefore, this part of the project describes the characterization of two Ste20-like kinases, with an in depth analysis of the *dst1* kinase as continuation of a Diploma project (Batsios, 2005) and the characterization of *krsB*. The projects include the generation and characterization of gene knockouts, preparation of anti-kinase antibodies, the expression of GFP-tagged kinase constructs for localization studies and the expression of recombinant kinases with *E. coli* for biochemical characterizations.

(2) Actin isoforms and the role of arginyl-transferase Ate1 as a possible actin isoform regulator.

*D. discoideum* contains more than 17 actins with minor differences in their protein sequences. These minor differences might enable different regulation of actin isoforms, for example by post-translational modifications. The genome of the model organism *D. discoideum* contains one homologue of Ate1. It was previously shown that depletion of the Ate1 enzyme reduced the rate of actin arginylation in mammalian cells (Karakozova et al., 2006). Beta-actin arginylation at the leading edge was postulated to prevent actin filaments from aggregating, thereby allowing the formation of loose networks. Goal of this part of the work was to study the effect of an *ate1* gene knockout in cells and its effect on the actin cytoskeleton in *D. discoideum*.

## 2. Materials and Methods

### 2.1 Materials

Cell culture plates, 24 wells	Nunc
Cell culture dishes $\varnothing$ 100 mm $\times$ 20 mm	Greiner bio-one
Cell culture dishes, $\varnothing$ 3.5 mm with glass bottom Tubes	MatTek Corporation
Dialysis membranes Type 8, 20, 27, 25A	Biomol
Gel drying membrane	Festata
Gel-blotting-paper GB002	Whatman
Nitrocellulose membrane Protran BA85	Whatman
Parafilm	American National Can
PCR tubes 0.5 ml, Petri dishes, $\varnothing$ 92 mm $\times$ 16 mm	peQLAB
Pipettes, 10 und 25 ml, 15 ml and 50 ml tubes	Nunc/Greiner
1.5 ml centrifuge tubes	Sarstedt
Pipette tips	Gilson
Plasmid DNA Purification Maxi Kit	Macherey Nagel
QIAprep Spin Miniprep and Gel Extraction kits	Qiagen
Sterile filter, 0.22 $\mu$ m Millex GV	Sarstedt
Ultracentrifuge tubes 1.5 ml	Beckman
X-ray film X-omat AR 5	GE Healthcare



### 2.1.1 Computer programs

Adobe photoshop CS2, Acrobat Reader 7.0	Adobe Systems
AskSam 4.0	Seaside Software
AxioVS40 V4.3.101	Carl Zeiss Vision GmbH
CorelDraw 12 2003	Corel Corporation
DIAS 3.4.1	Solltech Inc.
DeepView/Swiss PdB Viewer	gsk GlaxoSmithKline
ImageJ 1.34n	Wayne Rasband
Microsoft Office 2003	Microsoft
Unicorn Software for Äkta	GE Healthcare

### 2.1.2 Reagents

Unless and otherwise mentioned standard laboratory chemicals used were purchased from Bio Mol, Fluka, Merck, Roth, Serva or Sigma and had the degree of purity "p.a."

Adenosine-3', 5'-cyclic monophosphate (cAMP)	Sigma
Adenosine-5'-trisphosphate-Na <sub>2</sub> - Salt	Serva
BCIP (5-Bromo-4-chloro-3-indolylphosphate-p-toluidin-salt)	Gerbu
Bovine serum albumin fraction V	PAA
DE52 (Diethylaminoethyl-cellulose)	Whatman
[ $\gamma$ - <sup>32</sup> P] ATP	ICN
HL-5C (AX-Medium)	Formedium

LB-Medium	Formedium
NBT (Nitro blue tetrazolium)	Sigma
Nickel-NTA agarose	Qiagen
NP-40 (Nonylphenylpolyethylenglycol)	Fluka
Oligonucleotides	ThermoFischerScientific

### 2.1.3 Media

All media and buffers used were prepared with deionised water, which had been filtered over an ion exchanger (Millipore) and were sterilized either by autoclaving or by passing through a micro filter.

### 2.1.4 Buffers

<b>10 × Tris/Borate-Buffer (TBE, pH 8.3)</b>		<b>TE-Buffer (pH 8.0)</b>
890 mM	Tris/HCl	10 mM Tris/HCl
890 mM	Boric acid	2 mM EDTA
20 mM	EDTA	

### 2.1.5 Instruments and centrifuges

Aekta FPLC system and fraction collector RediFrac	GE Healthcare
Axiovert microscopes 25, 35, M200	Zeiss
Dounce homogenisor	Braun/ Wheaton

## Materials and Methods

---

Eagle Eye II	Stratagene
Electroporator	BioRad
Fluorescence-spectrometer (LS55)	PerkinElmer
Heating block/Shaking thermomixer 5436	Eppendorf
Nuclepore-filter	Whatman
PCR-Thermocycler Uno	Biometra
pH-Meter pH526	WTW
Photometer ultrospec 2100 pro	Amersham
Protein transfer Trans-Blot SD	BioRad
Quartz cuvettes	Starna
Superose 12 10/300 GL	GE Healthcare
Ultrasonicator 820/H	Elma
UV-transilluminator IL-200-M	Bachofer
Vortex	Bender & Hobein
Waterbath	GFL. Ika. Infors. Kühner
Centrifuges: Optima LE-80K, TL ultracentrifuges, GS-6KR centrifuge, J2-21M/E centrifuge, J6-HC centrifuge	Beckman
Rotors: JA-10, JA-14, JA-20 Ti 35, Ti 45, Ti 70, TLA 100.3	Beckman

Table top centrifuge 5415

Eppendorf

### 2.1.6 Bacteria strains

*Klebsiella aerogenes*

(Williams and Newell, 1976)

*E. coli* strains:

*E. coli* B2

DH5 $\alpha$

GE Healthcare

JM 105

Invitrogen

Expression strains:

*E. coli* BL21 ArcticExpress RIL

Stratagene

*E. coli* Rosetta

Novagene

*E. coli* BL21 RIL

Stratagene

### 2.1.7 *D. discoideum* strains

AX2-214

Laboratory wild type

*ate1* minus strain

from Dr. Müller-Taubenberger

*ate1* rescue (GFP-Ate1 in *ate1* minus)

this study

*dst1* minus strain

this study

*dst1* rescue (GFP-DstA in *dst1* minus)

this study

GFP-DstA in wild type

this study

GFP-DstA Reg in <i>dst1</i> minus	this study
GFP-DstA reg in wild type	this study
<i>krsB</i> minus strain	this study
<i>krsB</i> rescue (GFP-Krs2 in <i>krsB</i> null)	this study
GFP-Krs2 in wild type	this study
GFP-Krs2 Reg in wild type	this study
GFP-Krs2 aReg in wild type	this study
GFP-Krs2 CALP in wild type	this study
GFP-Krs2 CALP1,2,3 in wild type	this study

### 2.1.8 Vectors

pDGFPXaMCS-Neo	(Dumontier et al., 2000)
pGEX 5x-1	GE Healthcare
pGEX 6P-1	GE Healthcare
pLPBLP	(Faix et al., 2004)
pQE 30/31/32	Qiagen
pUC 18/19	(Yanisch-Perron et al., 1985)

## 2.2 Methods

### 2.2.1 Molecular Biological Methods

Standard molecular biological methods were used to generate various GFP- and GST-expression constructs. Genomic DNA from *D. discoideum* was isolated using the Roche High Pure PCR Template Preparation Kit following the protocol for mammalian cell culture. The genomic DNA was stored at 4°C.

Total RNA from different developmental time points was purified from *D. discoideum* with the Qiagen RNeasy Mini Kit. RNA was stored at -70°C for long term storage or was used immediately. RNA was transcribed and amplified into DNA using the Qiagen One Step RT-PCR kit with gene specific primers, at 45°-50°C for 30 min, followed by incubation at 95°C for 15 min and normal PCR cycles.

Polymerase chain reactions (PCRs) were performed with Taq Polymerase in PCR buffer (20 mM Tris pH 8.8, 10 mM KCl, 10 mM (NH<sub>4</sub>)<sub>2</sub>SO<sub>4</sub>, 2 mM MgCl<sub>2</sub>, 0.1 mg/ml BSA, 0.1% Triton X-100) using 30 cycles with variable annealing temperatures for 60 s and an elongation temperature of 72°C for 60 s for every 1000 bp. Extraction and purification of DNA from Tris-borate-EDTA agarose gels were performed using the QIAquick gel extraction kit (Qiagen) according to the manufacturer's instructions. PCR products were cloned into the appropriate plasmids using standard restriction enzyme mediated cloning.

Chemically competent cells were prepared following the CaCl<sub>2</sub> method (Mandel and Higa, 1970) and transformed with a heat shock protocol (Cohen et al., 1972). Plasmids were isolated from *E. coli* using alkaline lysis miniprep (Holmes and Quigley, 1981) or the silica-based anion-exchange Maxiprep kits from either Machery & Nagel or Qiagen.

### 2.2.2 Biochemical Methods

#### 2.2.2.1 SDS-Polyacrylamide Gel Electrophoresis and Western blotting

Protein mixtures were separated by discontinuous SDS-PAGE (Laemmli, 1970) and stained with Coomassie Brilliant Blue R 250. Alternatively proteins were visualized by semi-dry Western blotting following a modified Towbin protocol (Towbin et al., 1992). Blots were developed after BSA blocking in NCP buffer (10 mM Tris/HCl, 0.15 M NaCl, 0.05%

Tween 20, 2% NaN<sub>3</sub>) with alkaline phosphatase conjugated secondary antibodies and BCIP.

### 2.2.2.2 GST-tagged protein expression

Constructs in pGEX vectors were transformed into Rosetta, BL21 RIL or ArcticExpress RIL cells. Cultures were inoculated in LB (10 g bacto-tryptone, 5 g yeast extract, 86 mM NaCl) or LB rich medium (20 g bacto-tryptone, 10 g yeast extract, 86 mM NaCl) (Sambrook and Gething, 1989) and grown overnight at 37°C. Cells were diluted tenfold and grown at 21°C to an OD<sub>600</sub> of 0.4 - 0.8. Expression was induced with usually 0.5 mM IPTG and cells were grown overnight at 21°C. After harvesting and washing following routine procedures, cells were resuspended in lysis buffer (1 x PBS (70 mM Na<sub>2</sub>HPO<sub>4</sub>, 30 mM KH<sub>2</sub>PO<sub>4</sub>, 150 mM NaCl, 0.1% NaN<sub>3</sub>, pH 6.5), 1 mM DTT, 1 mM EDTA, 5 mM benzamidine, 1 mM PMSF, protease inhibitor cocktail (Sigma)), opened by sonication in the presence of 0.5 mg/ml lysozyme. Lysates were centrifuged at 10,000 g for 45-60 min at 4°C and the supernatants were coupled to glutathione-sepharose 4B (Sigma) by recycling for 3-4 h. The matrix was washed with 10-20 column volumes of lysis buffer and the bound proteins were eluted with lysis buffer containing 20 mM reduced glutathione (pH 7.2). The presence of protein in different fractions was tested by Bradford's method (Bradford, 1976). Protein containing fractions were analysed on SDS-PAGE. The appropriate fractions were pooled and dialysed against PBS.

If pGEX 6P-1 vector were used for expression, the GST tag could be removed by PreScission protease. Following elution of the GST fusion protein from glutathione sepharose, the eluate was dialysed extensively against PBS containing 1 mM EDTA and 1 mM DTT in order to remove reduced glutathione and protease inhibitors from the sample. 10 µg of enzyme were used to cleave 1 mg of GST fusion protein. Cleavage was carried out at 4°C overnight on a rotatory shaker. Once digestion was complete, the sample was passed through a washed and equilibrated glutathione sepharose to remove free GST and the PreScission protease from the protein of interest.

Wild type cells were harvested and lysed in degassed TEDABP-Buffer (10 mM Tris/HCl, 1 mM EGTA, 1 mM DTT, 0.02% NaN<sub>3</sub>, 1 mM benzamidine, 0.5 mM PMSF, pH 8.0) by freeze thaw and passed through a filter. The total lysate was centrifuged and used for size exclusion gel chromatography. The supernatant was applied to a Superose 12 10/300 GL

column (GE) that was controlled by the Äkta. 500 µl fractions were collected and blotted against the appropriate antibodies.

Polyclonal antibodies for DstA and Krs2 were generated in haemophilic New Zealand rabbits. Protein solutions mixed (1:1) with adjuvant were injected into the rabbits. After the primary booster polyclonal serum was for the antibody titer by western blot. In both cases a dilution of 1:10 000 of the original serum was sufficient for western blot use.

### **2.2.2.3 Immunoprecipitation and Nanotrap**

For immunoprecipitations the *D. discoideum* cells were harvested by centrifugation at 1,200 g for 3 min, washed twice with phosphate buffer and resuspended at a density of  $1 \times 10^8$  cells/ml in cold 25 mM HEPES buffer pH 7.4. One millilitre of the cell suspension was sedimented for 2 min at 2,000 g and the pellets incubated with IP-lysis buffer (25 mM HEPES pH 7.4, 50 mM NaCl, 1 mM EGTA, 5 mM benzamidine, and 1 mM DTT, 5% glycerol, 1% N-octylpolyoxyethylene (Bachem), 1 mM PMSF and protease inhibitor cocktail (Sigma)). The crude lysates were spun for 10 min at 15,000 g and the clear lysates were each supplemented with 100 µg of polyclonal antibodies together with 150 µl of protein A-Sepharose CL-4B slurry (Sigma) equilibrated in IP-lysis buffer. After 2 h of incubation at 4°C, the beads were sedimented, washed seven times with 1 ml IP-lysis buffer, and bound proteins eluted with SDS sample buffer (Faix et al., 2001). Nanotrap was performed as described (Rothbauer et al., 2008). After immunoprecipitation kinase assays were performed essentially as described (Eichinger et al., 1998). The signals were visualized on autoradiography films (Hyperfilm, GE Healthcare) and developed in CURIX 60 (Agfa).

### **2.2.2.4 Two-dimensional gel electrophoresis**

Aliquots containing less than 100 pg of protein were adjusted by the addition of 2 ml of a solution containing 7.0 M urea, 2.0 M thio urea, 4% CHAPS (Sigma), 4% servalyt, 0.4 g/ml ampholytes (Pharmacia Biotech Inc.), 0.2 M DTT and protease inhibitors. Samples were then applied to the top of the naked IPG strips and incubated over night at room temperature covered with mineral oil. The swollen strips were subjected to electrophoresis for 1 h at 300 V and 16 h at 3500 V. The gel reservoir was filled with mineral oil. Following electrophoresis, IPG strips were extruded and equilibrated for 15 min into equilibration buffer 1 (50 mM Tris-HCl (pH 8.8), 6 M urea, 30% glycerol, 2% SDS and



0.1 M DTT) and 15 min in equilibration buffer 2 (50 mM Tris-HCl (pH 8.8), 6 M urea, 30% glycerol, 2% SDS and 0.15 M IAA). Second dimension gels were freshly cast in the Ettan DALTsix gel caster. Slab gels consisted of 12% acrylamide-bisacrylamide, 0.07% w/v SDS, 37 mM Tris-HCl, pH 8.8, 0.05% w/v ammonium persulfate, and 0.025% v/v TEMED. The first dimension IPG strips were secured on top of the slab gels. The proteins were subject to electrophoresis overnight at 10 mA/gel in gel running buffer consisting of 0.1% SDS, 25 mM Tris/HCl, and 185 mM glycine. Following electrophoresis gels were stained with Coomassie blue solution.

### 2.2.3 Cell Biological Methods

#### 2.2.3.1 *D. discoideum* growth in liquid medium and on agar plates

Wild type AX2 strain was cultured axenically (Watts and Ashworth, 1970) in either AX medium (14.3 g peptone, 7.15 g yeast extract, 50 mM glucose, 3.5 mM Na<sub>2</sub>HPO<sub>4</sub>, 3.5 mM KH<sub>2</sub>PO<sub>4</sub>, in 1 l H<sub>2</sub>O) or in HL5 medium (pH 7.5) (5 g yeast extract, 10 g proteose peptone, 50 mM glucose, 8.5 mM KH<sub>2</sub>PO<sub>4</sub>, made up to 1 l with H<sub>2</sub>O) in Erlenmeyer flasks on an orbital shaker at 120 rpm at 22°C. The media were supplemented with the appropriate antibiotics when cultivating the mutants. For all cell biological studies, cells were allowed to grow maximally up to a cell density of 6 x 10<sup>6</sup> cells/ml to avoid the stationary phase.

For long term storage spores of mature fruiting bodies developed on Soerensen phosphate agar plates (Malchow et al., 1972) (10 g Bacto-agar, dissolved in 1 l Soerensen buffer) were resuspended in Soerensen phosphate buffer (pH 6.0) (14.6 mM KH<sub>2</sub>PO<sub>4</sub>, 2 mM Na<sub>2</sub>HPO<sub>4</sub>) and shock-frozen in liquid nitrogen and stored at -80°C. Alternatively, the cells of *D. discoideum* can be frozen in freezing medium (1.1 ml containing 900 µl of HL5 or AX medium, 100 µl of horse serum and 100 µl of DMSO) following a stepwise temperature gradient (4°C for one hour, -20°C for 2-4 h and then stored at -80°C).

*D. discoideum* were transformed with the appropriate plasmids by electroporation (Kimmel and Faix, 2006). Clones were isolated by spreader dilution on SM Agar plattes (9 g agar, 10 g peptone, 50 mM glucose, 1 g yeast extract, 4 mM MgSO<sub>4</sub>, 16 mM KH<sub>2</sub>PO<sub>4</sub>, 5.7 mM K<sub>2</sub>HPO<sub>4</sub> in 1 l with H<sub>2</sub>O, pH 6.5) with *K. aerogenes* lawn.

Centrosome isolation was essentially done as described (Schulz et al., 2006). *Dictyostelium* actin was isolated as described (Eichinger et al., 1991).

### **2.2.3.2 Analysis of cell shape and cell migration**

Aggregation competent *D. discoideum* cells were plated onto glass coverslips in small plastic dishes, and cell migration was recorded at intervals of 10 s using an Axiovert-200 inverted microscope and the Axiovision software (Carl Zeiss, Jena, Germany). The time-lapse movies were analysed with the DIAS program (Solltech, Oakdale, IA). For shape analysis, the outlines of single cells were drawn manually. Chemotaxis experiments were performed with micropipettes and a micromanipulator system (Eppendorf, Hamburg, Germany) essentially as described previously (Gerisch and Keller, 1981).

### **2.2.3.3 Chemotaxis**

To monitor the chemotactic motility to a micropipette containing cAMP, wild type and transformant cells were harvested and washed in Soerensen phosphate buffer, resuspended at a density of  $1 \times 10^7$  cells/ml, and put on a shaker at 100 rpm essentially as described (Parent et al., 1998). After at least 6 h of starvation, cells were spotted onto chambered cover glasses. Once cells were attached, the chambers were filled with 3 ml of phosphate buffer and presented with a micropipette filled with 10  $\mu$ M cAMP positioned near the cells, and images of moving cells were recorded as above. Adobe Photoshop and ImageJ software packages were used to process data. For the folic acid assay, cells were harvest from plate and then spotted onto the chambered coverglass and presented with a micropipette containing 1 M folic acid (Sigma). Images were collected as above.

### **2.2.3.4 Phagocytosis and pinocytosis assay**

*D. discoideum* cells were grown to densities below  $6 \times 10^6$  cells/ml, harvested, washed, and resuspended in Soerensen phosphate buffer to a density of  $2 \times 10^6$  cells/ml in a 100 ml Erlenmeyer flask. Tetramethyl rhodamine isothiocyanate (TRITC)-labeled yeast cells (120  $\mu$ l;  $10^9$  cells/ml) or TRITC-Dextran were added to 20 ml of the *D. discoideum* cell suspension. Samples of 1 ml were withdrawn every 20 min and added to 100  $\mu$ l of trypan blue solution (20 mg/ml dissolved in 20 mM sodium citrate containing 150 mM NaCl), which quenches the fluorescence of non-internalized yeast cells. After 3 min of agitated incubation, cells were spun and the supernatant was removed carefully. After re-suspension in Soerensen phosphate buffer, fluorescence was measured in a fluorimeter using 544 nm

light for excitation and recording emission at 574 nm. The highest fluorescence of the wild type was taken as 100%.

### **2.2.3.5 Phototaxis**

Phototaxis efficiency of the wild type and mutants was tested as described previously (Darcy et al., 1994) using a sterile inoculation loop slugs were transferred onto water agar plates from the edges of colonies growing on *K. aerogenes* lawns. The plates were wrapped in a dark coloured box with a 2 mm wide opening for the entry of light. Plates were incubated at 21°C for at least 48 h. To visualize the slugs and their tracks, cells were transferred onto a nitrocellulose membrane and were stained with amido black.

### **2.2.3.6 Indirect immunofluorescence**

Studies of subcellular localization were also performed via indirect immunofluorescence. For this assay, coverslips were washed with 3.6% HCl followed by dH<sub>2</sub>O. Exponentially growing *D. discoideum* cells were harvested, washed twice with Soerensen buffer, and  $1 \times 10^6$  cells were allowed to attach to the coverslips for 15 min, after which excess fluid was removed and the cells were fixed in cold methanol for 10 min at -20°C followed by 30 min air drying. Alternatively, cells could be fixed with paraformaldehyde/picric acid solution (2% paraformaldehyde, 10 mM Pipes, 15% saturated picric acid, pH 6.0) for 15 min and then washed several times with PBS/glycine and PBG (0.5% BSA, 0.05% fish gelatine, 1xPBS, passed through 0.5 µm filter). The cells were then permeabilized with 70% ethanol for 5 min at room temperature and washed with PBS/glycine followed by PBG (Hagedorn et al., 2006).

After fixation, cells were incubated with undiluted hybridoma supernatants for at least 2 h before being washed with PBG and then subjected to 1 h incubation with fluorescently labelled goat anti-mouse IgG (diluted in PBG). F-actin was labelled either with Alexa 488, TRITC-labelled phalloidin or a monoclonal antibody against *D. discoideum* actin (Simpson et al 1984). Nuclei were stained either with DAPI (4, 6-diamidino-2-phenylindole, Sigma), TO-PRO3 or DRAQ3 diluted in PBG. After incubating with the secondary antibody cells were washed several times with PBG, PBS and briefly with dH<sub>2</sub>O before being embedded in gelvatol and kept at 4°C overnight.

Agar overlay assays of cells expressing GFP or RFP were performed as described (Fukui et al., 1987).

### **2.2.3.7 Reflection Interference Contrast Microscopy**

Reflection Interference Contrast Microscope imaging (RICM) (Verschueren, 1985) was performed with an inverted Zeiss LSM 510 laser scanning confocal microscope (LSM). Images were obtained using the 633 nm line of a He-Ne laser, a reflection mirror in place of the dichroic beam-splitter, a fully open pinhole, and a 100×/1.6 NA oil-immersion Neofluor lens. The second dichroic beam-splitter was removed from the light path. The cells were either in Soerenson buffer or in nutrient rich media. The parameters of the laser scanning system were adjusted so that focal contacts appeared black. For time lapse movies, about 100 images were collected at 10 s intervals. The contact area was selected manually and measured in the ImageJ software.

### **2.2.3.8 Total Internal Reflection Fluorescence Microscopy**

Total Internal Reflection Fluorescence Microscopy imaging (TIRFM) (Axelrod, 2003) was performed with the help of Dr. Wedlich-Soeldner as described (Riedl et al., 2008). Images were obtained using the appropriate laser and standard setting to visualize the surface area. The cells were either in Soerenson buffer or in nutrient rich media. The parameters of the laser scanning system were adjusted so that focal contacts appeared bright. For time lapse movies, about 100 images were collected at ms intervals.

### 3. Results

In this part the main outcomes concerning the Ste20-like kinases DstA and Krs2, and the Arginine transfer RNA protein transferase (Ate1) are presented. Important for this part were the generation and characterization of knockout strains. GFP fusions were used to analyze the subcellular localization of the investigated proteins. Furthermore, polyclonal antibodies were generated as an additional tool to investigate expression levels and biochemical properties of the proteins.

#### 3.1 Ste20-like kinases in *D. discoideum*

A database search for homologues of the severin kinase, the first described Ste20-like kinase in *D. discoideum* (Eichinger et al., 1998), identified 13 Ste20 kinase genes (Arasada et al., 2006). Of these 13, the genes *dst1* and *krsB* were chosen for an extensive characterization throughout this thesis. The kinase *krsB* was selected because of its interesting domain architecture with four calpain-III domains, *dst1* seemed promising because an initial characterization (Batsios, 2005) suggested a central role for this kinase during the onset of development and phagocytosis.

##### 3.1.1 The Ste20-like kinase DstA in *D. discoideum*

In a phylogenetic analysis of the Ste20 family in *D. discoideum* the kinase DstA falls into the group of GCK-III/Ysk kinases, which also includes DstB and Svka from the amoeba and the human kinases Ysk1/Sok1, Mst3 and Mst4 (Arasada et al., 2006). DstA has all the classical features of the GCK family. It contains two parts: (1) A conserved N-terminal catalytic domain (23-280 aa) and (2) a 457 aa long C-terminal region with unknown, but probably regulatory function (281-737 aa) (Figure 4 A). In addition to all subdomains that characterize Ser/Thr-kinases, the Ste20-signature sequence 'GTP(Y/W)APEV' is also present in DstA (186-193) (Figure 4 A).

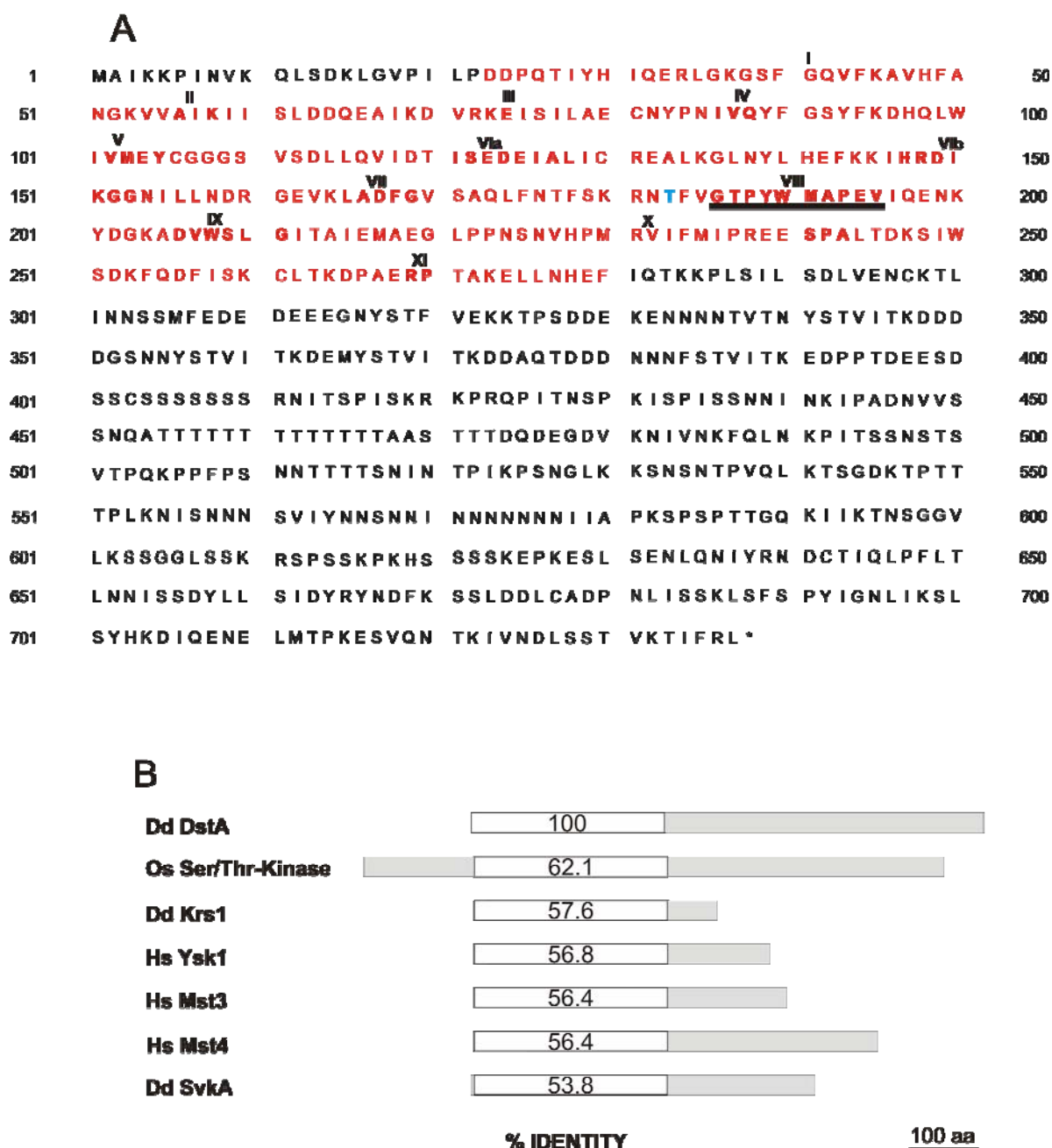


Figure 4. Domain architecture of DstA (adapted from Batsios 2005).

(A) The DstA protein consists of the catalytic domain (23-280 aa, red) and the regulatory domain (281-737 aa). All 12 canonical subdomains of kinase domains are present in DstA and labeled with roman letters. The characteristic sequence for Ste20-like kinases is underlined in sub domain VIII. A potential autophosphorylation site, described for Krs1 and other GCK-III kinases (Arasada et al., 2006), at Threonine 183 is highlighted (blue). (B) Schematic comparison of DstA relatives. The kinases were arranged depending on the identity in their catalytic domains (white) in relation to DstA. (Dd, *Dictyostelium discoideum*; Os, *Oryza sativa*; Hs, *Homo sapiens*). The accession numbers for the kinases are: DstA (DDB0167905); Os S/T Kinase (AAR01688); Krs1 (DDB0191170); Ysk1 (O00506); Mst3 (Q9Y6E0); Mst4 (AAK29620); SvkA (DDB0191176).

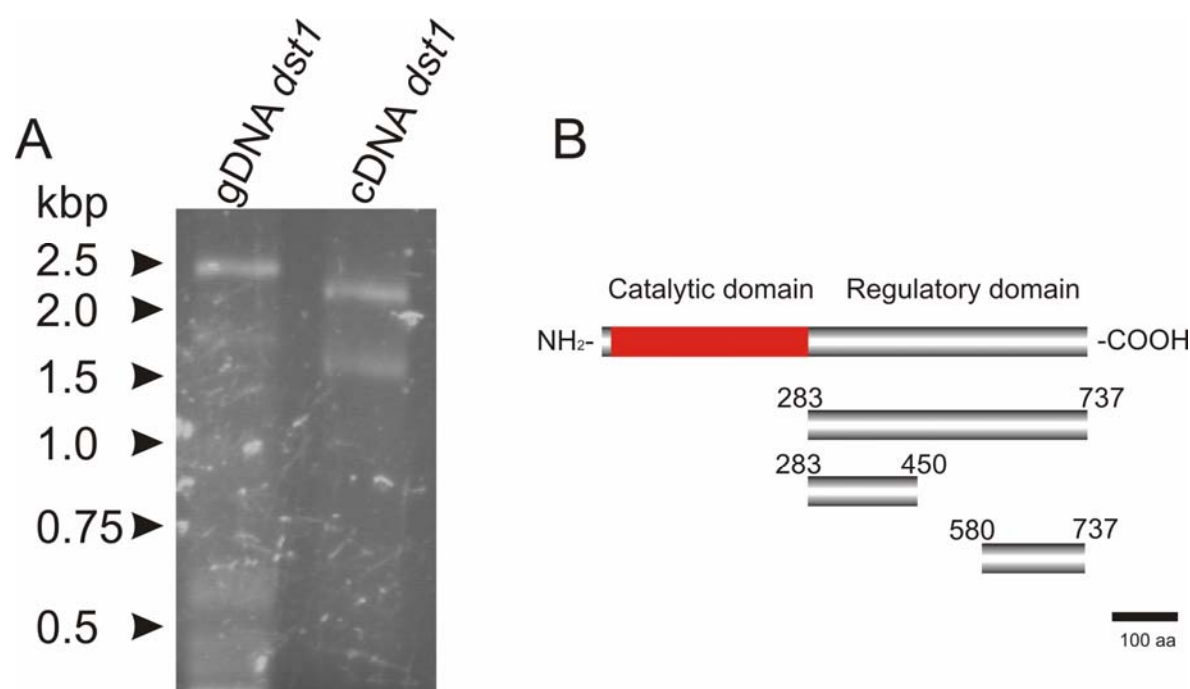


Figure 5. *Dst1* cDNA generation.

(A) The *dst1* gene was amplified by PCR using appropriate primers. *Dst1* cDNA was amplified by RT-PCR of RNA representing all developmental stages. The size of the amplified fragments corresponds to the expected size of *dst1* (gDNA: 2404 bp; cDNA: 2214 bp). (B) The amplified cDNA was used to express truncated proteins in *E. coli* and to use them for antibody generation. Three constructs of the DstA regulatory domain were expressed.

In database searches with the catalytic domain of DstA the highest degree of sequence homology was observed in kinases from the GCK-III subfamily, such as mammalian Mst3, Mst4 or Sok1 and uncharacterized representatives in plants with up to 62% identity. The closest relatives in *D. discoideum* are Krs1 (DDB0191170) and Severin kinase A (SvkA) (DDB0191176) with 57% and 53% identity in the catalytic domain. (Figure 4 B). The conserved catalytic domain of DstA also contains the putative autophosphorylation site, between subdomains VII and VIII at Thr182, that was described to be essential for kinase activity of Mst3 and Ysk1 (Lu et al., 2006; Preisinger et al., 2004). The C-terminus of DstA, on the other hand, showed no significant homologies to any known proteins.



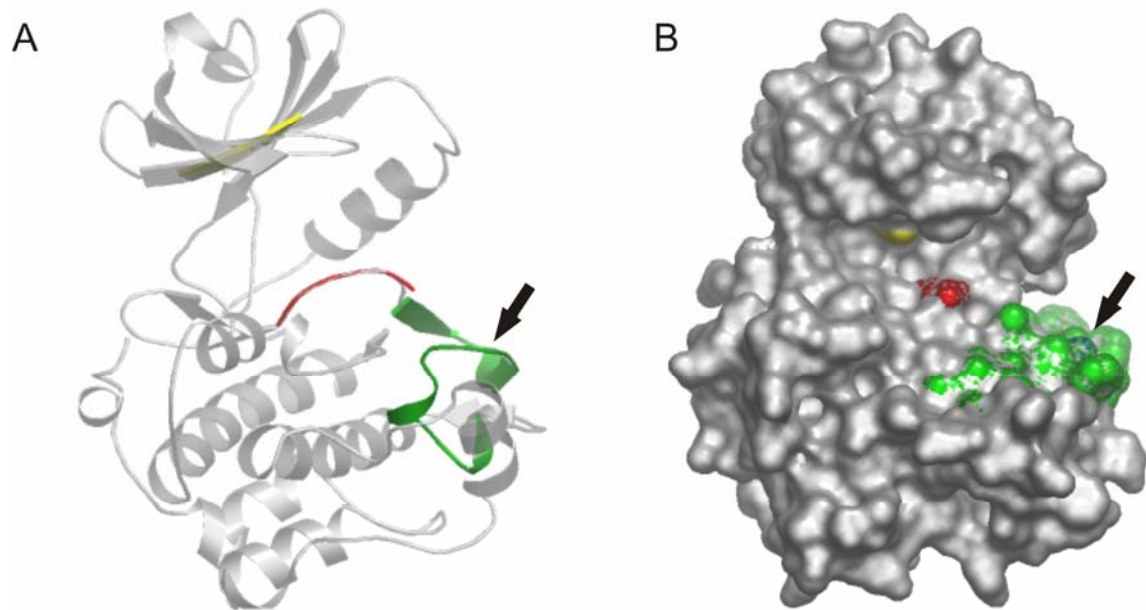


Figure 6. Tertiary model for the kinase domain of DstA.

Mst1 was used as template to predict the DstA kinase domain using the software tool Swiss Model (Arnold et al., 2006). (A) Ribbon diagram of the predicted DstA kinase domain. The ATP binding site (yellow), the activation segment (red) and the substrate binding site (green) are conserved on the surface area of DstA. (B) Surface model of DstA kinase domain (colors as in (A)). The autophosphorylation site (blue and black arrow) is exposed at the surface of the predicted substrate binding site.

The size of the full length gene and its cDNA was confirmed by PCR and RT-PCR respectively (Figure 5 A). The full length cDNA was then used for recombinant expression of parts of the kinase for antibodies generation (Figure 5 B). The high conservation of the kinase domain prompted us to use a bioinformatics approach to visualize the 3d structure of the kinase domain. As a template for this 3d model the 3d structure of the already crystallized GCK kinase homologue Mst1 was used (Hwang et al., 2007). The calculated structure for the catalytic domain of DstA shows that the potential autophosphorylation site at Threonine 183 is exposed at the surface of the substrate binding area (green) (Figure 6) making it possible that autophosphorylation regulates substrate recognition.

### 3.1.1.1 DstA antibodies

In order to further characterize the function of DstA polyclonal antibodies were generated in rabbits. For this *dst1* cDNA was amplified from RNA isolated from all developmental stages (Figure 5 A). The resulting cDNA was used to express fragments of the C-terminal part of DstA in *E. coli*. The DstA C-terminal domain was chosen as antigen because it has



no sequence homology to any other *D. discoideum* proteins. The full length regulatory domain (283-737aa) and two parts, the regulatory domain from amino acid 283 to 450 (aReg) and a fragment from amino acid 580 to 737 (Ct-Reg), of DstA were successfully expressed in *E. coli* and purified as GST fusion proteins (Figure 7).

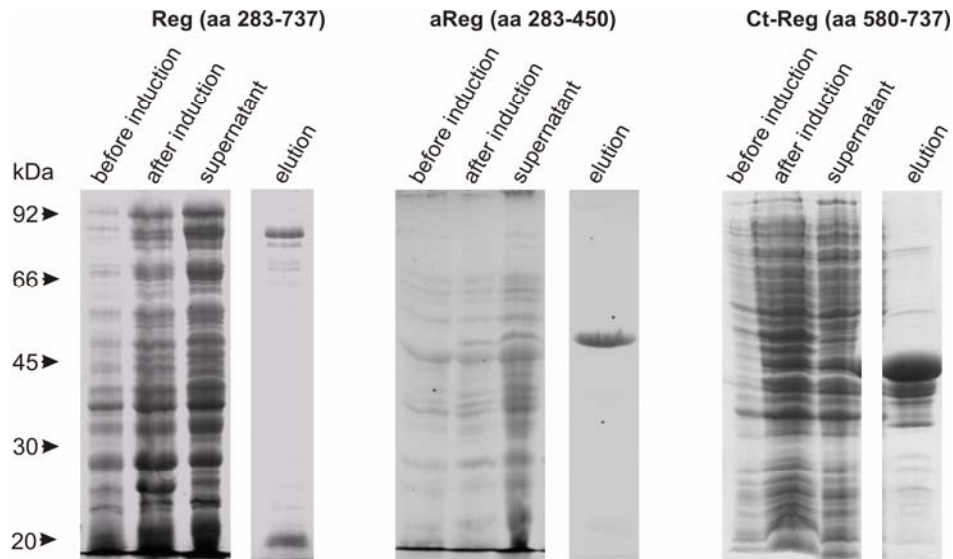


Figure 7. Expression and purification of two DstA fragments.

The DstA constructs Reg (aa 283-737) was cloned into expression vector pGEX 6P-1 and expressed in the *E. coli* strain BL21 ArcticExpress RIL. aReg (aa 283-450) and Ct-Reg (aa 580-737) were cloned into expression vector pGEX 5x-1 and expressed in the *E. coli* strain BL21RIL. The successful expression and purification of the recombinant proteins via glutathione beads is documented as Coomassie stained SDS-PAGE, with samples taken before induction, 4h after induction, supernatants after cell lysis and the eluted proteins.

The two shorter purified DstA fragments of the regulatory domain were mixed in a 1:1 ratio and injected together into New Zealand white rabbits. After two boosts, the serum of the animal was tested with western blot for the presence of anti-DstA antibodies. One specific band with a size corresponding to the endogenous DstA kinase (~82 kDa) was detected in *D. discoideum* cell lysates. The serum was useful for western blot analysis even in dilutions of 1:5000 (Figure 8). The full length regulatory domain (Reg, aa 283-737) was expressed at lower temperature in the *E. coli* strain BL21 ArcticExpress RIL, and purified after anti-DstA antibodies were generated (Figure 7).

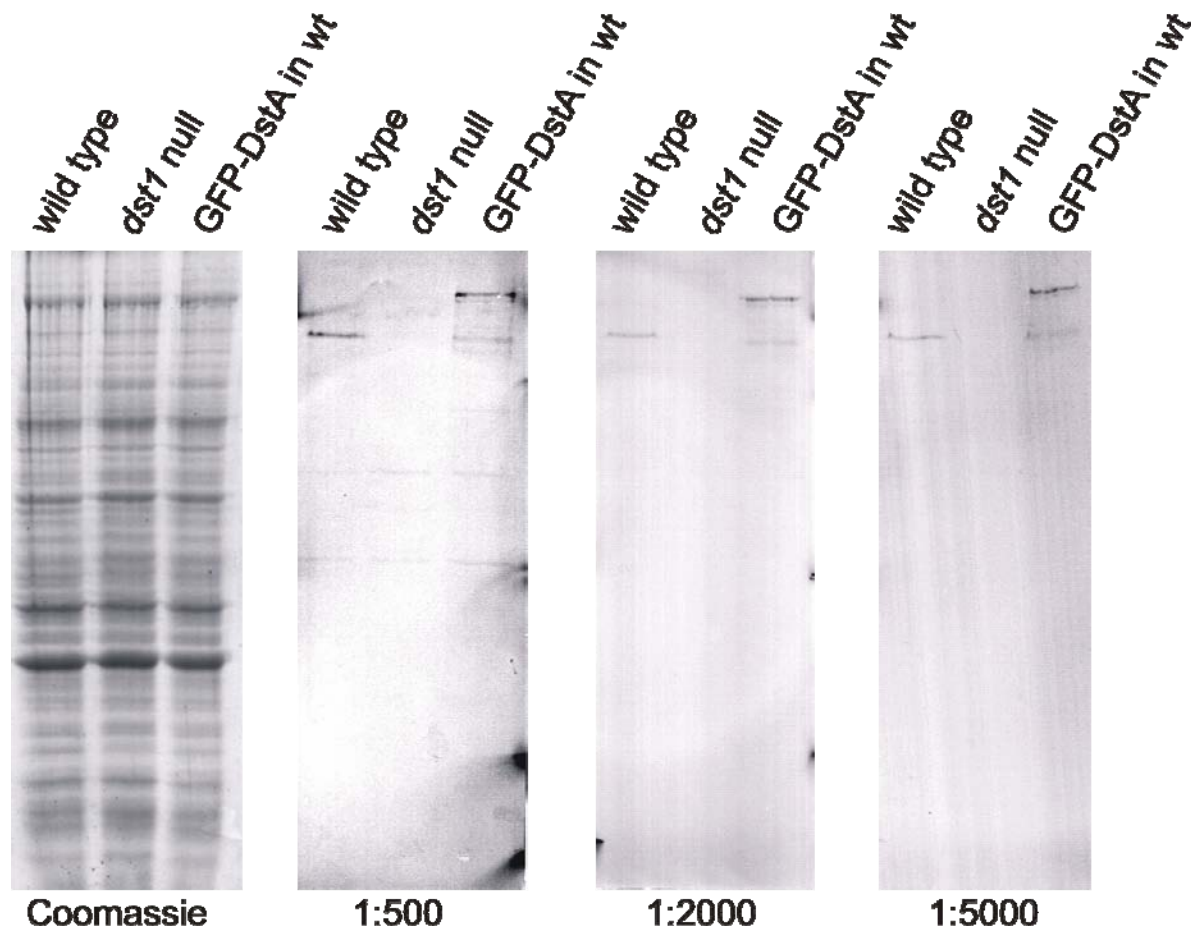


Figure 8. The anti-DstA antibody.

Western blot analysis of the generated anti-DstA serum with equal numbers of wild type, *dst1* null and GFP-DstA in wild type cells.

The anti-DstA antibodies were used to visualize the endogenous expression of the DstA kinase during *D. discoideum* development. For that purpose protein samples were prepared from every three hours of the wild type *D. discoideum* development and analyzed on western blots with anti-DstA antibodies. The DstA kinase is ubiquitously expressed during all stages of the *D. discoideum* development (Figure 9). Anti-DstA antibodies were perfectly suitable for western blot analysis but not for immunofluorescence. Wild type, *dst1* null and GFP-DstA cells were fixed with picric acid or methanol and incubated with anti-DstA antibodies and appropriate secondary antibodies. Non specific signals were visible in these fixations (not shown).

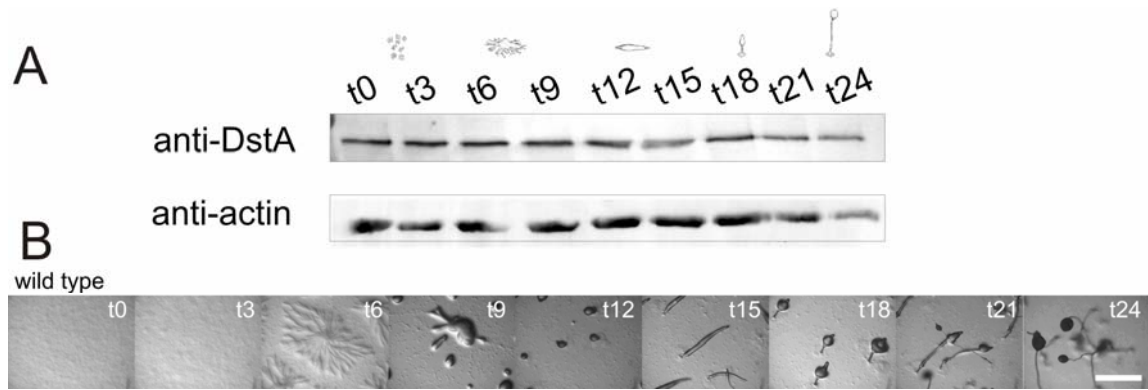


Figure 9. Expression of DstA during the *D. discoideum* development.

(A) DstA is equally expressed during all stages of *D. discoideum* development. Equal numbers of cells were collected every 3h hours throughout the development and analyzed using the anti-DstA antibody. Actin served as loading control. (B) The developmental cycle of wild type cells used in (A) is documented with images taken before cell lysis. Bar: 5 mm.

### 3.1.1.2 Subcellular localization of DstA

In order to investigate the subcellular localization of the DstA kinase three GFP tagged DstA constructs were generated and expressed in *D. discoideum*. The sizes of the expressed constructs were confirmed in anti-DstA western blots.

The GFP-DstA full length kinase in vegetative (not shown) and in polarized (t6) cells was visible in the cytosol of live cells, but not in the nucleus (Figure 10). In cells fixed with picric acid the GFP-DstA localization is also pronounced at the plasma membrane and in membranous intracellular structures, but not the nucleus (Figure 11 A). The C-terminal region of DstA expressed as GFP-DstA Reg (aa 283 - 737) in wild type and *dst1* null cells was mainly distributed in the nucleus and in the cytosol (Figure 11 B). The shorter construct GFP-DstA Ct Reg (aa 580 - 737) localized in fixed cells, similar to the full length kinase, with staining at the membrane and cytosol, but not in the nucleus (Figure 11 C). The generated anti-DstA antibody was also used for immunostains after picric acid/paraformaldehyde or methanol fixations, but due to a very high background, even in DstA knockout cells, no conclusion could be drawn. The localization of GFP-DstA constructs, expressed to similar levels as the endogenous DstA, suggest a mainly cytosolic distribution in *D. discoideum* (Figure 11). Under certain conditions a slight enrichment at the plasma membrane was observed.

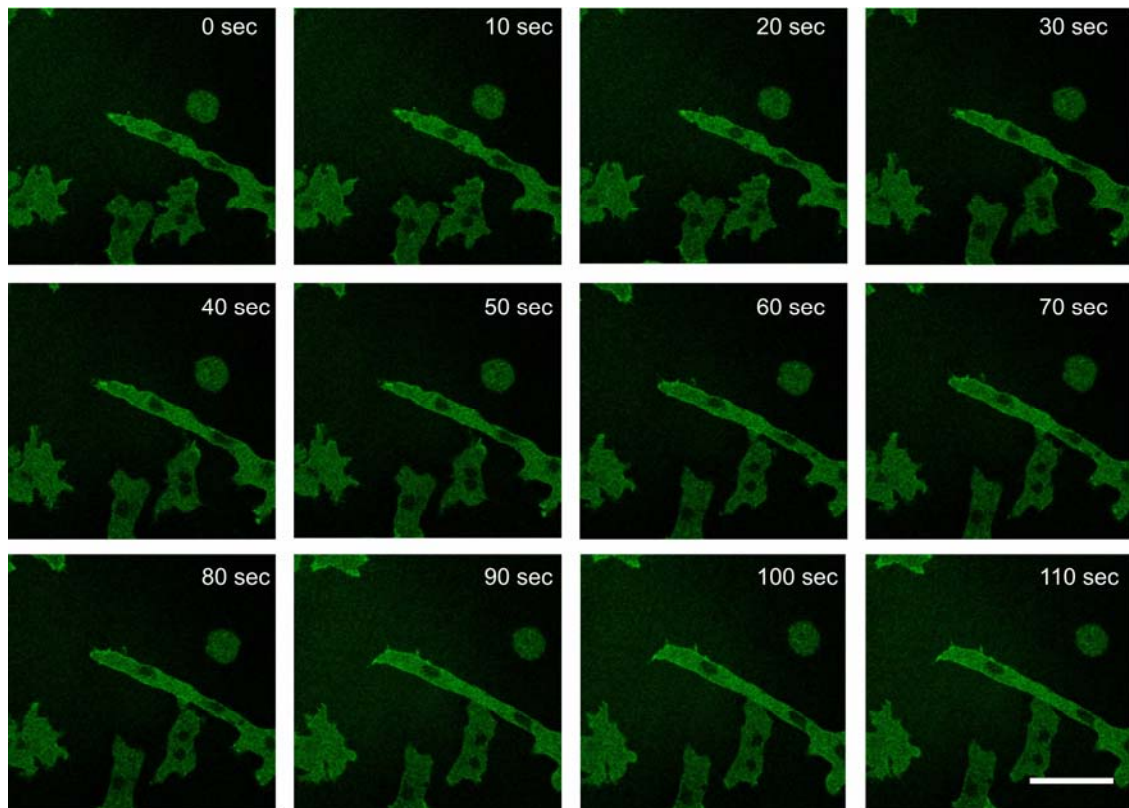


Figure 10. Subcellular localization of GFP-DstA in migrating polarized cells. GFP-DstA cells were starved for 6 hours and the polarized cells were observed with the confocal microscope. The kinase localizes throughout the cytoplasm, but not in the nucleus. Scale bar: 5  $\mu$ m.

The characteristic GFP-DstA membrane localization was further analyzed by immunostaining for co-localization with other molecules. First the membrane protein cortexillin II was chosen (Figure 12).

Cortexillin II localization in wild type and *dst1* null cells is not disturbed. Moreover, the GFP-DstA and not the GFP-DstA Ct Reg construct seemed to co-localize with cortexillin (Figure 12). The GFP-DstA protein also seemed to be in the cytosol but enriched around the nucleus. Actin, comitin and annexin VII were used as markers for co-localization studies (Figure 13). Actin and GFP-DstA do not co-localize in the immunostaining (Figure 13 A).

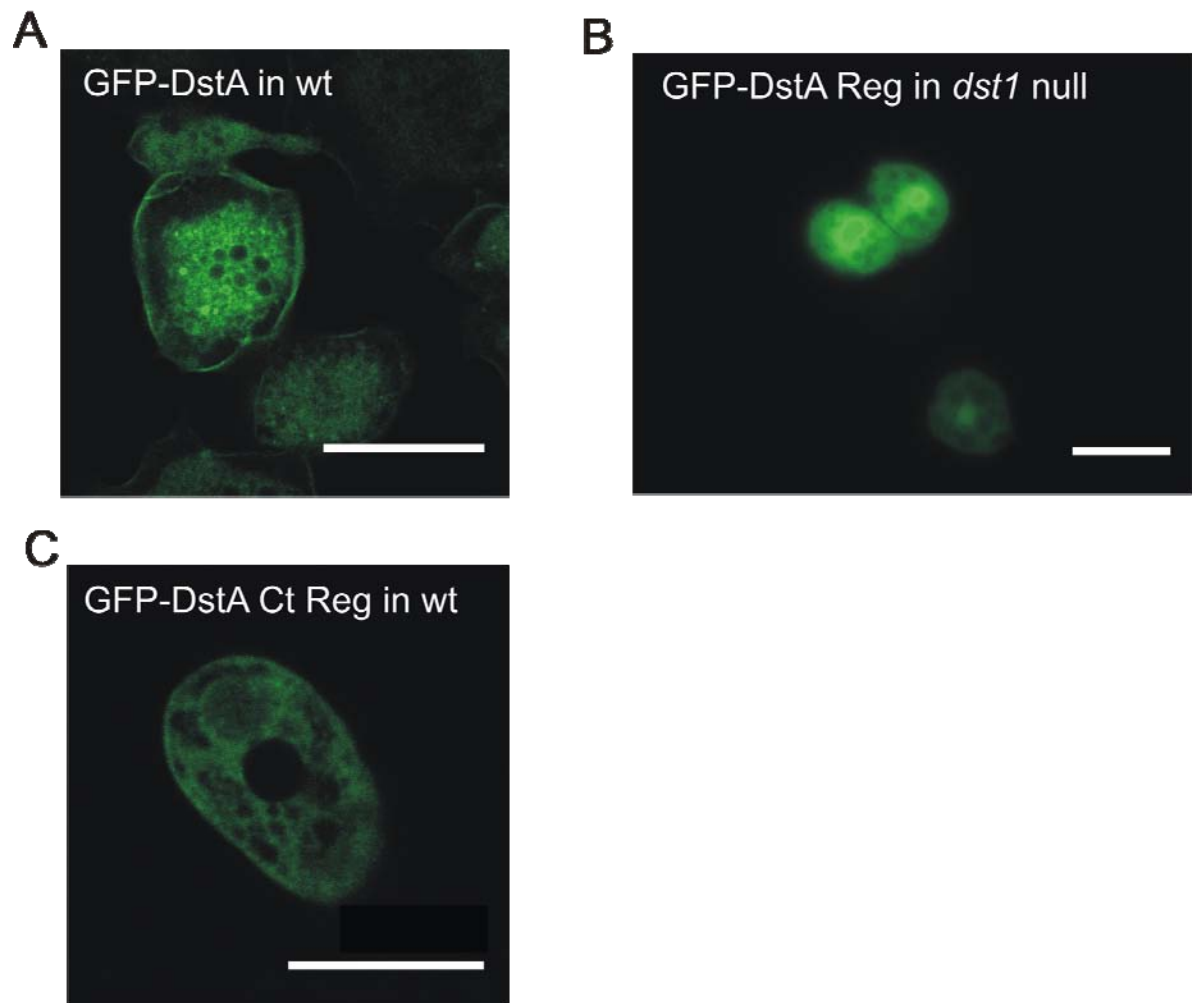


Figure 11. Subcellular localization of DstA.

(A) Localization of GFP-DstA in wild type and (B) GFP-DstA Reg in *dst1* null cells. Bar: 4  $\mu\text{m}$ . (C) Confocal image of GFP-DstA Ct Reg in wild type. Cells were fixed with picric acid (A and C) or observed alive (B). Images were taken with the confocal microscope (A and C) or the Axiovert (B). Bar: 2  $\mu\text{m}$ .

Also the golgi marker, comitin, did not co-localize with the GFP-DstA (Figure 13 B). Annexin VII is localized to the membrane and in the cytosol. This was thought to be co-localizing with GFP-DstA. Annexins are characterized by their calcium dependent ability to bind to negatively charged phospholipids. They are located in some, but not all membranous surfaces within a cell, which would be evidence of a heterogeneous distribution of  $\text{Ca}^{2+}$  within the cell (Doring et al., 1995). Annexins have been observed to play a role for the later stages of the exocytotic pathway near or at the plasma membrane, and in the transport and also sorting of endocytotic events. The localization of annexin VII partly overlapped with the DstA localization, especially at certain parts at the plasma membrane (arrows). Nevertheless the annexin VII localization is not disturbed in *dst1* null



cells (not shown). Coimmunostainings with TRITC-Phalloidin revealed that the actin cytoskeleton of *dst1* null cells is not disturbed (not shown).

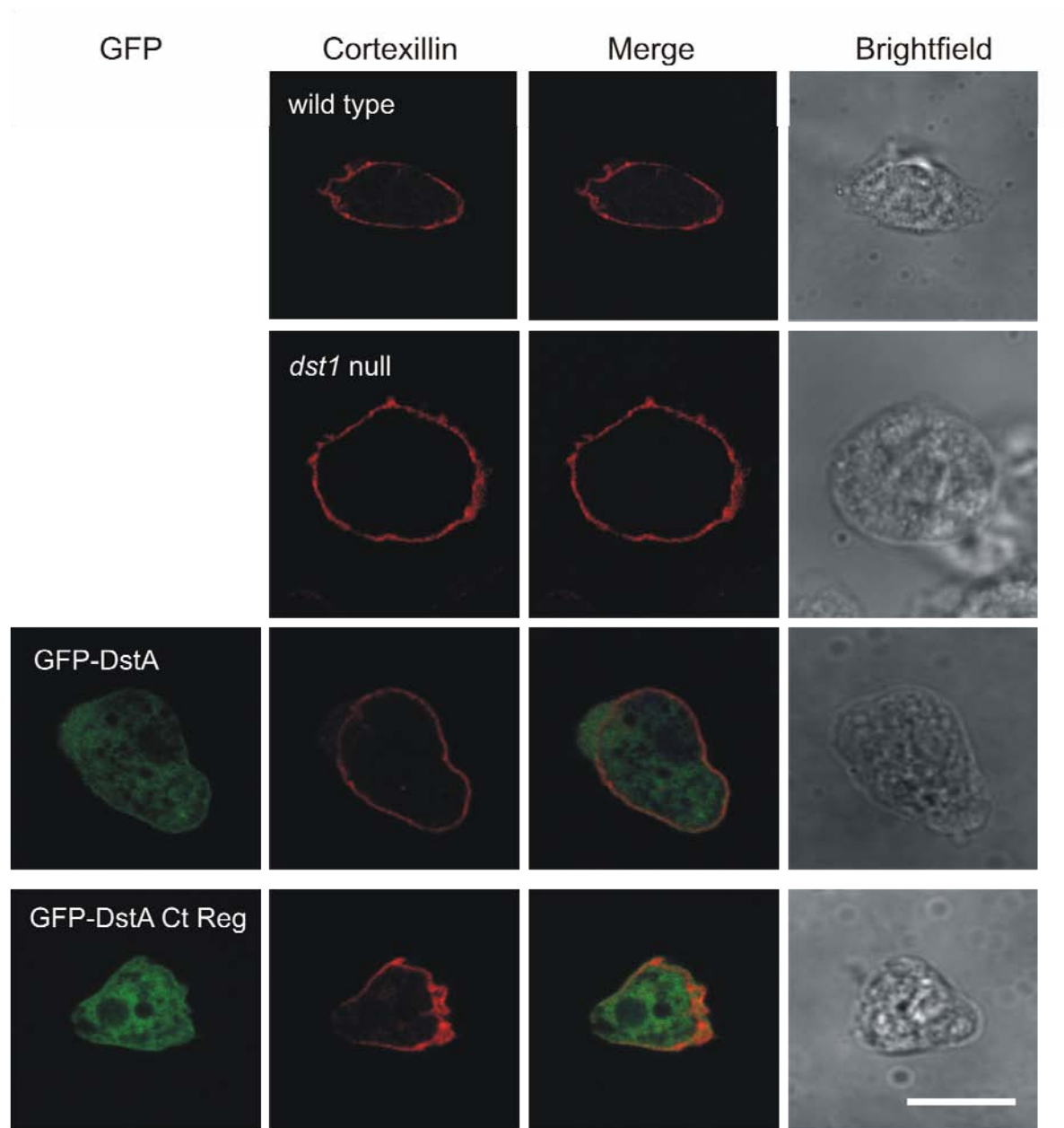


Figure 12. Colocalization of GFP-DstA with cortexillin II.

After picric acid fixation cells were incubated with anti-cortexillin II antibodies, followed by secondary Cy3 and TO-PRO. Images were taken with the confocal microscope. Bar: 2  $\mu$ m.

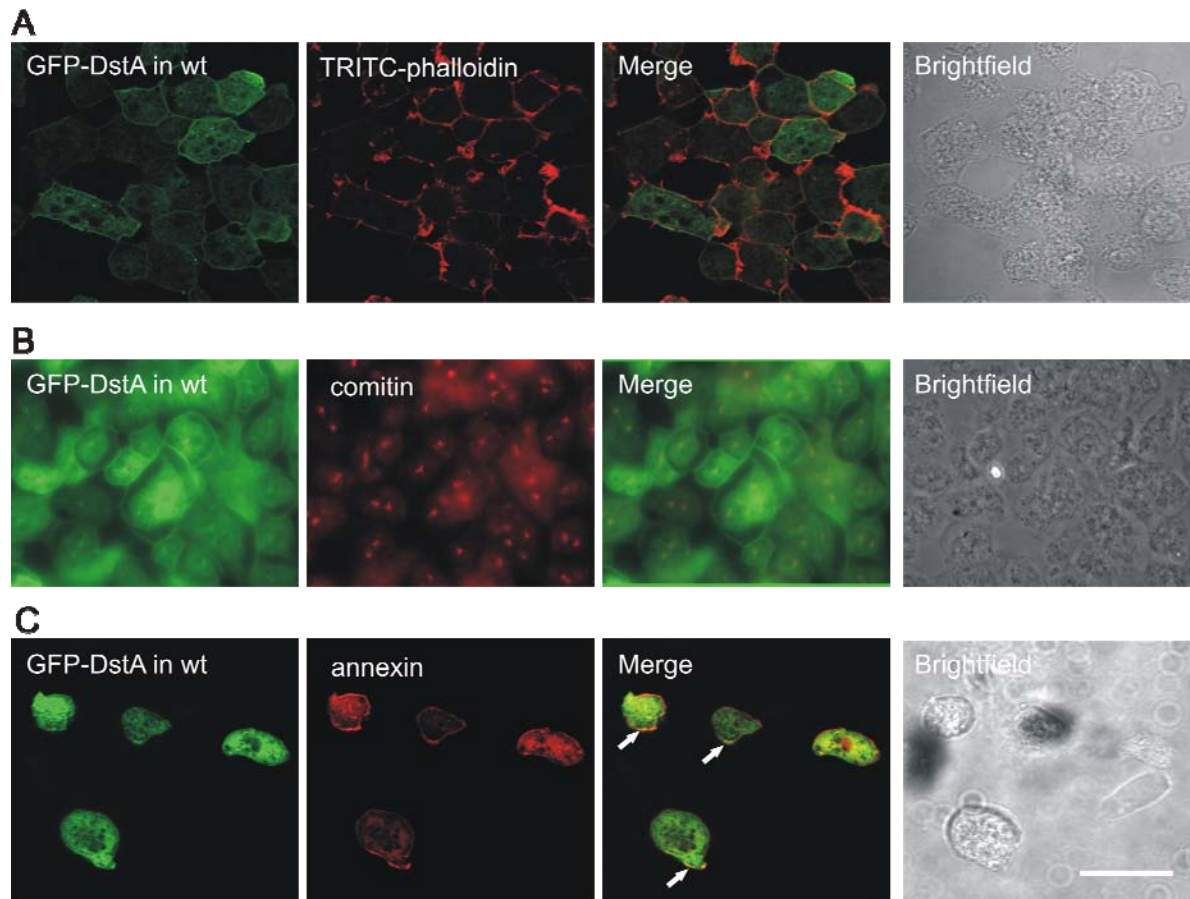


Figure 13. Co-localization of GFP-DstA with F-actin, comitin and annexin VII. GFP-DstA cells were fixed with picric acid and stained with (A) TRITC-phalloidin, (B) anti-comitin or (C) anti-annexin VII antibodies, followed by secondary cy3. After mounting images were taken with the confocal microscope (LSM 510) (A and C) or a fluorescence microscope (B). Arrows indicate the areas of partial co-localization of GFP-DstA with annexin VII. Bar: 4  $\mu$ m.

### 3.1.1.3 Isolation of *dst1* knockouts

The initial characterization of a DstA knockout mutant (Batsios, 2005) suggested a severe developmental defect (Figure 14). To further substantiate these results independent *dst1* null clones were generated and confirmed with the new anti-DstA antibody (Figure 14 C). An initial analysis of the independent knockout clones c2, d5, x2, x4 and x5 showed the same phenotype for all mutants. So clone c2 was chosen for the in depth analysis of the DstA knockout phenotype throughout this project.

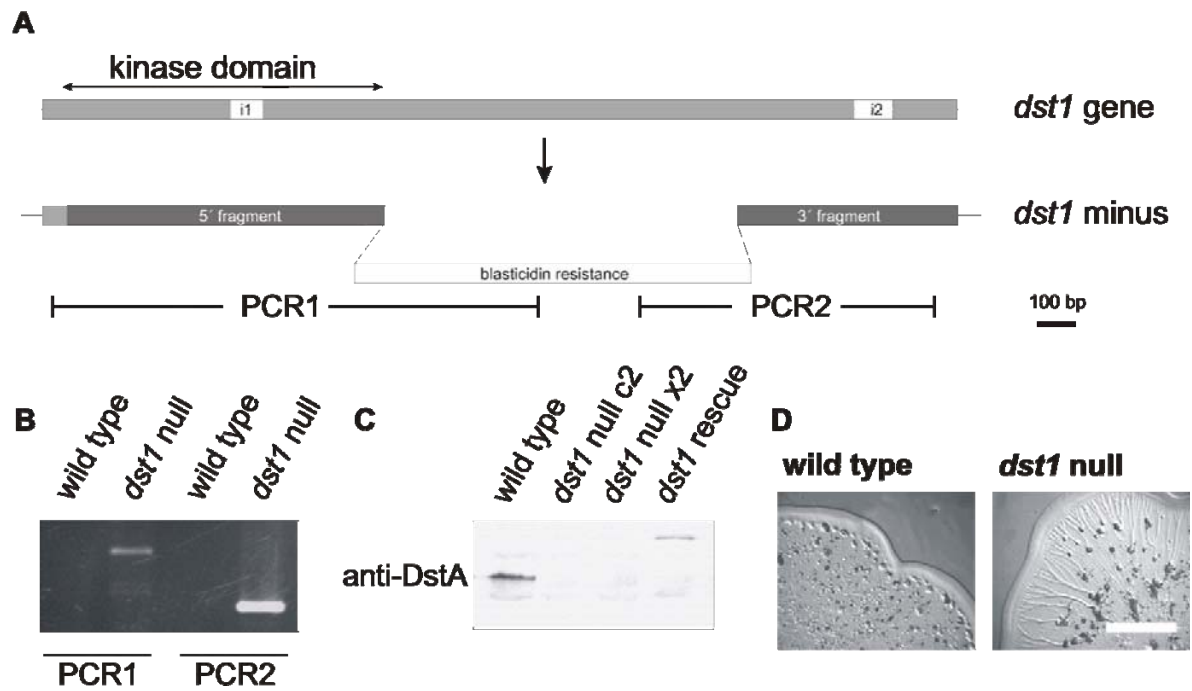


Figure 14. *Dst1* gene disruption (adapted from (Batsios, 2005)).

(A) Deletion of the *dst1* gene. Gene specific homologous recombination leads to the integration of a blasticidin-resistance cassette and inactivation of the DstA gene. (B) Identification of *dst1* null mutants by two knockout specific PCRs. (C) Confirmation of the DstA null mutants by anti-DstA western blot analysis. Expression of a GFP-DstA full length, under control of the actin15 promoter, was used to rescue the DstA knockout phenotype. (D) The first indication for a developmental phenotype of *dst1* null cells was the observation of long streams on bacteria lawn. Bar: 2 cm.

#### 3.1.1.4 Phenotype characterization of the *dst1* null

Wild type, *dst1* null, *dst1* rescue, GFP-DstA regulatory domain in *dst1* null cells and GFP-DstA in wild type cells were characterized and compared in order to draw conclusions for the function of DstA in *D. discoideum*. The first observation was that *dst1* null cells form long streams on bacteria lawns (Figure 15 A), indicating that the initial phase of the development is disturbed. Detailed analysis of stream formation, by plotting the length of the streams over the number of streaming events (Figure 15 B), showed that normal wild type behaviour is that the streams are getting shorter the bigger the streaming area gets. Interestingly, *dst1* null streams get longer over time, fall back to the initiating state and grow bigger again. Another finding, linking DstA to the early phase of development, was that *dst1* null cells form aggregates when growing in medium on petri dishes (Figure 15 D and E), a behaviour normally part of the developmental cycle of starving cells.



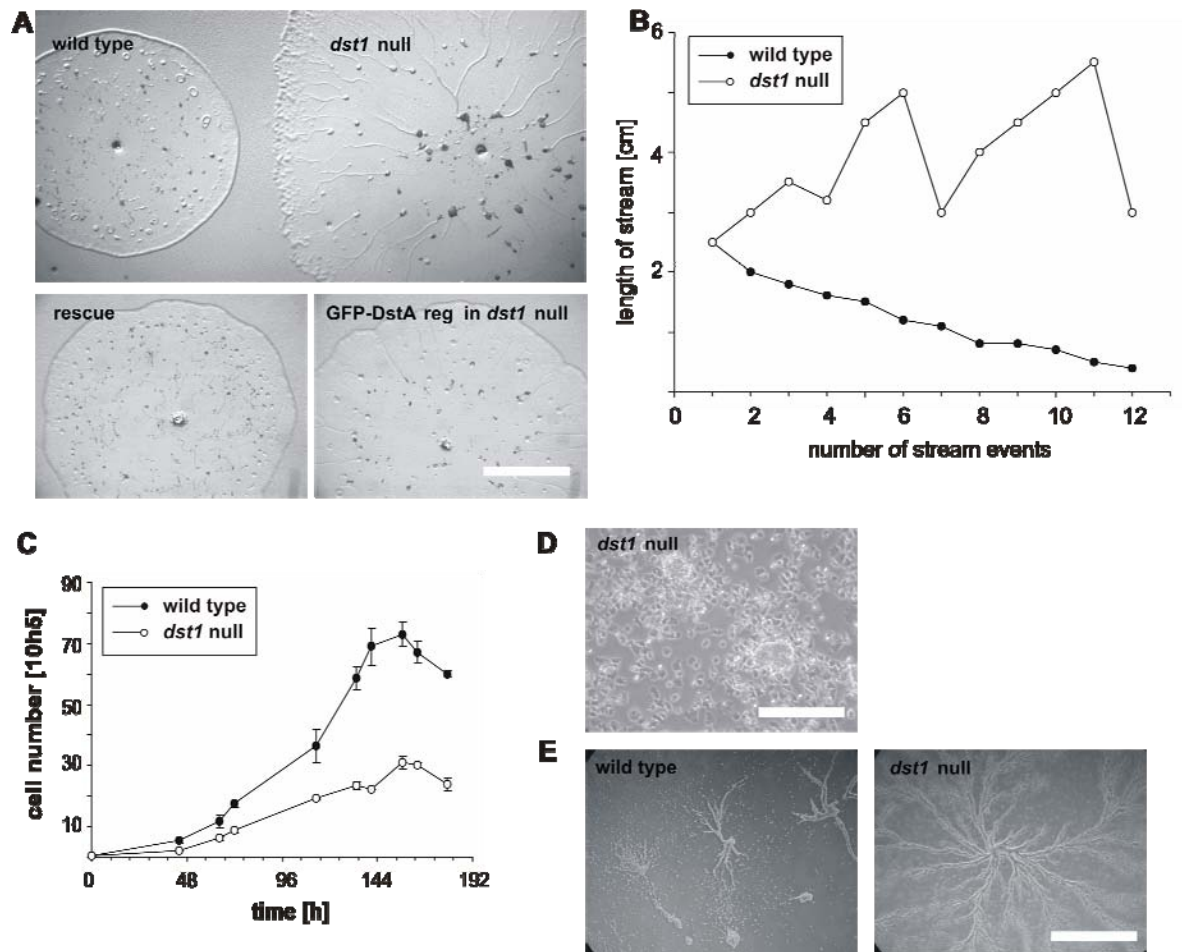


Figure 15. Characterization of the *dst1* null phenotype.

(A) *dst1* null cells form aberrant long streams on bacteria lawns. Cells were transferred to the middle of an *E. coli* B2 lawn. After two days the size of the colonies and length of stream were documented. Expression of GFP-DstA but not the GFP-DstA regulatory domain alone could rescue the observed phenotype of the DstA knockout. Bar: 2 cm. (B) The length of the streams formed by the starving amoeba was measured and plotted against the number of streaming events. (C) A comparison of growth rates from *dst1* null and wild type cells showed that the mutant grows considerably slower in shaking culture. (D) The *dst1* null cells already start to aggregate in growth medium where there should be enough nutrients present. Error bars indicate standard deviation. (E) When the nutrients are withdrawn, the *dst1* null cells frequently aggregate towards a single centre whereas the wild type would form several aggregation centers under same conditions. Bar: 0.5 cm.

There are several possible explanations for this phenotype. First, the knockout cells have a severe defect in phago- and/or pinocytosis that result in cells that starve while surrounded by abundant food. Second, DstA could be part of a signaling pathway that normally prevents well fed cells from entering the developmental cycle and to go into developmental commitment. Third, *dst1* null cells secrete starvation signals even in the presence of nutrients initiating the developmental cycle prematurely. These three hypotheses were further investigated in the *dst1* null.

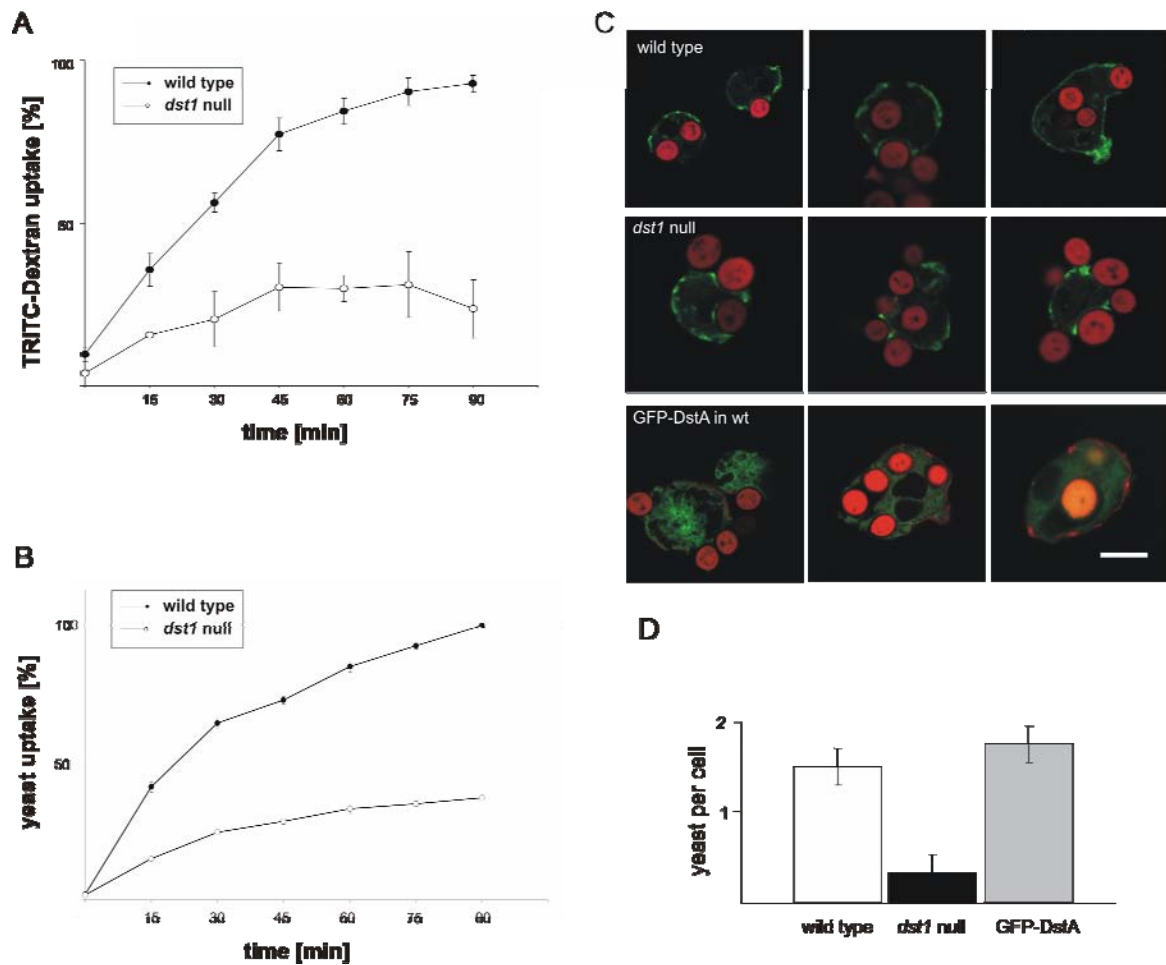


Figure 16. *Dst1* null cells have a defect in phagocytosis.

(A) Pinocytosis assay. TRITC-dextran uptake was recorded for *dst1* null and wild type cells. (B) Phagocytosis assay. The uptake of fluorescent yeast was measured for wild type and *dst1* null cells. (C) Cells were incubated for 1h with TRITC-yeast fixed with picric acid and engulfed yeast counted. The yeast uptake was disturbed in *dst1* null cells. Wild type and *dst1* null cells express GFP-Coronin. GFP-DstA cells were stained for coronin (red) after fixation. Bar: 1  $\mu$ m. (D) Quantification of yeast uptake in fixed cells revealed reduced phagocytosis by *dst1* null cells after incubation with yeast for one hour. Error bars indicate standard deviation.

To address the question of phagocytosis or pinocytosis defects the growth in liquid medium was investigated. The *dst1* mutants show a severe growth defect when grown in liquid medium, where cells can only rely on pinocytosis to take up nutrients (Figure 15 C). The reduced doubling time of the mutant would be in agreement with a pinocytosis defect. On the other hand, *dst1* null cells were not able to grow to normal cell densities ( $2.5 \times 10^6$  compared to  $8.0 \times 10^6$ ), which could be an indication for a secreted density factor. To quantify the pinocytosis defect, the uptake of fluorescent TRITC-dextran was measured (Figure 16 A). The knockout had only 30% of the pinocytosis capacity compared to the wild type.

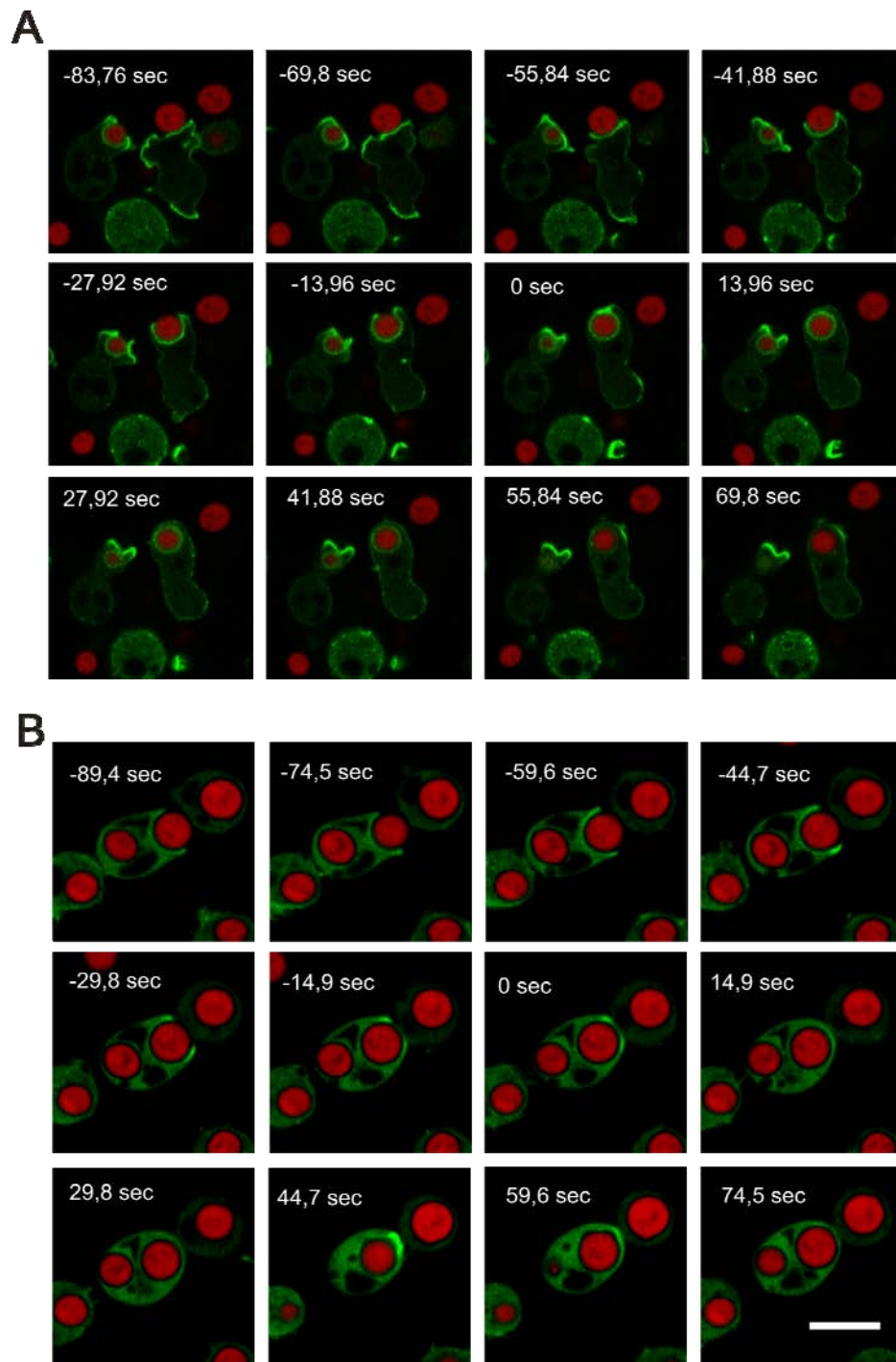
A similar result was obtained in the phagocytosis assay with TRITC-labelled yeast (Figure 16 B), where the knockout engulfed only 40% compared to normal *D. discoideum* cells. In order to confirm the observed phagocytosis defect, we incubated wild type, *dst1* null cells expressing GFP-coronin and GFP-DstA for 1h with TRITC labelled yeast. After picric acid fixation single cells undergoing phagocytosis were observed (Figure 16 C). Our previous finding confirmed that *dst1* null cells did not take up as many yeast particles as the wild type even after 1 hour of incubation with yeast. Another finding while looking at fixed cells expressing GFP-DstA was, that DstA functions during phagocytosis without localizing to the phagocytic cup (Figure 16 C), where else coronin localization was not effected during this process. The random motility of vegetative *dst1* null cells was normal indicating that overall actin machinery is not disturbed (not shown).

In order to follow the phagocytosis in the mutant strain live cell fluorescence microscopy was performed. Wild type cells expressing GFP-Lim $\Delta$ coil an F-actin marker and *dst1* null expressing the actin binding protein GFP-coronin were observed during TRITC-yeast uptake (Figure 17). Even though *dst1* null cells show a drastic phagocytosis defect, they are able to take up yeast and the phagocytosis marker coronin localized normally. *Dst1* null cells form a phagocytic cup but have problems finishing the process of phagocytosis. When compared to the wild type, single *dst1* null cells take ~90 sec to close the phagocytic cup from the first contact with the particle (Figure 17 A). The normal process of phagocytosis in wild type cells is faster and takes only ~45 sec from contact to closure of the phagocytic cup (Figure 17 B).

Taken together *dst1* null have a pinocytosis and phagocytosis defect that could cause the initially observed phenotype of premature development in the presence of abundant food. The defect of *dst1* null cells in pinocytosis would explain the reduced growth rates. On the other hand because pinocytosis and phagocytosis are regulated by different pathways in *D. discoideum* and *dst1* null cells show defects in both, our second hypothesis that *dst1* null cells are prematurely developed and that the observed defect, had to be tested.

It is known that *D. discoideum* cells which have entered the developmental program for more than 6 hours (Kato et al., 2007) do not perform bacteria phagocytosis which represents a commitment to development. In the same study it has been shown that cAMP pulses are necessary to induce both commitment and the loss of phagocytosis in starving cells, whereas starvation alone is not sufficient. So it is possible that the observed

pinocytosis and phagocytosis defects of *dst1* null are a secondary effect observed in cells that have begun the developmental cycle.



To address the issue how far into the developmental cycle *dst1* null cells have proceeded in the presence of nutrients (time point t0) we tested for the expression of several development marker proteins (Figure 18). The expression of the developmental markers contact site A (CsA), a cell adhesion protein normally expressed after 6 hrs into the development (Bakthavatsalam et al., 2007) and prespore A (PsA) expressed normally at t12 (Alvarez-Curto et al., 2007) was investigated by western blot. Whereas the expression of the late developmental marker PsA showed no significant differences between wild type and *dst1* null (Figure 18 A), CsA in *dst1* null cells was expressed 3 hrs into the development. This is not considerably earlier than in the wild type and suggests that DstA does not influence initial stages of the *D. discoideum* developmental cycle. *Dst1* null cells do not express CsA at the vegetative cell stage (t0). If *dst1* null cells in nutrient media are not ahead in the developmental program this might suggest that the observed phagocytosis defect is the primary defect of *dst1* null cells.

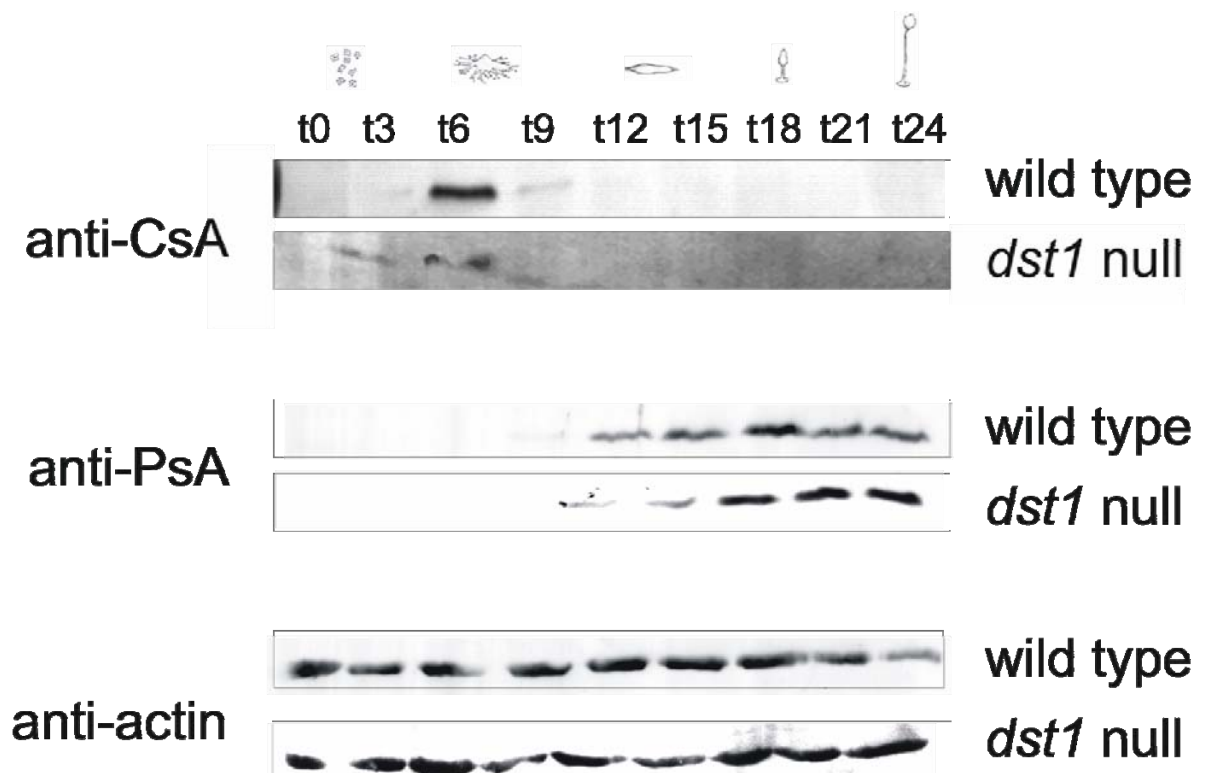


Figure 18. Expression of the developmental markers CsA and PsA in *dst1* null cells. Western blot analysis of developmental markers in *dst1* null cells.

Overall, the development of *dst1* minus cells culminating into fruiting bodies was rather normal (data not shown). A slight increase in the size of the fruiting bodies and a parallel decrease in the number of end structures, which we would explain with the bigger



catchment area of *dst1* null cells due to the tendency of *dst1* null cells to make longer streams, resulting in more cells per fruiting body, were observed. A second observation was that during the development *dst1* slug migration (Figure 19) is inhibited.

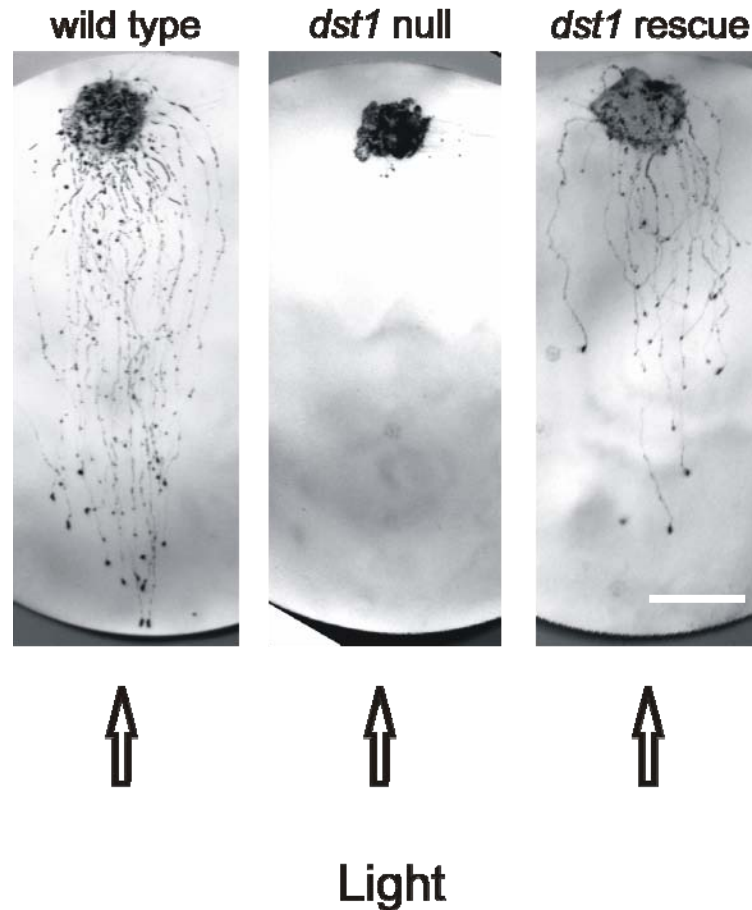


Figure 19. Phototaxis of *dst1* null aggregates.

In aggregated *dst1* null cells the multicellular slug migration is affected. Bar: 2 cm.

The third hypothesis, that a secretory factor produced by the *dst1* mutant leads cells to aggregate in medium and to stream on bacteria lawns was also investigated. In several experiments fresh HL5 growth medium with conditioned medium that was collected from cultures of streaming *dst1* null cells were compared. *Dst1* null cells incubated with fresh HL5 medium took ~48h longer to stream when compared with *dst1* null cells in conditioned medium. Surprisingly, the conditioned medium had no effect on wild type cells under similar conditions. These experiments led us to conclude that *dst1* null cells conditioned the medium with a factor that has an effect on *dst1* null but not on wild type cells. An explanation could be that, as suggested before, *dst1* null cells have already entered the developmental cycle making them susceptible for the secreted factor, whereas the undeveloped wild type does not sense this factor.

To further characterize this secreted factor several experiments were performed. Using filters with different pore sizes showed that the factor passes a filter size of 10 kDa. With that experiment the large counting factor, a cell density sensor (Brock and Gomer, 1999), could be excluded as the responsible molecule for aggregation and streaming in *dst1* null cells. *Dst1* cells produce a small factor that lead *dst1* null cells but not wild type cells to aggregate and stream in the vegetative cell stage.

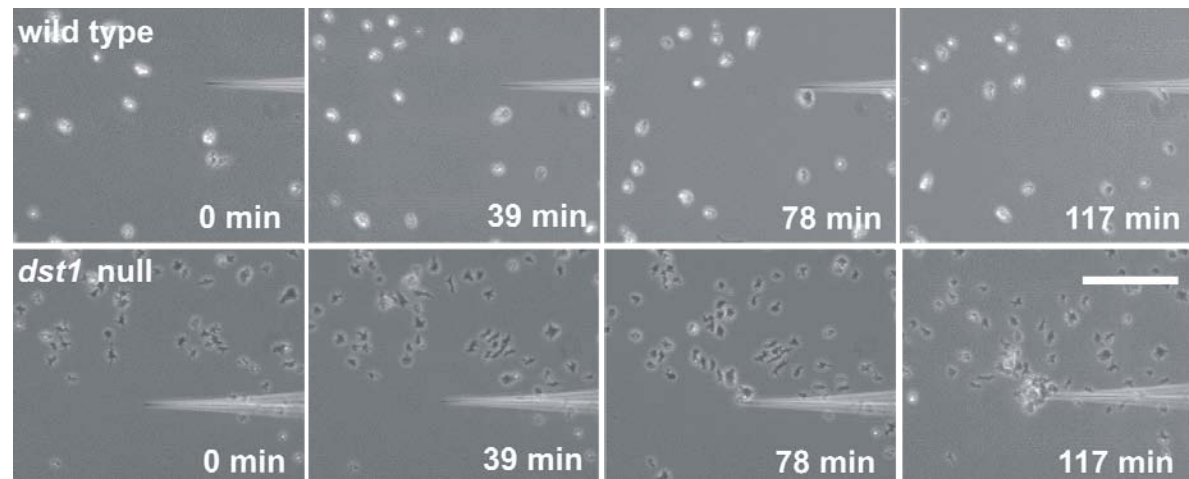


Figure 20. Chemotaxis of vegetative cells towards cAMP.

Vegetative *dst1* null cells react to the chemoattractant cAMP in growth medium. Wild type and *dst1* null cells were harvested from shaking cultures or petri dishes and plated on glass bottom dishes. Cells were stimulated with a capillary filled with 0.1 mM cAMP. After one hour of stimulation *dst1* null cells started to migrate towards the gradient in medium. Bar: 2 mm.

During the developmental program of *D. discoideum* cAMP is the molecule that leads cells to aggregate. cAMP pulses are sufficient to induce both commitment and the loss of phagocytosis in starving cells, but starvation alone is not sufficient (Kato et al., 2007). To investigate aggregate formation in liquid medium, a standard capillary assay with vegetative cells in HL5 medium was performed. Surprisingly, *dst1* null cells react to the chemoattractant cAMP after 1 hour of stimulation (Figure 20). Wild type cells do not react even after 2-3 hours as expected. The experiment was repeated in phosphate buffer and nutrient medium, with cells coming from shaking culture or petri dish. Under all conditions the wild type did not react to the cAMP filled capillary, whereas the *dst1* knockout reacted after an initial phase of acclimatization. *Dst1* knockout cells coming from a petri dish (where streams can be formed) and *dst1* null cells incubated in phosphate buffer reacted considerably faster to the chemoattractant.

An explanation could be that *dst1* null cells produce cAMP and express the cAMP receptor 1 (cAR1) already in the vegetative state or at least at an earlier time point than wild type cells. In order to confirm the expression of cAR1 in *dst1* null cells western blot analysis had to be performed. This did not work because of the poor quality of the cAR1 antibodies.

To summarize, a knockout for *dst1* was generated and was found to be defective in endocytosis and development. The cells aggregate and stream in the presence of nutrients and grow slower in liquid cultures compared to wild type cells. *Dst1* cells are defective in uptake of liquid and yeast. The mutant is not entering development significantly earlier than wild type cells but is able to produce cAMP and the cAR1(not shown) at the vegetative cell stage and react to that. We suggest an involvement of DstA in pathways that are regulating cAR1 expression and/or cAMP production. The knockout is therefore developing prematurely and as a secondary effect reduces endocytosis and growth.

### **3.1.1.5 Interactors for DstA**

Several approaches were undertaken to identify interactors for the DstA kinase. Based on the successful expression of three different C-terminal DstA constructs as GST fusion proteins (Figure 7) GST-pull-downs with *D. discoideum* lysate were performed. Unfortunately, no interaction partner could be pulled down using this method.

The same negative results were obtained using the GFP-DstA expressing strains for immunoprecipitations. Neither the conventional anti-GFP polyclonal antibodies, used successfully to precipitate cortexillin II interactors (Faix et al., 2001), nor engineered GFP antibodies developed for the new Nanotrap system (Rothbauer et al., 2008) could reveal DstA interactors. These results led us to conclude that DstA, as most other kinases, is involved in a “kiss and run” process for phosphorylation and does not make a stable binding with a substrate in the conditions used in our assays.



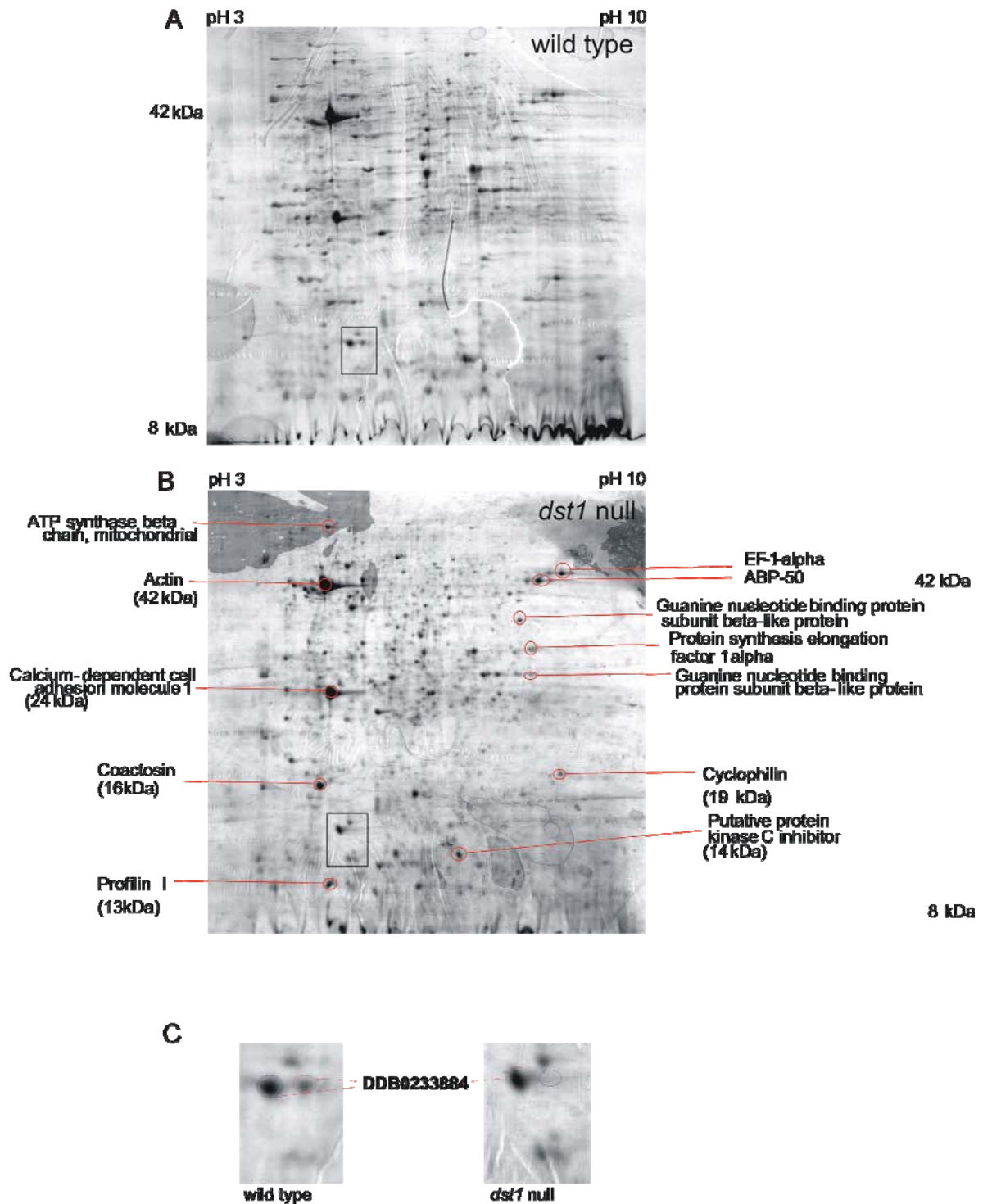


Figure 21. Identification of the ADF/Cofilin over 2D-PAGE.

(A and B) 2D-PAGE identified a spot of approximately 16 kDa size at a pI of ~5 that is affected in the *dst1* null proteome, suggesting differences in phosphorylation (box). Prominent spots were characterized with MALDI-TOF to facilitate orientation on 2D-PAGE from *D. discoideum* cells. (C) The boxed areas from A and B are magnified to highlight the protein spot that is absent in *dst1* null cells. It was subsequently identified as DDB0233884 an ADF/Cofilin protein of *D. discoideum*.

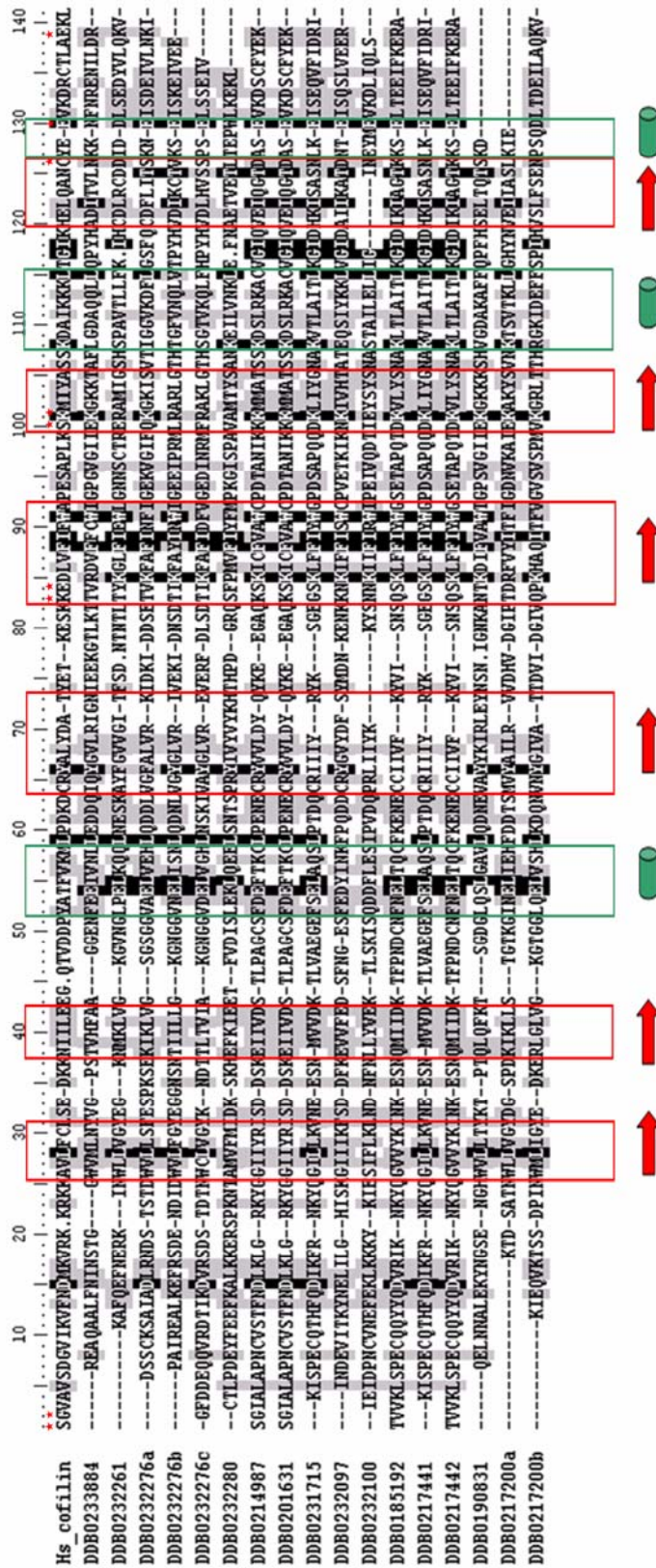


Figure 22. Multiple alignment of DDB0233884 with ADF/cofilins from *D. discoideum*. DDB0233884 misses residues (red stars) which have been reported to be important for actin binding in *S. cerevisiae* ADF/Cofilin (Ojala et al., 2001) and are present in Hs\_cofilin (CAA64685). Predicted secondary structure elements are shown in red and green.

As no direct interactors for DstA were found in the different pull-down approaches a proteomics approach was chosen to unveil parts of the DstA signaling network. Therefore changes in the proteome of *dst1* null compared to wild type cells were investigated using 2D-PAGE (Figure 21 A and B). MALDI-TOF analysis identified several prominent spots as *D. discoideum* proteins present in both the wild type and *dst1* null (Figure 21 A and B). Interestingly, we could observe differences in the proteome of *dst1* when compared to the wild type. Our main observation was a missing protein spot at around 20 kDa size in the proteome of *dst1* null (Figure 21 C). MALDI-TOF identified this spot as DDB0233884 a protein of the ADF/Cofilin family in *D. discoideum*. The spot pattern suggests that, in wild type cells, DDB0233884 is present in two post-translational modifications that differ in their isoelectric points. In the DstA knockout the more positive charged form disappears, which could suggest that loss of DstA increases the phosphorylation of DDB0233884.

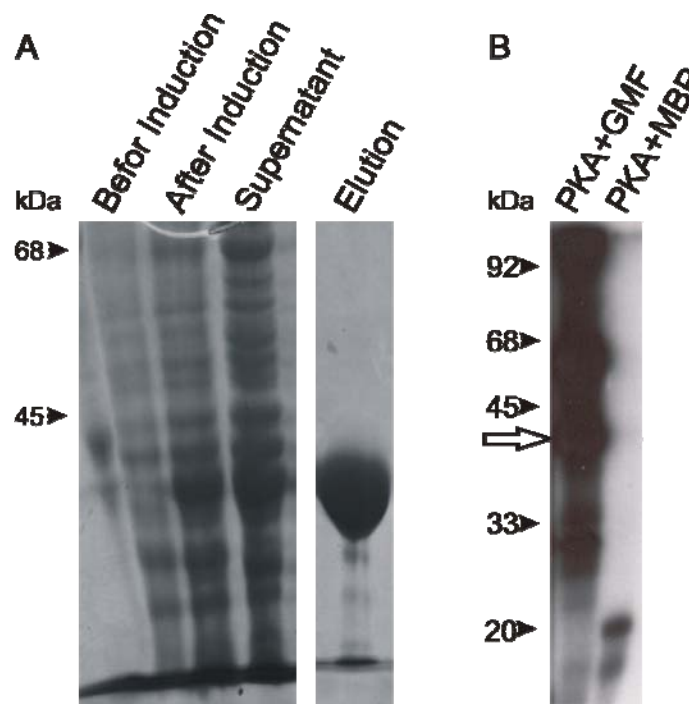


Figure 23. GMF is phosphorylated by PKA *in vitro*.

(A) Purification of the recombinant GST-GMF. Samples were taken after every purification step. Here shown are the samples before induction, 4h after induction, supernatants after cell lysis and the eluted proteins. (B) *In vitro* kinase assays with PKA, and GMF. Arrow indicates the phosphorylated GST-GMF by PKA.

Detailed sequence analysis of the identified ADF/Cofilin revealed that it belongs into a subfamily of ADF/Cofilins, together with the Glia maturation factors (GMFs), which do not contain several conserved residues responsible for actin binding (Maciver and Hussey,

2002). GMFs were firstly identified as growth and differentiation factors acting on neurons as well as glia in the vertebrate brain. It is unlikely that the identified DDB0233884 is a real actin depolymerization factor (ADF) because it does not contain the residues important for actin-binding (Figure 22). Its highest homolog in mammals is the human Drebrin-Like Protein.

The GMF-like protein was expressed as GST-fusion protein to further characterize this potential target of a DstA signaling cascade. The gene was cloned into the expression vector pGEX 6P-1 (Figure 23 A) and after purification the GST-fusion protein was used for pull-down and actin spin down assays. No binding partner could be identified and no binding to G- or F-actin was detected, suggesting that the GMF-like (DDB0233884) really lacks the ADF/cofilin domain.

We used the GST-GMF-like protein as substrate for *in vitro* kinase assays using immunoprecipitated GFP-DstA (not shown). GFP-DstA readily phosphorylated several *in vitro* substrates, such as severin, the domain of severin (DSC112C), casein and myelin basic protein (MyBP), but no phosphorylation of GMF-like was observed. This confirmed the first impression from the 2D-PAGE that GMF-like is not phosphorylated by DstA, but rather DstA somehow induces the dephosphorylation of GMF *in vivo*. GMF-like can be phosphorylated *in vitro* with the kinase PKA (Figure 23 B). PKA is a positive control for a functional kinase. We conclude that the identified GMF-like is not a direct target for DstA but might be a downstream target of the pathways DstA is involved in. A GFP-GMF-like construct was cloned but could not be transformed into *D. discoideum* for localization studies.



### 3.1.2 The Ste20-like kinase Krs2 in *D. discoideum*

#### 3.1.2.1 Sequence analysis of Krs2

We used the amino acid sequence of the SvkA catalytic domain in a proteome wide screen for homologue kinases and were able to identify 13 members of the GCK group of Ste20-like kinases in *D. discoideum*. One of these kinases is Krs2 and was named because of its strong homology to the mammalian kinases Krs1/Mst2 and Krs2/Mst1 (Kinases responsive to stress) (Goldberg et al., 2006). The gene (DDB0216375 or *krsB*) coding for Krs2 is located on the first chromosome of *D. discoideum* and contains three exons coding for the 1106 aa long protein with a molecular mass of ~122 kDa (Figure 24 A). The two introns have a size of 303 bp and 102 bp, respectively. The full length gDNA (3,723 bp) was obtained by PCR using DNA isolated from vegetative cells.

The kinase domain at the N-terminus of Krs2 (Figure 1 A, B) is related to Mst1 and Mst2 from *H. sapiens* the most with 60% sequence identity (Figure 1 C). The closest relative in *D. discoideum* is Krs1 (Arasada et al., 2007) with 58% identity. Following the catalytic domain a coiled-coil domain (aa 334 to 381) is predicted by “Coils” (Lupas et al., 1991) as was shown for other Ste20-like kinases (Arasada et al., 2006; Creasy et al., 1996). The very carboxy terminal of the protein is especially interesting as it displays a unique stretch of four calpain-III domains (Figure 24 A, B) normally part of a membrane anchoring domain in proteases of the calpain family. These calpain-III domains in Krs2, and two similar domains in the protein CplA (Huang et al., 2003), are the only proteins with similarities to calpains in *D. discoideum*. The active site with the cysteine has not yet been identified in CplA and definitive proof of a proteolytic function has not been found in the amoeba (Huang et al., 2003).

The similarity of Krs2 to Mst1 and Mst2 (Figure 1 C) suggests that Krs2 is one of two representatives of the GCK-II subfamily in *D. discoideum*. Even an autophosphorylation site surrounding Thr176, described to be important for activity in other subfamily members (Deng et al., 2003; Stegert et al., 2005) seems to be conserved in Krs2. The GCK-II subfamily in other organisms comprises the before mentioned mammalian Mst1 and Mst2 (Creasy and Chernoff, 1995; Katoh et al., 1995; Schinkmann and Blenis, 1997) and the fly kinase Hippo, which were described as key players in apoptosis.

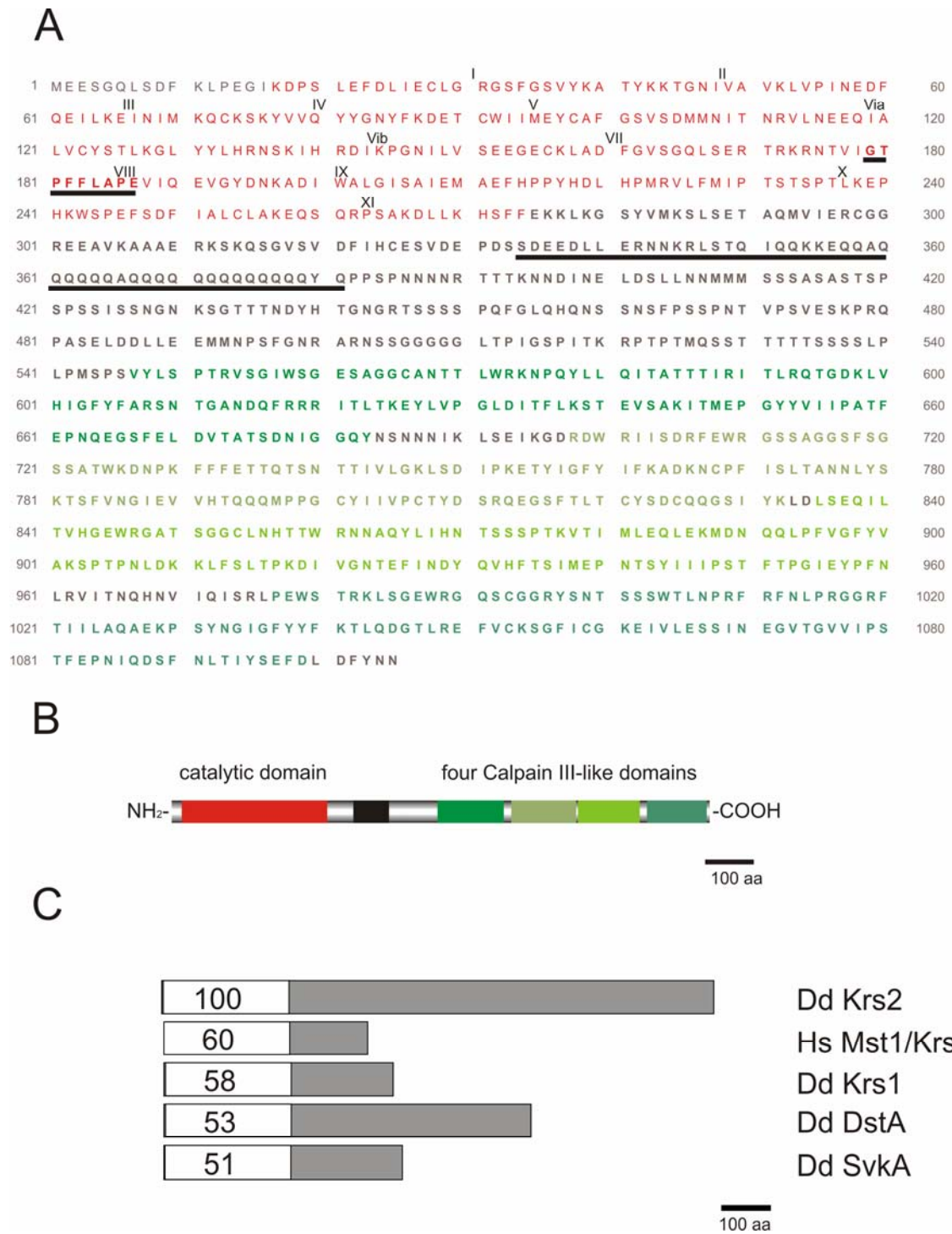


Figure 24. Domain overview of Krs2.

(A) The Krs2 protein consists of the catalytic domain (aa 17-274, red) and the regulatory domain (aa 275-1105) with four calpain-domain III (green). The 12 canonical subdomains of kinase domains are present in Krs2 and labeled with roman letters. The characteristic sequence for Ste20-like kinases is underlined in subdomain VIII. A predicted coiled-coil region is underlined from residues 334 to 381. (B) Schematic representation of Krs2 with the N-terminal catalytic domain (17-274 aa) of Krs2 (red). The regulatory domain (275-1106 aa) of Krs2 contains a linker domain (gray) with a possible coiled-coil domain (black) and four calpain III-like domains (green variants). (C) Schematic alignment of homologous

kinases based on the identity of the kinase domain (white). The sequence identity of the catalytic domains was calculated in relation to Dd Krs2. The used abbreviations: Dd, *Dictyostelium discoideum*; Os, *Oryza sativa*; Hs, *Homo sapiens*. The database access numbers are: Krs2 (DDB0216375); Mst1/Krs2 (CAI95634); Krs1 (DDB0191170); DstA (DDB0167905); SvkA (DDB0191176).

As *D. discoideum* has no caspase mediated programmed cell death pathways (Olie et al., 1998) the intriguing question is why amoeba expresses two kinases of the GCK-II family. Studying Krs2 in *D. discoideum* can help to unveil possible parallel/ secondary signaling pathways that are masked by the predominant role of GCK-II kinases for apoptosis in higher organisms.

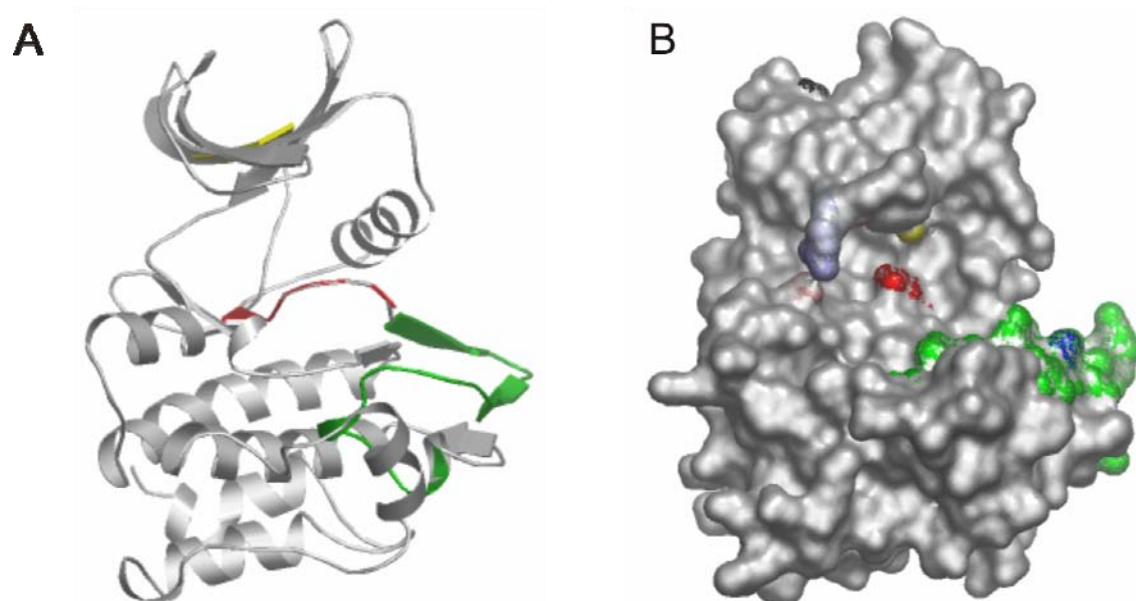


Figure 25. Tertiary model of the kinase domain of Krs2.

The published structure of Mst1 was used as template to predict the 3D fold of the kinase domain of Krs2. (A) Ribbon diagram of the predicted DstA kinase domain. The ATP binding site (yellow), the activation segment (red) and the substrate binding site (green) are conserved in DstA. (B) Surface model of DstA kinase domain. Colors show the same as in (A). The predicted autophosphorylation site at Thr176 (blue) is exposed at the surface of the predicted substrate binding site. An unusual feature of the calculated Krs2 kinase domain is the close proximity of Arg31 (purple) and Asp105 (pink). The opposite charges of these residues may stabilize the kinase fold (made with AstexViewer).

We used SwissModel (Arnold et al., 2006) to model the kinase domain of Krs2 towards the known structure of Mst1. The possible autophosphorylation site Thr176 is calculated to be part of the surface that makes contact to the substrate. Additionally, the 3D model postulates an unusual interaction between Arg31 and Asp105 (Figure 25) that bridges the ATP-binding pocket. These finding would be interesting for further investigations concerning a possible novel way to regulate for kinase regulation.

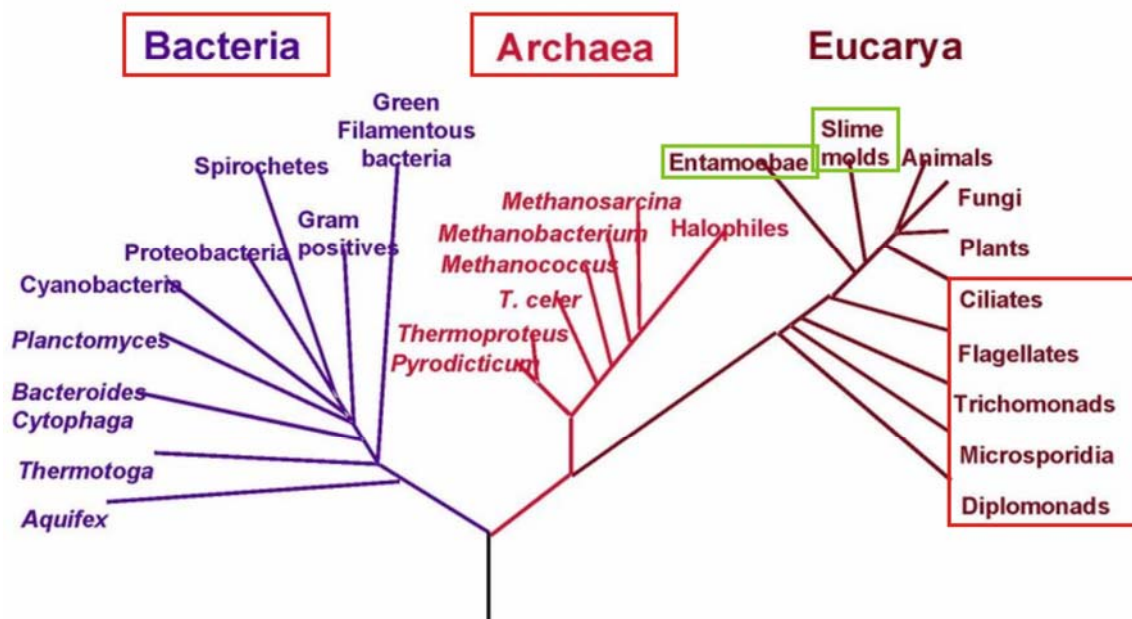


Figure 26. Phylogenetic tree for calpain cystein proteases and calpain III-like domains. Red boxes indicate organisms that completely lack calpain cystein proteases and calpain III-like domains. Green boxes indicate organisms that contain proteins with calpain III-like domain. Animals, Fungi and Plants have functional calpain cystein proteases (Tree adapted and modified from <http://darwin.nmsu.edu>).

Krs2 contains four calpain III-like domains at the C-terminus. These domains were described as possible interactors of lipids and cytoskeleton components. It has been reported that interaction between microtubules and Calpain 6 is mediated by domain III (Tonami et al., 2007) and PIP<sub>2</sub> binding to m-Calpain is mediated by domain III (Shao et al., 2006). Sequence alignments show that the calpain III-like domains of Krs2 are most similar to calpain-like cysteine proteases in plants, fish, insects, worms and mammals. In a search only in *Entamoeba histolytica* a calpain III-like domain is part of a protein kinase. The first hit in a BLAST for the fourth calpain III-like domain of Krs2 is a flagellar associated protein (XP\_001698317) of *Chlamydomonas reinhardtii*.



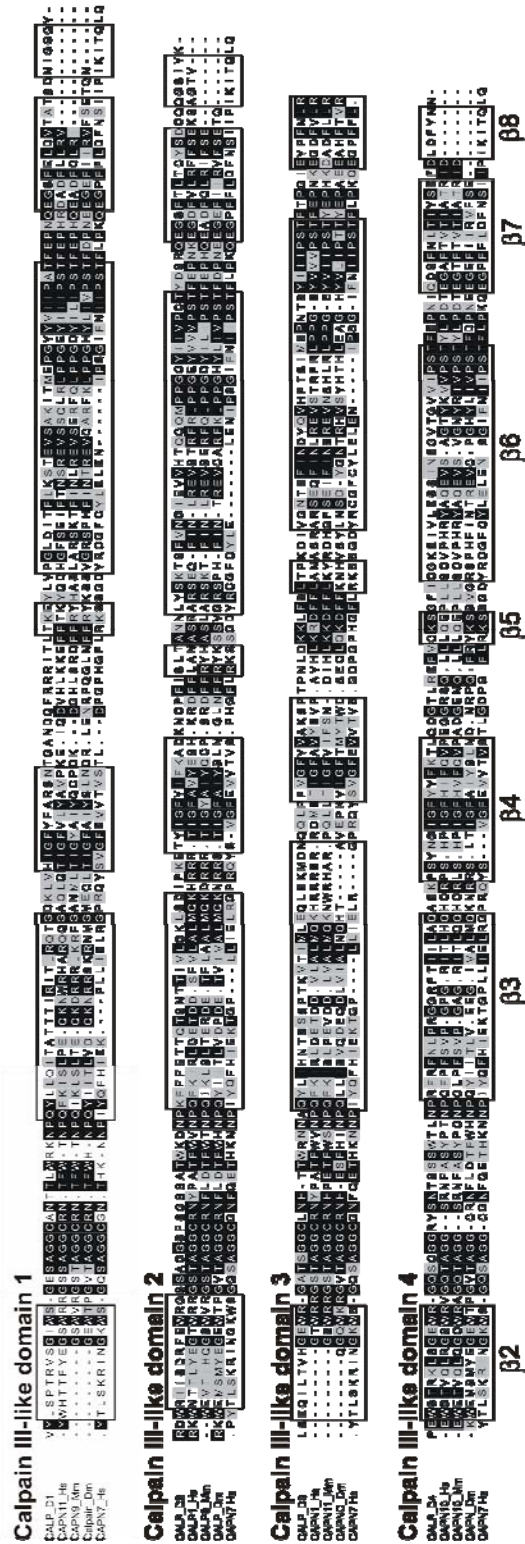


Figure 27. Multiple alignments of the calpain III-like domains of Krs2.

A BLAST search with all four calpain III-like domain from Krs2 was used to retrieve similar protein sequences which were subsequently aligned using BioEdit. Identical and similar residues are shown in black or gray respectively. The distal C2-like domain of human Calpain 7 was included in the alignment as it was used as template for the 3D model. The boxes show the seven beta-sheets formed in the known structure of Calpain 7.

Calpain III-like domains are not conserved in all organisms (Figure 26). Bacteria and archaea do not have calpains and lack calpain III-like domains. Dictyostelid cellular slime molds are the first eucaryota with the presence of calpain III-like domains but lack functional calpain cysteine proteases. Fungi and plants have calpain III-like domains with members like *Arabidopsis thaliana*, *Ricinus communis*, *Oryza sativa* and *Hordeum vulgare* which have predicted calpain systems. Lower animals belong to porifera, annelida and moluscs do not have calpain III-like domains but the rest of the animals have functional calpain protease systems. In mammals functional calpain systems including all subdomains were firstly identified. Calpain-like proteases with domain III in budding yeast were found.

A multiple alignment of several calpain III-like domains (Figure 4) highlights two clusters at the N- and C-termini that are conserved in all species. The calpain III-like domains of Krs2 were more than 25% identical to the other sequences. To get an idea of the 3D structure of the calpain III-like domains of Krs2 the distal C2-like domain of human Calpain7 was used as a template to model three of the four calpain III-like domains from this kinase (Figure 28 A). Because the homology of the third predicted calpain III-like domain to any crystallized structures available is very low this domain was not calculated. The predictions show a conserved pattern of  $\beta$ -sheets for all calpain III-like domains modeled (Figure 28 A-D). Small differences are predicted concerning the size of the acidic loop which is formed between beta sheets 4 and 5 ( $\beta$ 4- $\beta$ 5) and varies in length and amino acid composition. The N and C-termini of the calpain III-fold in all models are facing one side of the 3D structures.

Taken together, Krs2 is a GCK-II in *D. discoideum* with a highly conserved catalytic domain and a unique stretch of four calpain III-like domains in its C-terminus with similarities to calpain III-like domains in other organisms.

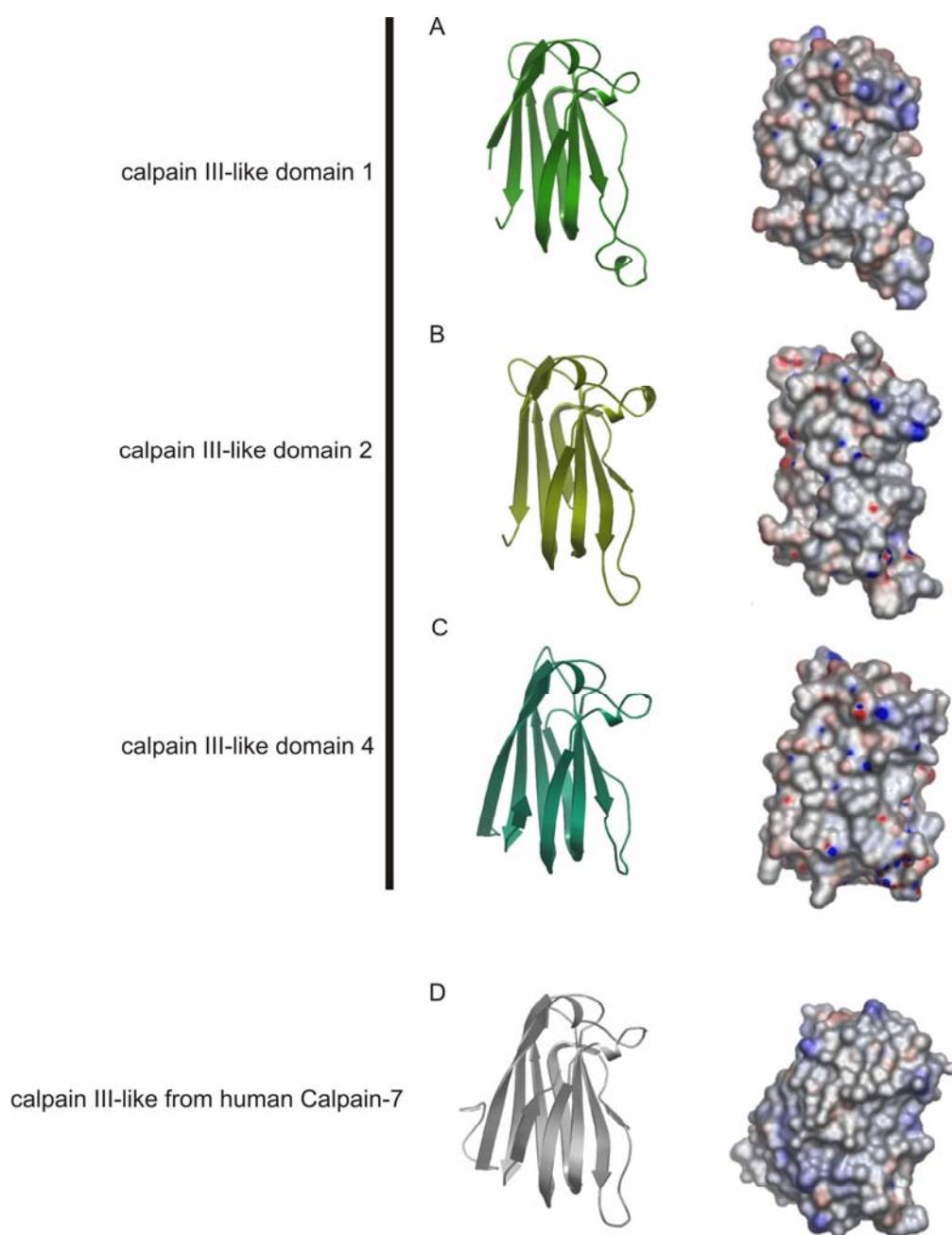


Figure 28. Predicted structures for the calpain III-like domains of Krs2.

The calpain III-like domains 1, 2 and 4 of Krs2 (A-C) were modeled using the crystal structure of distal C2-like domain of human Calpain-7 as template (D). The calpain III-like consists mainly of anti parallel  $\beta$ -sheets. In the 3D structure of the template and in the models the N- and C-termini of the calpain III-like domains are in close proximity on one side of the fold (left side in Figure 5). This might suggest that the calpain III-like domain can be transferred as a complete module into another protein without changing the structure of the target protein. For the arrangement of the four calpain III-like domains of Krs2 this might suggest a clover like arrangement, with the four domains as leaves and the N and C termini forming a node. In this arrangement the surface facing to the right would be accessible for protein-protein interactions. Blue spots show the positively and red the negatively charged surface area (made with AstexViewer).

### 3.1.2.2 Generation of Krs2 antibodies

In order to characterize the expression and localization of Krs2 polyclonal antibodies were generated. The Krs2 regulatory domain has no sequence homology to any other proteins in *D. discoideum* and therefore this region was chosen as antigen to generate antibodies.

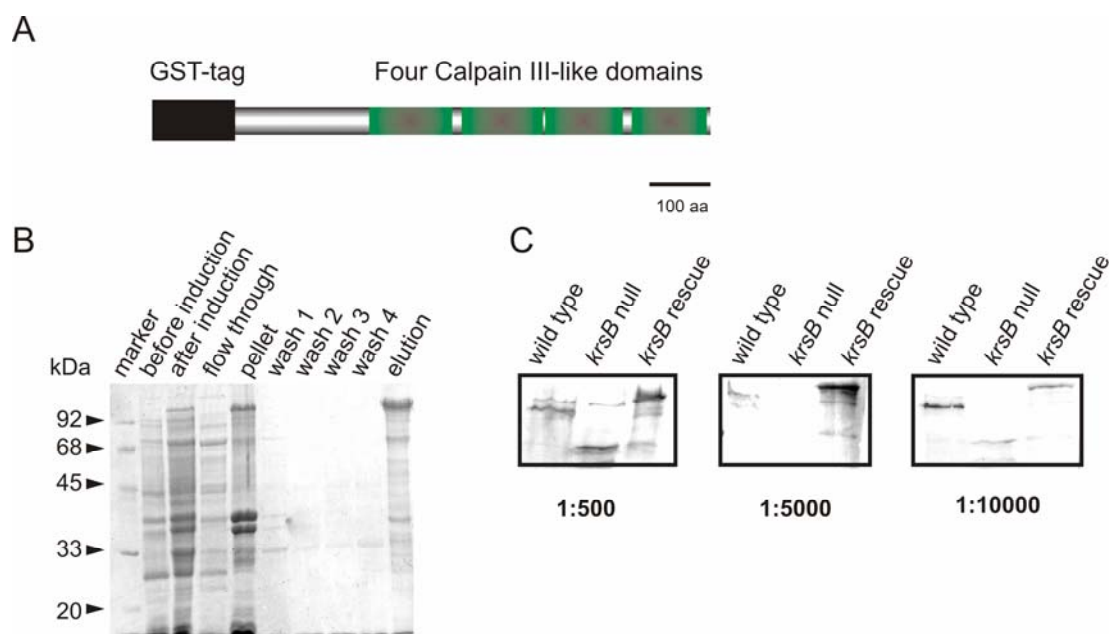


Figure 29. Expression and purification of the GST-Krs2 C-terminal domain.

(A) Schematic view of the purified fragment. The part of the *krsB* gene coding for the regulatory domain (320-1106 aa) was cloned into pGEX 6P-1 expression vector. The construct was expressed recombinant in the *E. coli* strain BL21RIL. (B) Purification of the recombinant protein. Samples were taken after every purification step. The samples before induction, 4h after induction, supernatants and pellet after cell lysis, the flow through, three wash steps and the eluted protein are shown. (C) Western blot analysis with indicated serum dilutions. A serum dilution of 1:10000 was sufficient to recognize the correct bands in the lysates.

The complete C-terminal domain (320-1106 aa) was cloned into a GST expression vector (pGEX 6P-1) (Figure 29A). After expression and purification of the GST tagged Krs2 regulatory domain this antigen was injected into New Zealand white rabbits. After two boosts, the serum of the animals was tested by western blot for the presence of anti-Krs2 antibodies. The analysis showed that antibodies recognize one band with a size corresponding to the endogenous kinase (121.6 kDa) (Figure 29). The dilution 1:10 000 of the serum gave the lowest background on western blots.

### 3.1.2.3 Subcellular localization of Krs2

Even though the generated antibodies were useful for western blot analysis the anti-Krs2 antibodies produced a very high background in immunofluorescence. In order to study the subcellular localization of the kinase GFP tagged Krs2 constructs were generated. The sizes of these constructs expressed in *D. discoideum* were confirmed by western blot with both anti-Krs2 and anti-GFP antibodies (Figure 35 B).

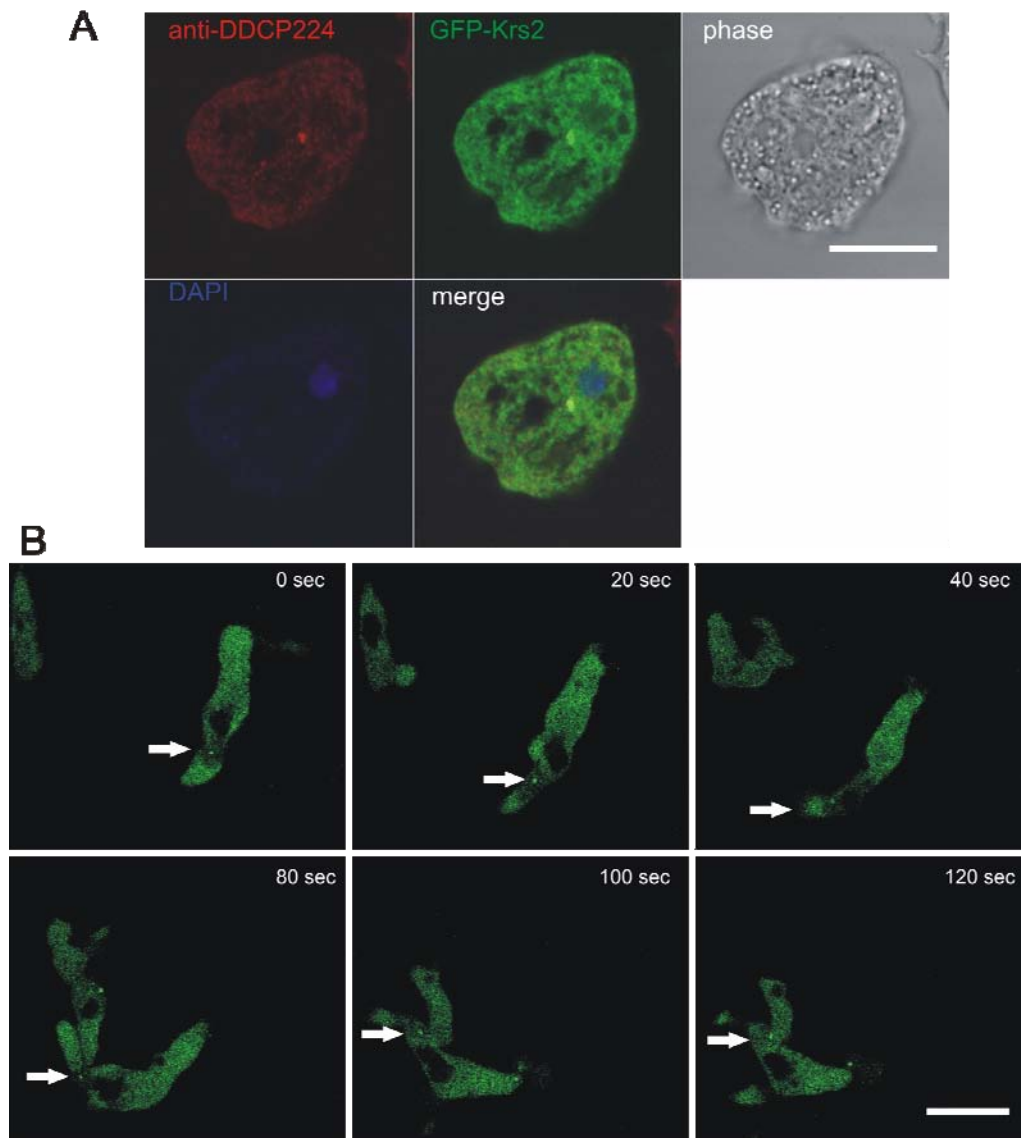


Figure 30. Subcellular localization of GFP-Krs2.

(A) Colocalization of GFP-Krs2 and DDCP224. Wild type cells expressing GFP-Krs2 were fixed and immunostained with the centrosomal marker. Pictures were taken using the confocal microscope (LSM 510, Carl Zeiss). Bar: 1  $\mu$ m. (B) Organization of the MTOC in developed cells. Wild type cells expressing GFP-Krs2 were developed for 6-7 h. Cells were plated and imaged by confocal microscopy. Arrows indicate the MTOC position during cell migration. Bar: 2  $\mu$ m.



The expression of GFP-Krs2 revealed that full length Krs2 is cytosolic and strongly enriched at the centrosome (Figure 30 A). The centrosomal localization was confirmed by co-staining with the centrosomal protein DDCP224 (Graf et al., 2000) (Figure 30 A). Live cell imaging of polarized GFP-Krs2 expressing cells showed that also during chemotaxis the kinase localizes to the centrosome (Figure 30 B).

To map the sequence of the Krs2 protein responsible for the centrosomal localization several truncations of the kinase were expressed. The findings indicate that the localization signal lies within the unique C-terminus of Krs2. In live cells the complete C-terminal portion of Krs2 (Krs2 aREG, 275 to 546) did not show the centrosomal localization when expressed as GFP fusion protein. On the other hand, expression of the four calpain III-like domains showed nearly the same localization as the full length kinase to the centrosome and cytosol, and in addition also entered the nucleus. Removing the very C-terminal calpain III-like domain abolishes the localization to the centrosome, and resulted in a peculiar enrichment of the protein at the nuclear membrane (Figure 31). Therefore the very C-terminal calpain III-like domain is important for the MTOC localization.

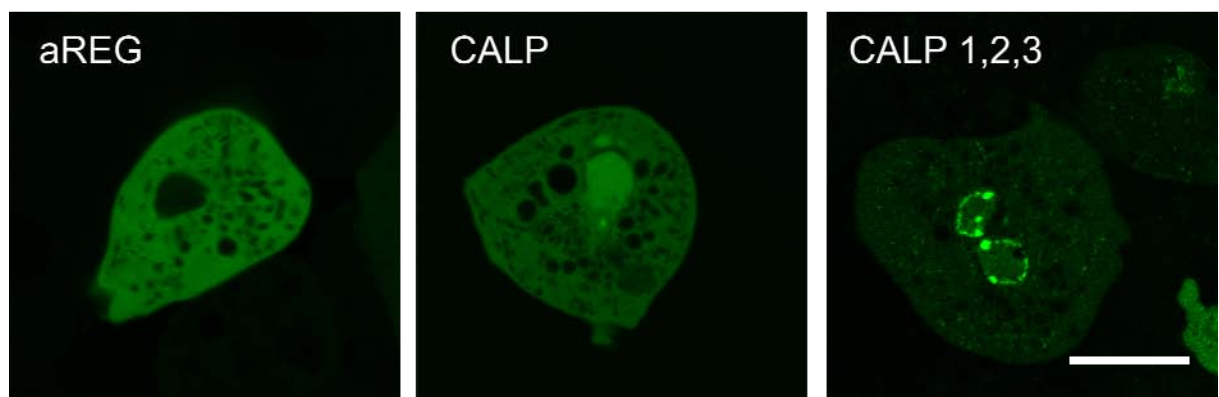


Figure 31. Subcellular localization of Krs2 GFP-tagged truncations in live cells. Wild type cells were transformed with GFP tagged Krs2 truncations and observed with the confocal microscope. GFP-aREG Krs2 did not clearly localize to the centrosome, the four calpain III-like domains (GFP-CALP) stain the centrosome, the nucleus and the cytosol. A construct lacking the last calpain III-like domain (GFP-CALP 1,2,3) showed a localization at the nuclear membrane. Bar: 1  $\mu$ m.

To confirm the role of the four Krs2 calpain III-like domains for the centrosomal localization fixed cells with anti-tubulin antibodies were investigated (Figure 32). Under these conditions the full length (FL), the C-terminal domain (REG) and the four calpain III-like domains all showed a staining at the centrosome. And again removal of the last calpain

III-like domain diminished this centrosomal localization and lead to a peculiar accumulation at the nuclear membrane.

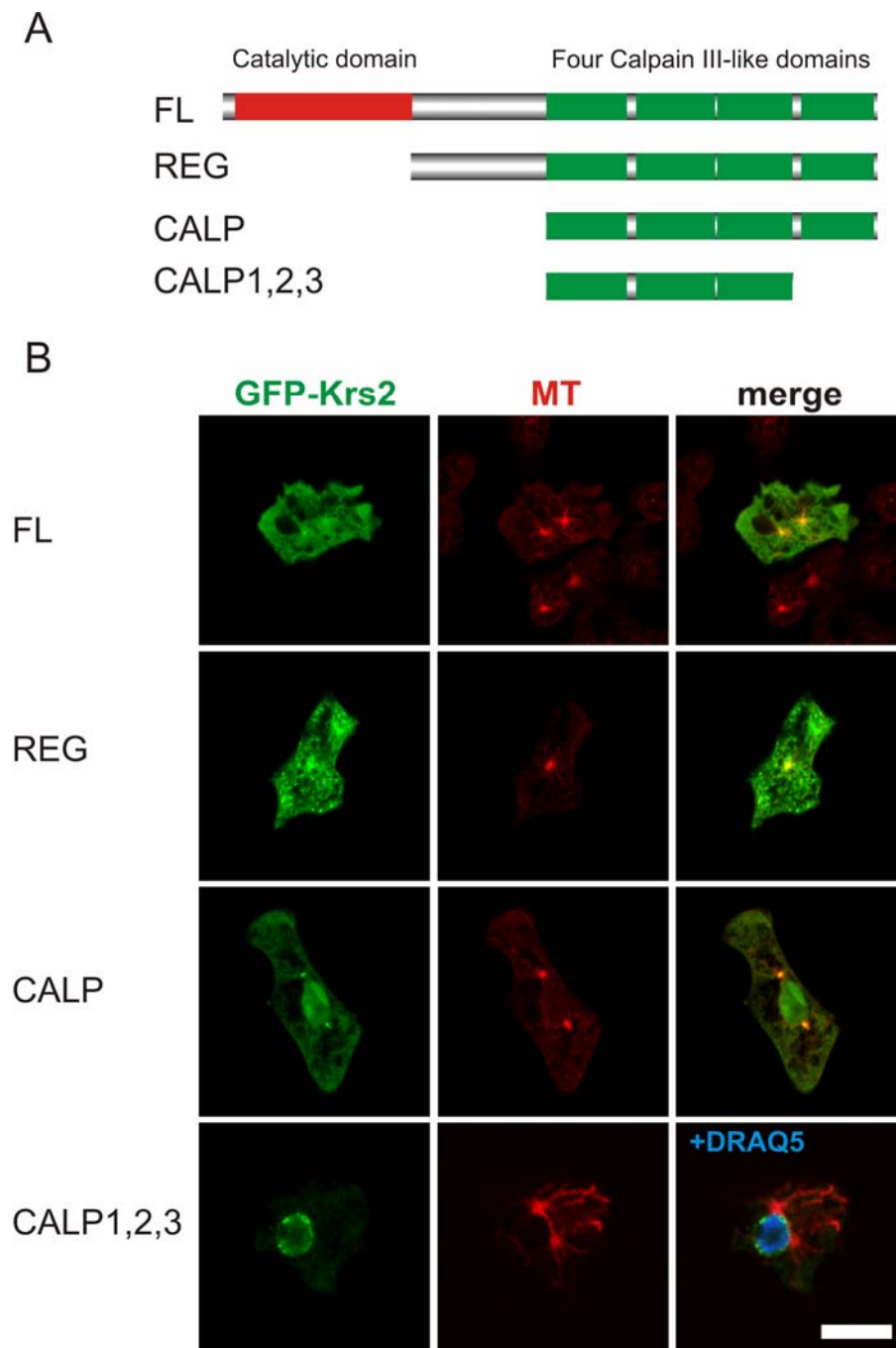


Figure 32. Localization of Krs2 truncations in fixed cells.

The localization of the indicated constructs expressed in wild type cells was acquired by fluorescent microscopy. Shown are cells fixed and immunostained for tubulin. Bar: 2  $\mu$ m.

In order to substantiate the centrosome localization a centrosome preparation with wild type cells was done. The purified centrosome fractions were used for western blot analysis with anti-Krs2 antibodies. The signal in the centrosome fraction confirmed the finding that Krs2

localizes to the centrosome (not shown). Subsequently, GFP-tagged truncations of the Krs2 C-terminus were generated for further localization studies: CALP 1 (547-683aa), CALP 2 (697-832aa), CALP 3 (834-962 aa), CALP 2,3,4 (697-1106 aa), CALP 2,3 (697-962 aa), CALP 3,4 (834-1106 aa) and CALP 1,2 (547-832 aa). These constructs were also cloned into the GST expression vector and can be expressed, purified and used for biochemical assays.

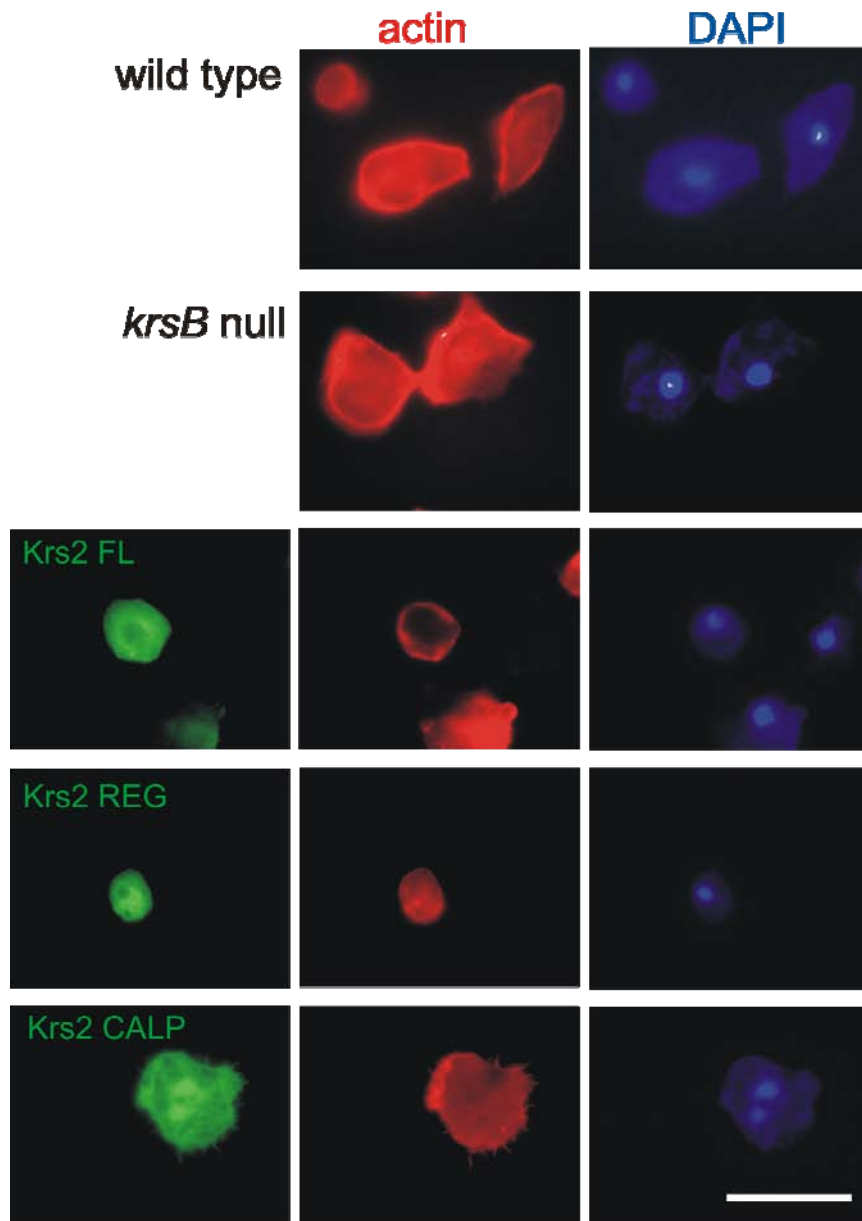


Figure 33. Actin localization in *krsB* mutants.

Cells were fixed with picric acid, stained with TRITC-phalloidin/ DAPI and observed under the confocal microscope. The GFP constructs show the previously described localization patterns. Actin is not affected in any of the cell types that were used here. Bar: 3  $\mu$ m.



As the localization of Krs2 to the centrosome suggest a role for this kinase in the microtubule network, we expressed GFP-tubulin in *krsB* knockout cells (see below). The Krs2 knockout had no aberrant numbers of centrosomes and did not show any obvious abnormalities concerning the microtubule system.

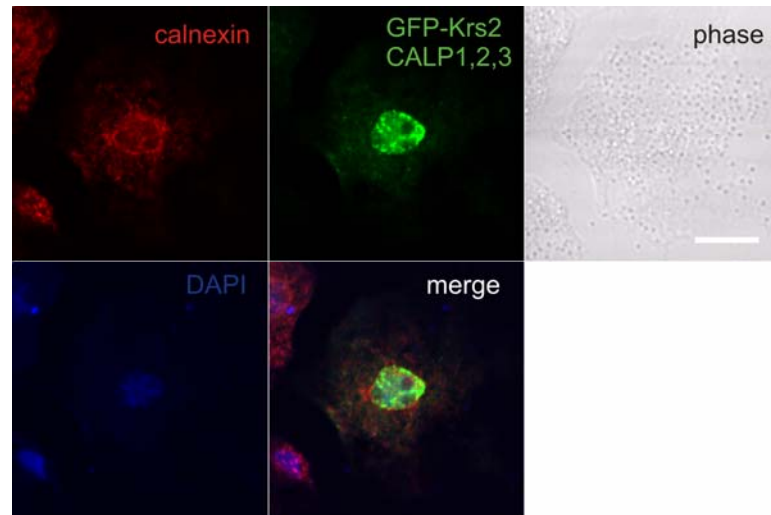


Figure 34. GFP-Krs2 CALP 1,2,3 is not co-localizing with calnexin. Cells were fixed with picric acid, stained with calnexin antibodies/ DAPI and observed under the confocal microscope. Bar: 0.5  $\mu$ m.

In order to visualize the F-actin system in the generated mutant lines we fixed the cells with picric acid and stained the F-actin system with TRITC-phalloidin. There was no difference seen between wild type and *krsB* null cells concerning the actin localization. This was later also shown with the ectopic expression of GFP-actin and GFP-Lime $\Delta$ coil in the knockout. The full length and truncated GFP constructs expressed in the wild type background showed the expected localization in the green signal and did not show any difference in the actin cytoskeleton when compared to the wild type.

The actin localization was not disturbed in any of the generated mutants (Figure 33). In order to investigate the peculiar localization pattern of the GFP-CALP 1,2,3 construct we co-immunostained these cells with the ER marker calnexin. The signal of GFP-CALP 1,2,3 does not overlap with calnexin leading us to conclude that these three calpain III-like domains of Krs2 are not localized at the ER, but instead accumulated at the nuclear membrane (Figure 34). However, as the full length protein did not show this localization, we conclude that it is an unusual overexpression artifact of the three Krs2 calpain III-like domains.

### 3.1.2.4 Isolation of *krsB* knockouts

To learn more about the *in vivo* function of Krs2, we generated *krsB* null mutants. The *krsB* gene was disrupted by introducing a blasticidin resistance cassette that terminates translation between subdomains IX and XI of the kinase domain (Figure 35 A).

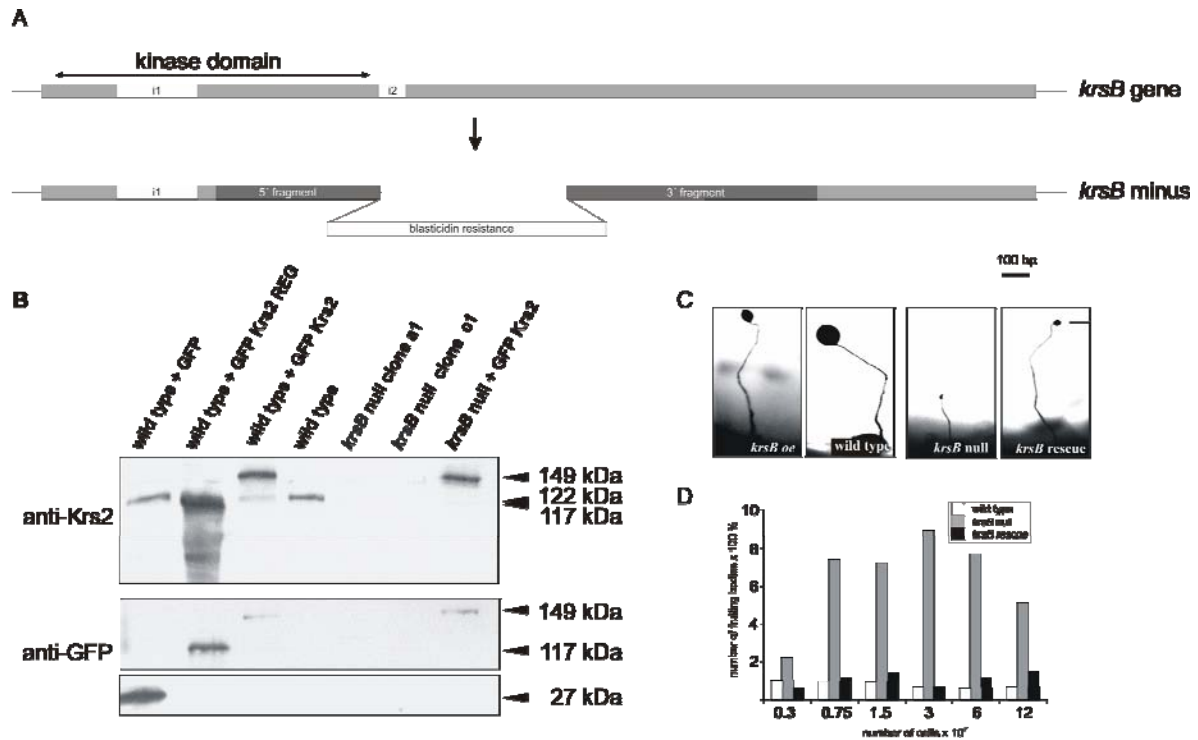


Figure 35. *KrsB* knockout generation.

(A) Scheme depicting the disruption of the *krsB* gene. Two fragments of the kinase were amplified by PCR from genomic DNA and cloned flanking a blasticidin resistance cassette. Homologous recombination led to *krsB*<sup>minus</sup> cells. (B) Blasticidin resistant clones were tested for knockout events by western blot and PCR (not shown). The western blot also shows the expression of GFP-Krs2 constructs in the wild type and *krsB* null background. The endogenous kinase is 122 kDa and the GFP-Krs2 REG construct 117kDa (see arrows). (C) Typical fruiting bodies obtained after three days on phosphate agar of wild type, and rescue and knockout cells. Bar: 6 mm. (D) The number of fruiting bodies and spores per area was counted for different cell densities.

Transformants, resistant to blasticidin, were screened for successful recombination events by PCR (not shown) and confirmed by western blots (Figure 35 B). Two independent knockout clones were isolated. The initial characterization of the *krsB* null cells showed that growth in axenic cultures and on *K. aerogenes* lawn was normal (not shown).

Interestingly, even though the chronology of the development was normal, the resulting fruiting bodies were drastically reduced in size (Figure 35 C), but showed normal

proportion of stalk to spores size. The smaller size was compensated by an increased number of fruiting bodies per area (Figure 35 D). This indicates that Krs2 somehow influences the development of *D. discoideum*.

### 3.1.2.5 Characterization of the *krsB* null phenotype

The most intriguing phenotype observed during the initial characterization of the *krsB* null cells was the drastically reduced size of the fruiting body (Figure 35C). Concomitant, *krsB* null cells developed 10-times more fruiting bodies per area, independent of cell density (Figure 35 D). This phenotype was rescued with the expression of GFP-Krs2 in the *krsB* null cells.

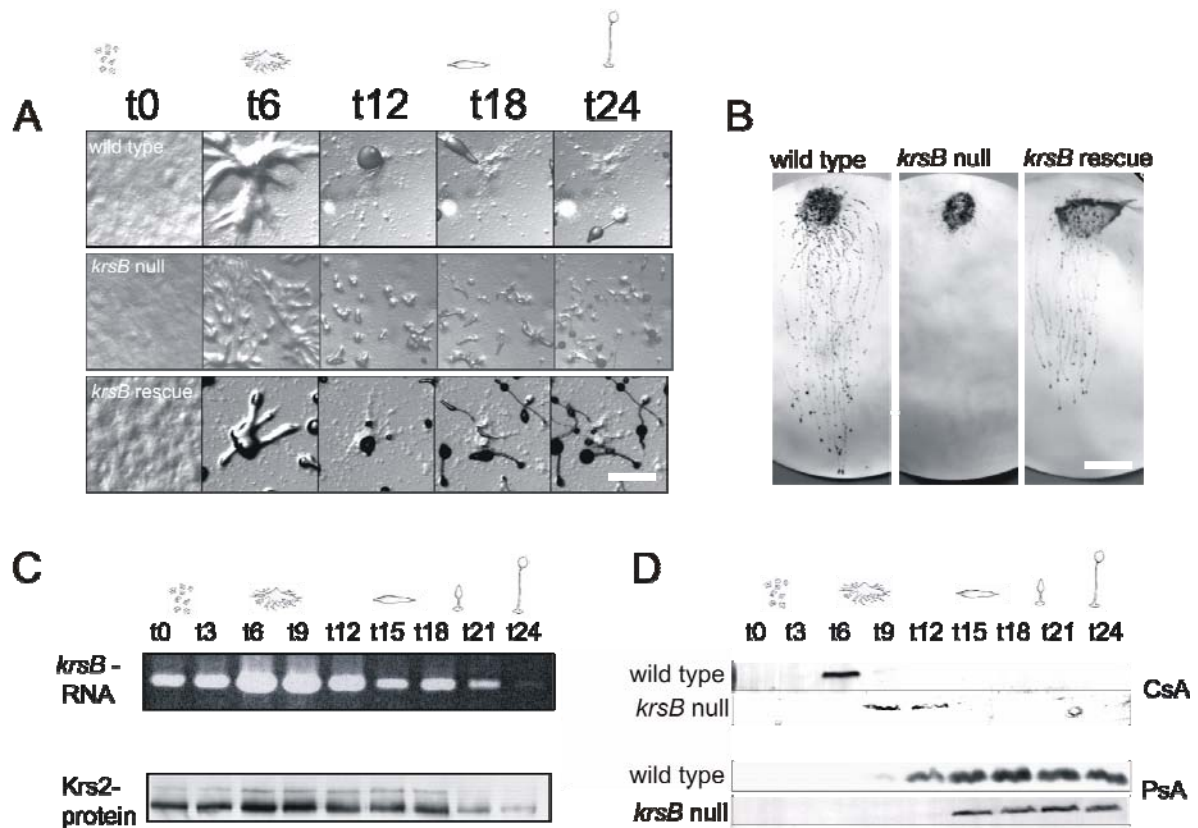
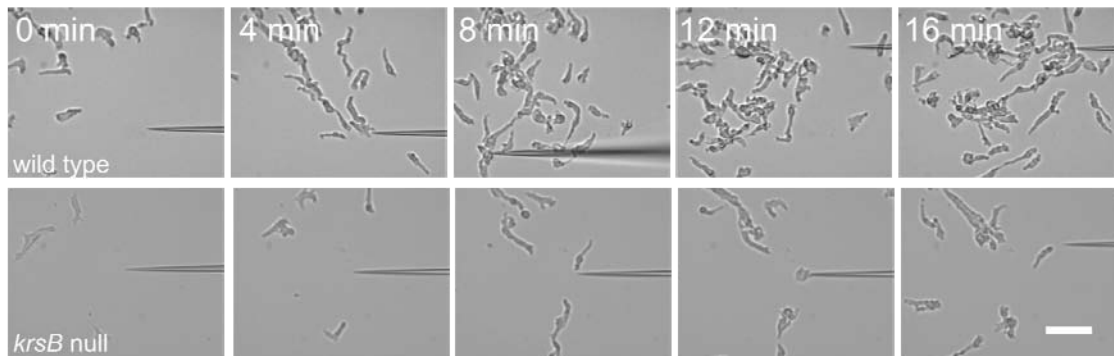


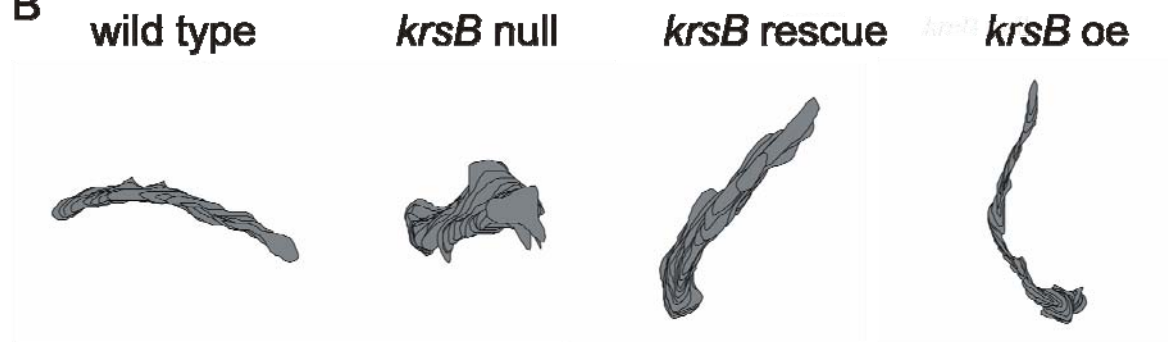
Figure 36. *KrsB* null development.

(A) Development of starved cells on phosphate agar show the normal chronology for the *krsB* null cells, but resulting in smaller fruiting bodies. Bar: 5 mm. (B) Phototaxis of *D. discoideum* slugs on water agar towards a light source, visualized with Amido black. Bar: 2 cm. (C) Expression of Krs2 during the developmental cycle. RT-PCR and western blot with antibodies against Krs2 show equal expression throughout the 24 hours of wild type development. (D) Western blot for the expression of CsA and PsA during the development of *krsB* null cells.

A



B



C

	Speed [ $\mu\text{m}/\text{min}$ ]	Persistence [ $\mu\text{m}/\text{min-deg}$ ]
wild type	$14,3 \pm 6,1$	$5,9 \pm 3,4$
<i>krsB</i> null	$6,1 \pm 0,6$	$2,2 \pm 0,3$
<i>krsB</i> rescue	$11,4 \pm 4,1$	$4,8 \pm 2,3$
<i>krsB</i> oe	$13,8 \pm 0,4$	$6,9 \pm 0,8$

D

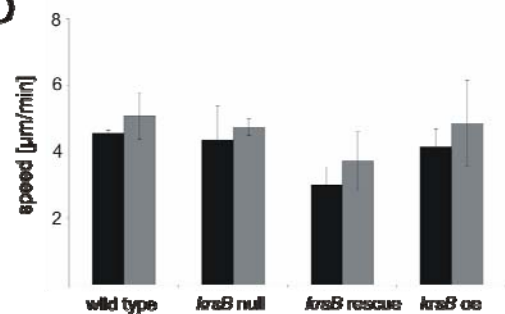


Figure 37. *KrsB* null cells have a chemotaxis defect.

(A) Aggregation competent cells were positioned near a capillary that was filled with  $10^{-4}$  M of the chemoattractant cAMP and cell motility measured for 100 frames with 20 sec time intervals (B) Single cell movement during chemotaxis. Representative cells from wild type, *krsB* null, rescue and the GFP-Krs2 overexpressor are shown. Bar: 2 mm. (C) The speed of chemotacting cells. The numbers average the data from about 30 cells each and indicate that a knockout of *krsB* leads to slower and less polarized cell movement. Cell movement was recorded at 3 frames per minute and analyzed using the DIAS software program (Soll Tech., USA). (D) Vegetative cells were plated on a glass bottom petri dish in medium (black) or phosphate buffer (gray) and cell motility measured for 100 frames with 20 sec time intervals. The speed from about 30 cells was analyzed using DIAS.

During the development, *krsB* null cells began to stream normally towards an aggregation centre, but before the normal size of these aggregates was reached, the streams fell apart and formed small aggregates that developed into tiny fruiting bodies (Figure 36 A). As multicellular intermediates of the developmental cycle, *D. discoideum* forms slugs that can

move towards light before the cells continue to culminate into fruiting bodies. The *krsB* knockout was able to form these slugs (not shown), but they did not move towards the light source, a phenotype which is rescued by the introduction of the GFP-Krs2 into the knockout (Figure 36 B).

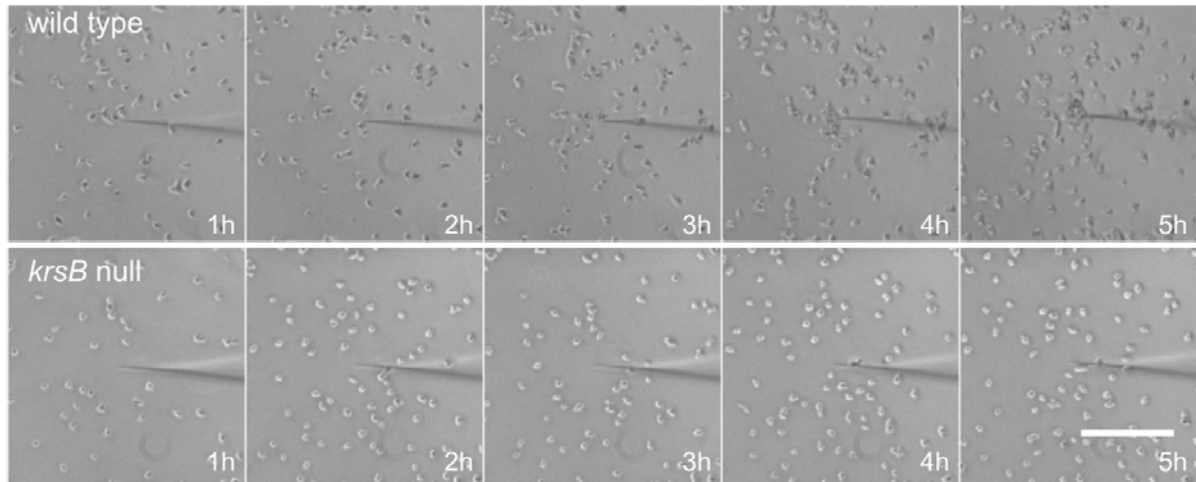


Figure 38. Chemotaxis of vegetative wild type vs *krsB* null cells with folic acid. Bar: 3 mm.

Non quantitative RT-PCR showed that *krsB* mRNA was present during all stages of *D. discoideum* development (Figure 36 C). Western blot analysis of wild type showed a small increase in Krs2 expression when streams form (t6 - t9) and at the slug stage (t18) (Figure 36 C). Even though the development of *krsB* minus cells is normal the developmental marker contact site A (CsA) and prespore A (PsA) were expressed slightly later than usual (Figure 36 D).

The formation of streams and aggregates in *D. discoideum* relies on chemotaxis towards cAMP. As observed with time-lapse movies of aggregating *krsB* null cells, the cAMP waves formed in mutant streams have a longer frequency than wild type cells (not shown). To characterize the chemotactic response of *krsB* null cells, the cells were starved for 5 – 6 hours and then presented with a micropipette releasing cAMP. Time lapse movies revealed that while wild type cells covered several cell lengths towards the micropipette, the *krsB* null cells moved extremely slow and without consistent direction (Figure 37 A and B). Cell tracking shows that during chemotaxis *krsB* null cells only reach half the speed and persistence as the wild type (Figure 37 C). The phenotype is reversed in the rescue strain and the overexpression of Krs2 in wild type does not have any effect on the chemotactic

behavior of the cells. This is a specific defect of polarized chemotacting cells, because vegetative cells showed a normal random motility (Figure 37 D).

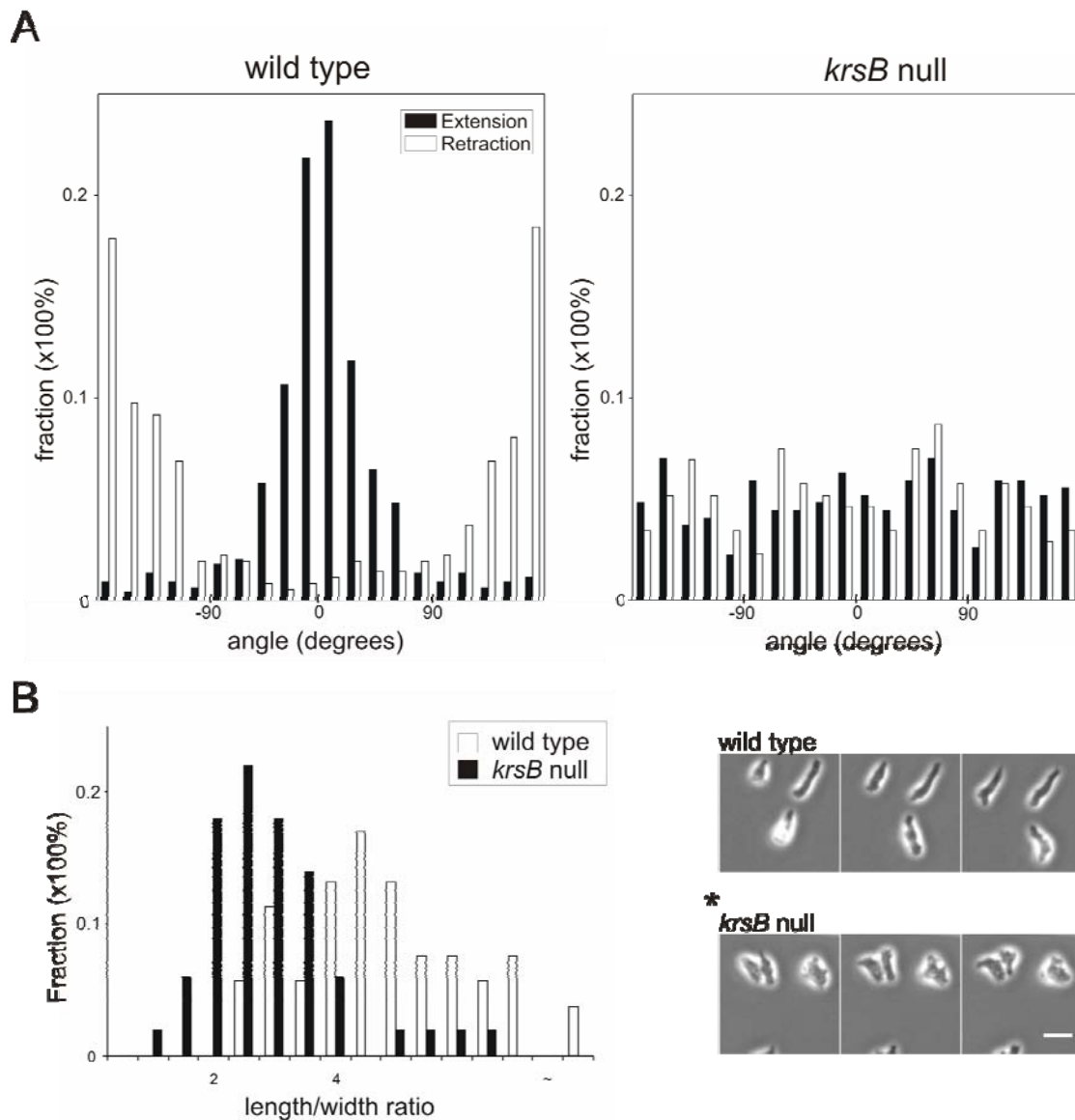


Figure 39. Chemotactic responses and induced cell polarity.

(A) Developed wild type and *krsB* null cells migrating to a micropipette releasing 10  $\mu$ M cAMP were recorded by time lapse microscopy. The distribution of tip angles for extending (black) and retracting (white) pseudopods relative to the direction of cAMP gradient was measured. 0° points refer directly to the microcapillary. The data represent 40 wild type and 20 *krsB* null cells. (B) Histogram of cell length/width ratio distribution of chemotacting cells. The distance from the leading edge, as defined by the front of protrusions, to the trailing tail was taken as cell length. The width was measured at the leading edge. The length/ width ratio from wild type and *krsB* null cells were grouped to ranges of 0.5 intervals and the frequency of every ratio range is plotted as a histogram. Representative phase contrast images are shown on the right. The star indicates the position of the capillary for both. Bar: 2  $\mu$ m.



In order to analyze the chemotaxis defect, vegetative wild type and *krsB* null cells were tested for their migration pattern towards the chemoattractant folic acid. Folic acid chemotaxis revealed a defect of the Krs2 mutant, which migrated much slower towards the capillary (Figure 38). The migration defect we see during chemotaxis in *krsB* null cells is not dependent on the receptor but affects the molecular signaling pathways downstream of the receptors responsible for *D. discoideum* chemotaxis.

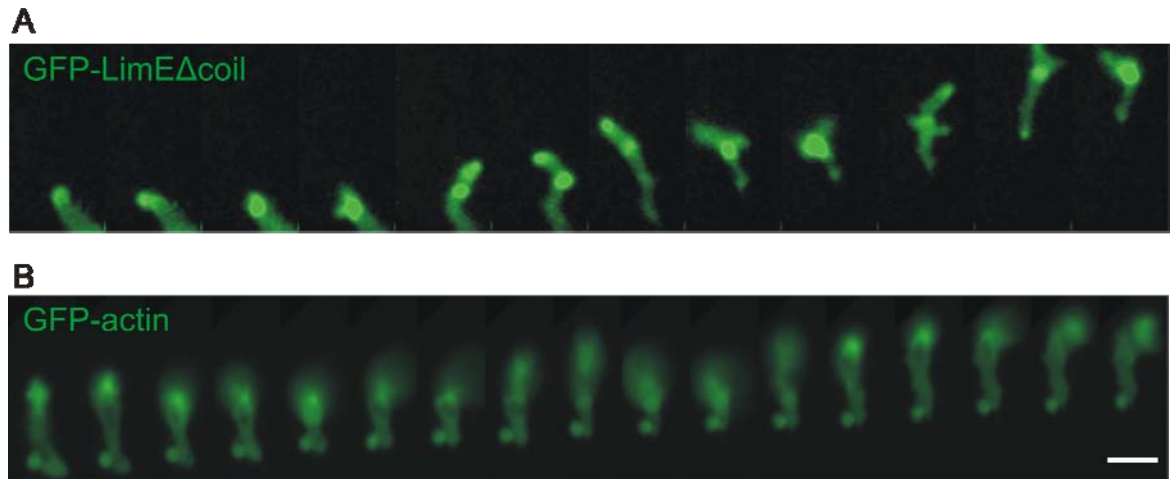


Figure 40. GFP-LimE $\Delta$ coil and GFP-actin expressed in *krsB* null cells during chemotaxis. The montage shows an average *krsB* null cell expressing (A) GFP-LimE $\Delta$ coil and (B) GFP-actin. The cAMP filled microcapillary is positioned at the upper right corner of each frame. The *krsB* mutant cells have a defect in making directional protrusions. Bar: 2  $\mu$ m.

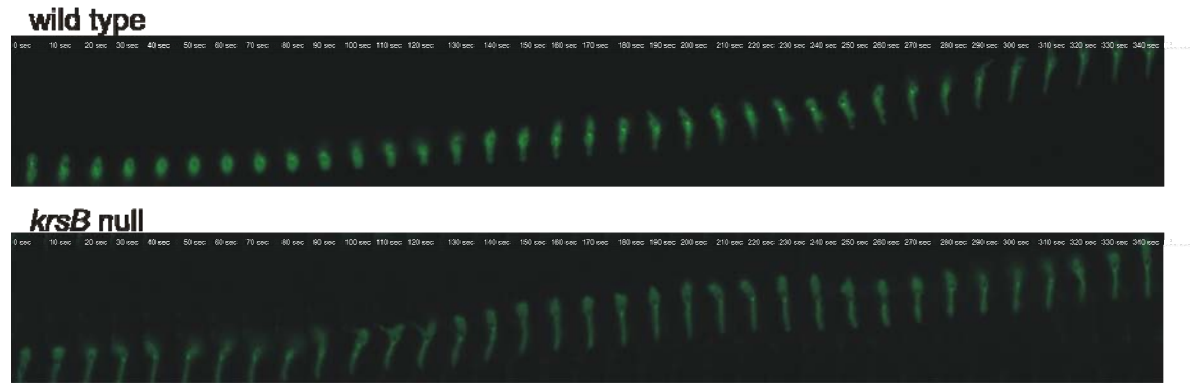
To understand this problem of *krsB* null cells, the formation of directional protrusions during chemotaxis was investigated. The directionality of newly formed pseudopodial extensions in relation to the chemotaxis gradient was measured. By comparing the cell outlines between adjacent frames of time lapse movies, we were able to detect both pseudopod extensions and retractions. These were plotted in relation to the angle of the micropipette. In contrast to the wild type cells that preferentially generate membrane extensions towards the cAMP source ( $0^\circ$ ) and made retractions at the rear of the cell ( $180^\circ$ ), the extensions and retractions in *krsB* null cells appeared completely random (Figure 39 A).

*KrsB* null cells are not well differentiated, as indicated by the rather round appearance (Figure 39 B). This is in contrast to the elongated and polarized shape of wild type cells expressing GFP-Krs2 under the control of the strong actin15 promoter (Figure 37 B). This was quantified by measuring the length-to-width ratios of wild type and mutant cells (Figure 39 B). The average length-to-width ratio in developed wild type cells was 4.9 ( $n =$

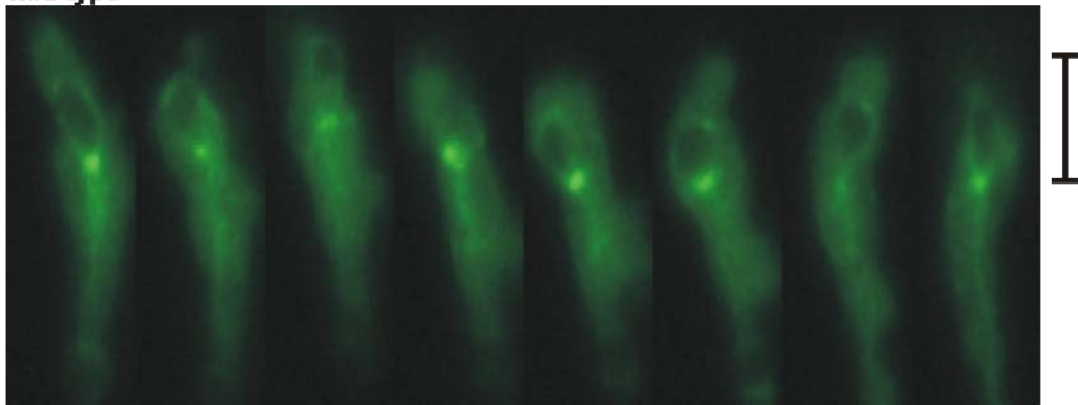


53), while the *krsB* null cells were more rounded and had a mean length to width ratio of 3.2 (n = 50).

**A**



**B wild type**



**krsB null**

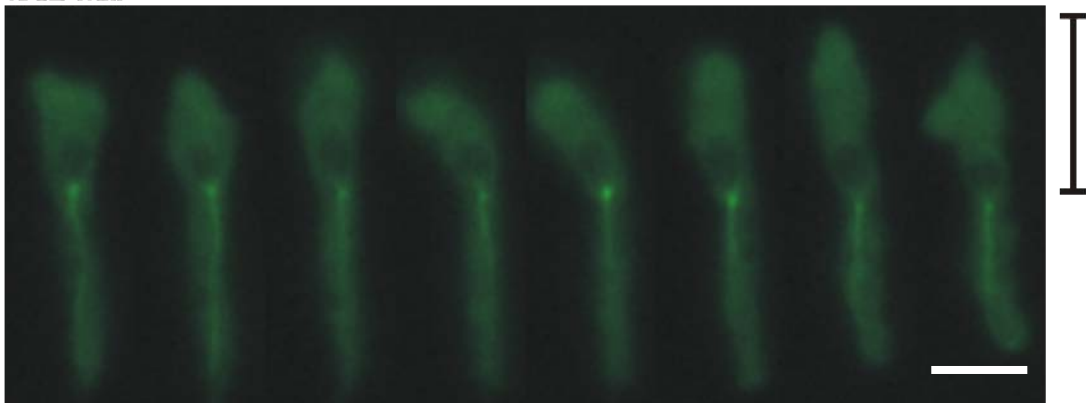


Figure 41. Chemotaxis of *krsB* null cells expressing GFP-tubulin.

(A) Single wild type and *krsB* null cell expressing GFP-tubulin during chemotaxis towards the cAMP gradient. Swapping protrusions are formed in the *krsB* null cell. (B) The distance from the MTOC to the front of the cell is longer in *krsB* null cells then the wild type. Bar: 2  $\mu$ m.

Time lapse microscopy of elongated *krsB* null cells expressing GFP-LimE $\Delta$ coil, GFP-actin and GFP-tubulin migrating towards a cAMP filled capillary confirmed the defect in chemotaxis. The cells did not only move slower towards the gradient but formed additional protrusions in other directions than the capillary (Figure 40 A, B). In addition, the leading front of these cells was often floating above the ground to any direction (Figure 40 B).

The expression of GFP-Krs2 constructs showed a localization of Krs2 to the centrosome, to investigate the tubulin system in developing cells, elongated *krsB* null cells expressing GFP-tubulin were observed during chemotaxis in a cAMP gradient (Figure 41 A). The MTOC in most of the cells was located behind the nucleus in the direction of migration, as observed for wild type cells. Interestingly, the nucleus of *krsB* null mutants is slightly more distant from the leading front than in the wild type cells (Figure 41 B). It seems that Krs2 is involved in the stabilization of protrusions at the leading edge. The role of the distant leading front to centrosome has to be further investigated.

### 3.1.2.6 Interactors for Krs2

The good expression of the C-terminal part of Krs2 prompted us to use this construct in a GST-pulldown approach to identify binding partners for this kinase. Unfortunately, after incubation of the GST tagged protein with total *D. discoideum* lysates, no interaction partner could be detected on SDS-PAGE.

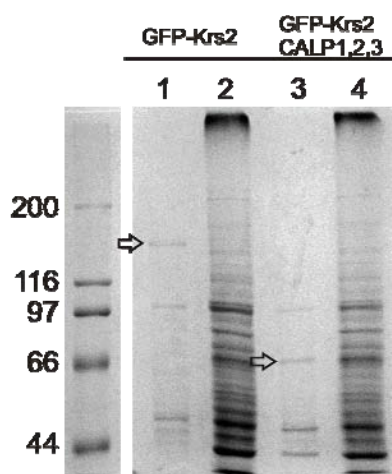


Figure 42. Nanotrap of Krs2 GFP constructs.

GFP-Krs2 full length (149 kDa) and GFP-Calp 1,2,3 (73 kDa) were immuno-precipitated (Lane 1 and 3) (arrows) with the Nanotrap matrix. The immunoprecipitated proteins were cut from the gel and identified using MALDI-TOF. Lanes 2 and 4 show the lysates used for this experiments.

Therefore, we used our GFP expression constructs (see below), in a "Nanotrap" immunoprecipitation approach. We were successful to purify the GFP-Krs2 full length kinase and the GFP-Calp1, 2, 3 domain (547-960 aa) from *D. discoideum*. But unfortunately again except for some unspecific proteins, always binding to the matrix, no interaction partners could be pulled down (Figure 42). These results led us to the conclusion that Krs2, as most other kinases, is involved in a "kiss and run" process for phosphorylation and does not make a stable binding with a substrate in the conditions used in our assays. In addition, as we could not detect the endogenous Krs2 in the GFP-Krs2 full length immunoprecipitation we conclude that Krs2 is not able to form a dimer neither with its predicted coiled-coil region nor with the calpain III-like domains.

## 3.2 Actin isoforms and actin modifications in *D. discoideum*

### 3.2.1 Actin isoforms in *D. discoideum*

To investigate the expression of actin isoforms (Figure 43 A) in *D. discoideum* 2D-PAGE was performed with wild type lysates. The pattern we observed on a representative 2D-PAGE after Coomassie staining is shown in Figure 43 B. Indicated spots were cut and used for MALDI/TOF analysis.

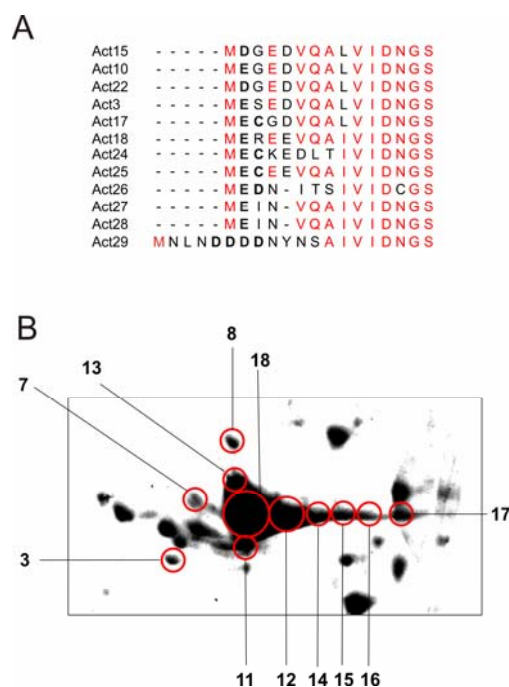


Figure 43. Isoactins in *Dictyostelium*.

(A) Alignment of the N-termini of *D. discoideum* actins. Main differences (bold) within the actin isoforms of *Dictyostelium* are found in the second/third amino acid position. Identical residues are shown in red. (B) 2D-PAGE of the *Dictyostelium* isoactins. The distribution of isoactins on the 2D-gel indicates a multitude of possible post-translational modifications. MALDI/TOF identified the circled spots as actin (see Table 1).

The main part of actin in *D. discoideum* consists of act15 (spot 18) and is coded by 17 identical actin genes. Interestingly, a subpopulation of act15 was found in most of the other spots which might be an indication for post-translational modification of this isoform. Several additional actin isoforms could be identified for example Act3 was detected in most exerted spots, an indication that this isoform is post-translationally modified. Act10 and Act23 of *D. discoideum* in spot 7 and 8 showed a high mobility shift which indicated a change in mass and pI, very likely generated by post-translational modifications.

**Table 4. Actin isoforms and Mascot based prediction for phosphorylation.**

Spot Number	Actin Isoform	Post-translational Modification
3	Act15, Act10	Phosphorylation (Thr 67, Thr78)
7	<b>Act15, Act3, Act10, Act23</b>	<b>Phosphorylation (Thr 67, Thr78)</b>
8	Act15, Act3, Act10, Act23	Phosphorylation (Thr 67, Thr78)
11	<b>Act15, Act3</b>	<b>Phosphorylation (Thr 67, Thr78, Tyr295, Ser 301 or Thr304-305)</b>
12	Act15, Act3	Phosphorylation (Thr 67, Thr78, Ser 301 or Thr304-305)
13	<b>Act15, Act3</b>	<b>Phosphorylation (Thr 67, Thr78, Ser 301 or Thr304-305)</b>
14	Act15, Act3	Phosphorylation (Thr 67, Thr78, Ser 301 or Thr304-305)
15	<b>Act15, Act3</b>	<b>Phosphorylation (Thr 67, Thr78, Ser 301 or Thr304-305)</b>
16	Act15, Act3	Phosphorylation (Thr 67, Thr78)
17	<b>Act3</b>	<b>No phosphorylation detected</b>
18	Act3, Act15	Phosphorylation (Thr78, Thr149 or Thr150, Ser156, Ser161, Thr163, Thr187, Thr195, Ser301, Thr304, Thr305, Thr 319, Ser324 or Thr325, Ser366, Ser369, Tyr70, Tyr280)

Of the peptides analyzed by MALDI/TOF several matched the actin isoforms in Table 4, to investigate if the unmatched peptides might represent peptides with post-translational modifications, we researched the peptide masses of several spots and used Mascot software settings that considered changes of peptide masses by phosphorylation. This analysis summarized in Table 4 would suggest that several of the unmatched peptides might be phosphorylated. To estimate if this *in silico* approach could have any relevance for the *in vivo* situation potential exposed phosphorylation sites were checked at the surface of actin (Figure 44). And indeed, some of the postulated phosphorylation sites should be accessible for kinases.

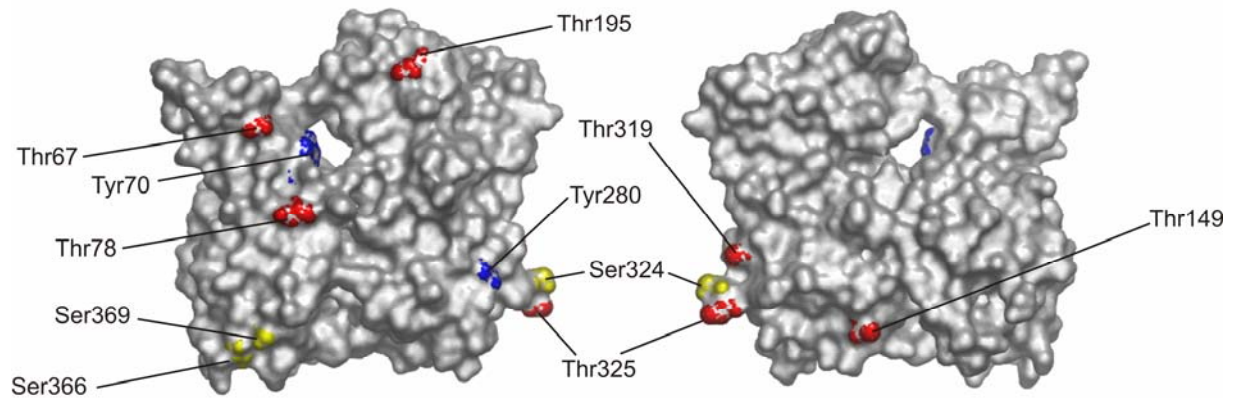


Figure 44. Predicted phosphorylation sites for Act15 of *D. discoideum*.

All possibly phosphorylated residues that were identified with MALDI/TOF are put on a 3D reconstruction of the surface of the actin molecule. Threonine (red), Serine (yellow) and Tyrosine (blue) residues are labelled.

In two of the spots (11 and 16) the N-terminus of act15 was present among the identified peptides. Interestingly, in both cases the assigned peptide would lack the N-terminal methionine. This would be an indication that act15 in *D. discoideum* has an open N-terminus, which would make it accessible for post-translational modifications like acetylation and/or arginylation.

### 3.2.2 The Arg-tRNA transferase (Ate1) in *D. discoideum*

The post-translational modification, arginylation, in *D. discoideum* has not been studied yet. In this part of the work *ate1* null cells were characterized in order to identify the function of Ate1 and to gain insights into a possible role of this enzyme in actin arginylation.

#### 3.2.2.1 Sequence analysis of Ate1

The gene coding for the Arg-tRNA transferase 1 (DDB0238346 or *ate1*) in *D. discoideum* is located on chromosome 1, has no introns, is 1890 bp long and encodes a protein of 629 aa (~74 kDa). Interestingly, the *D. discoideum* Ate1 protein has an unusual insert of 79 amino acids between amino acids 356 and 435 which is not present in Ate1 proteins of other organisms (Figure 47). Re-examining of this region in the genomic sequence published in Dictybase (dictybase.org), could suggest that the computational annotation of the Genome project missed a possible intron.



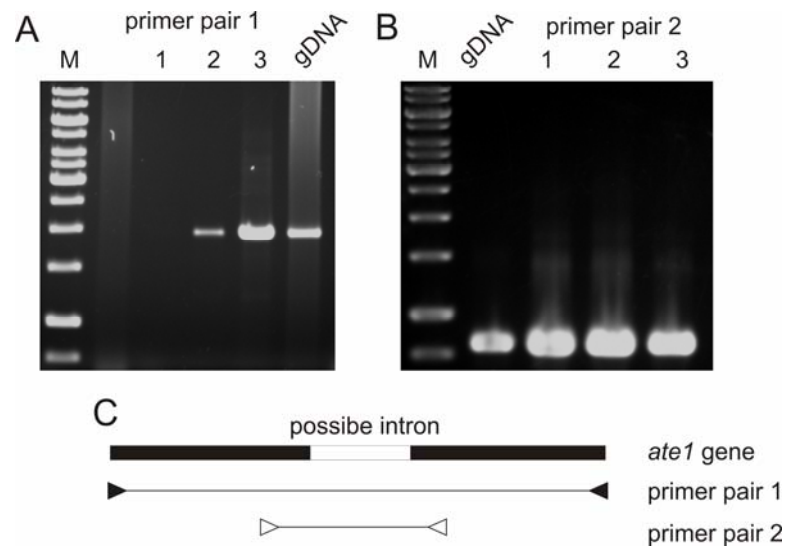


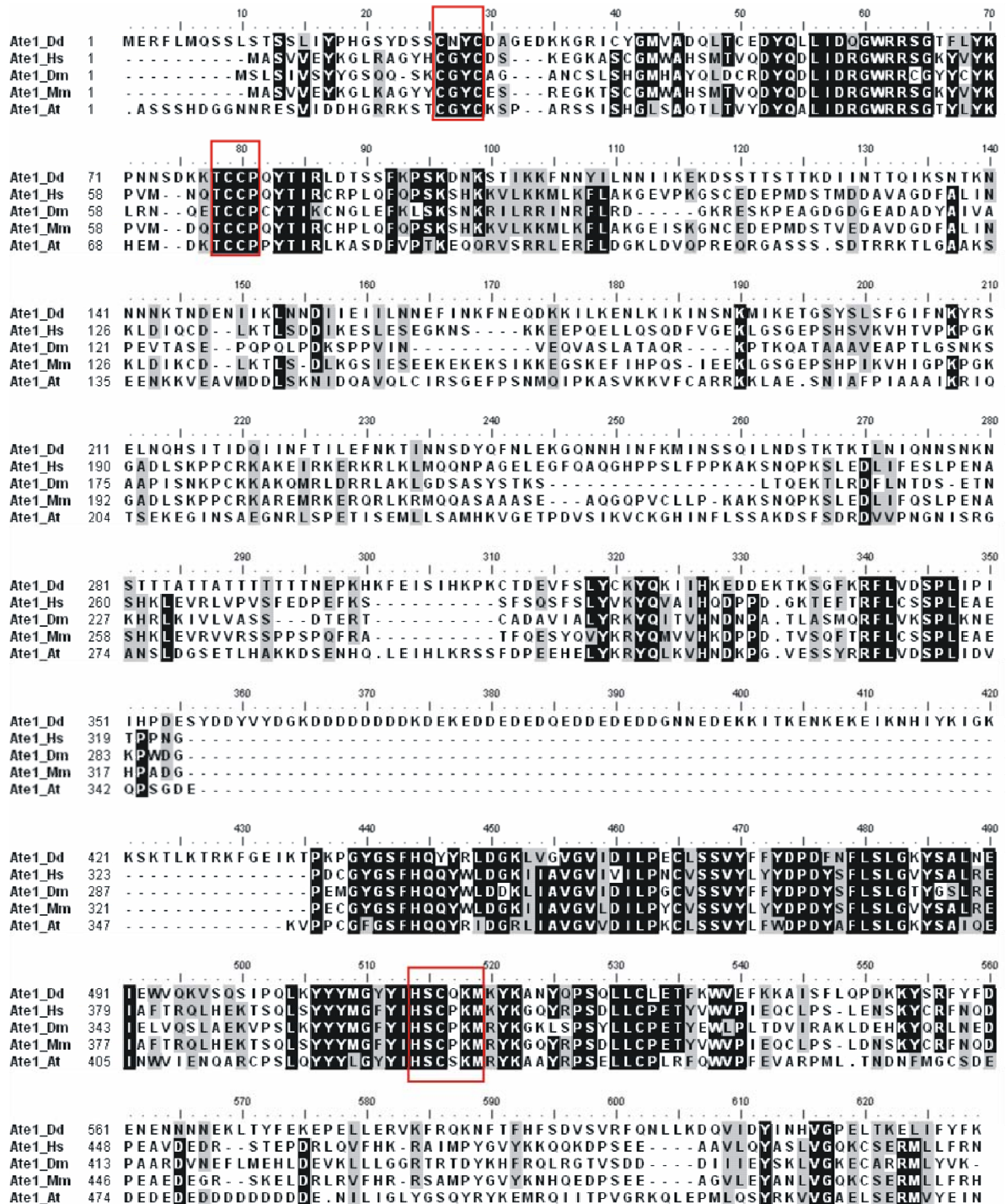
Figure 45. *Ate1* does not contain an intron sequence.

RNA from axenic cultures was isolated and RT-PCR was performed with two different oligonucleotide combinations. (A) Full length *ate1* amplification was successful with the RNA isolated from the GFP-Ate1 (lane 3) rescue and the GFP-Ate1 overexpressor (lane 2) cell lines and not with the wild type RNA (lane 1). The size of the *ate1* cDNA corresponds to the size of *ate1* gDNA. (B) A shorter fragment for Ate1 was amplified over RT-PCR with all isolated RNA.

This possible intron would have the conserved GT and AG consensus sequences and after splicing, would result in an Ate1 protein more similar to Ate1 in other organisms. Amplification and cloning of the full length *ate1* gene was performed from genomic DNA into an expression vector. After extraction of total RNA from axenical *D. discoideum* cells we were able to amplify the full length *ate1* cDNA over RT-PCR. The *ate1* cDNA has the same size as the gDNA. The possibility of an intron was excluded in the *ate1* sequence (Figure 45). An additional approach that confirmed this finding at the protein level was performed with the MALDI-TOF analysis of the immunoprecipitated GFP-Ate1. It revealed peptides matching the expected amino acid sequence without the existence of an intron at the suggested position.

The protein sequence is highly conserved with Arg-tRNA transferases in other organisms (Figure 46). All canonical sub domains which characterize Arg-tRNA transferases are present in Ate1 of *D. discoideum*. Interestingly, cysteine residues that have been reported to be important for *ate1* activity in *S. cerevisiae* (Balzi et al., 1990) are conserved in the DdAte1 (Figure 46, red boxes).

## Results



revealed that *Ate1* from *D. discoideum* is branching out after the plants but before the fungi (Figure 47) as in the evolutionary tree of the species (Eichinger et al., 2005).

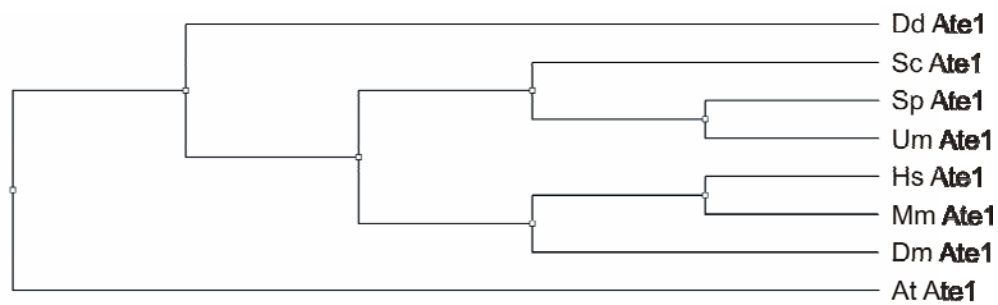


Figure 47. The phylogenetic tree of the *Ate1* proteins. *Ate1* proteins from *D. discoideum*, *S. cerevisiae*, *S. pombe*, *U. maydis*, *H. sapiens*, *M. musculus*, *D. melanogaster* and *A. thaliana* were used to generate a phylogenetic tree. The tree was generated with BioEdit by the neighbour joining method.

The *ate1* null cells, containing a blasticidin resistance cassette disrupting the *ate1* gene, were a kind gift from Dr. Annette Müller-Taubenberger (Figure 48 A). The knockout event in several clones was confirmed by PCR (Figure 48 B).

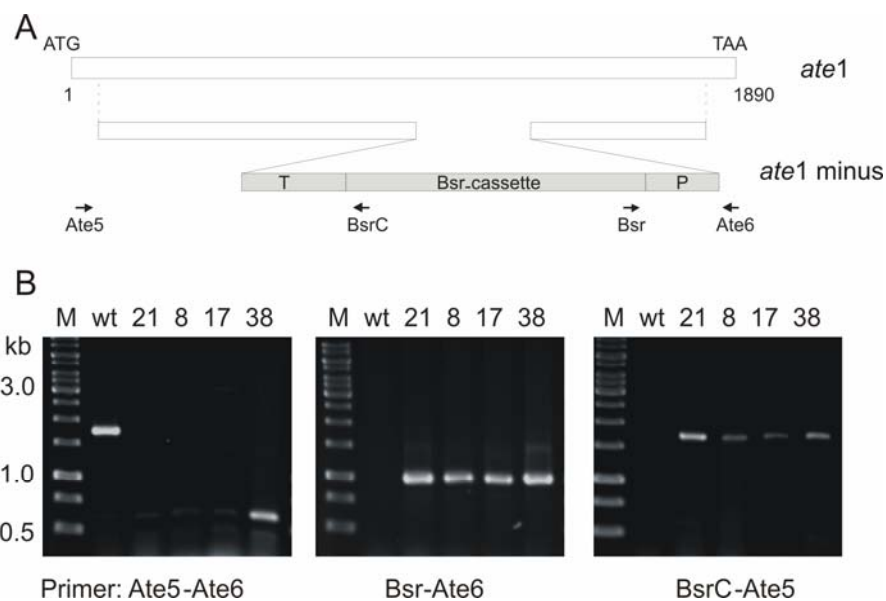


Figure 48. *Ate1* gene disruption and GFP-*Ate1* expression. (A) Inactivation of the *ate1* gene. Sequence specific homologous recombination leads to integration of a blasticidin resistance cassette into the target gene and loss of the parental gene. (B) Single *ate1* null clones were confirmed by PCR with the appropriate primer combinations.

In order to confirm that the observed *ate1* null phenotype is a direct consequence of the *ate1* knockout, a C-terminal GFP-Ate1 full length construct was introduced into the knockout to rescue the phenotype (Figure 49 A). The expression was confirmed by Western blot analysis with anti-GFP antibodies (Figure 49 B). A monoclonal rat anti-Ate1 antibody made against mouse Ate1-1 and Ate1-2 isoforms (from Dr. Anna Kashina), did not recognize the *D. discoideum* Ate1, on western blots of wild type or GFP-Ate1 expressing cell lysates.

### 3.2.2.2 Subcellular localization

Introduction of the Ate1-GFP into wild type and *ate1* null cells resulted in over expression of the constructs confirmed by western blot (Figure 49 B). In cells that express Ate1-GFP, the protein predominantly diffused in the cytosol. Interestingly, a nuclear localization was observed in a subpopulation of cells and rarely to flat protrusions, which were quite unusual for *D. discoideum* (Figure 49 A).

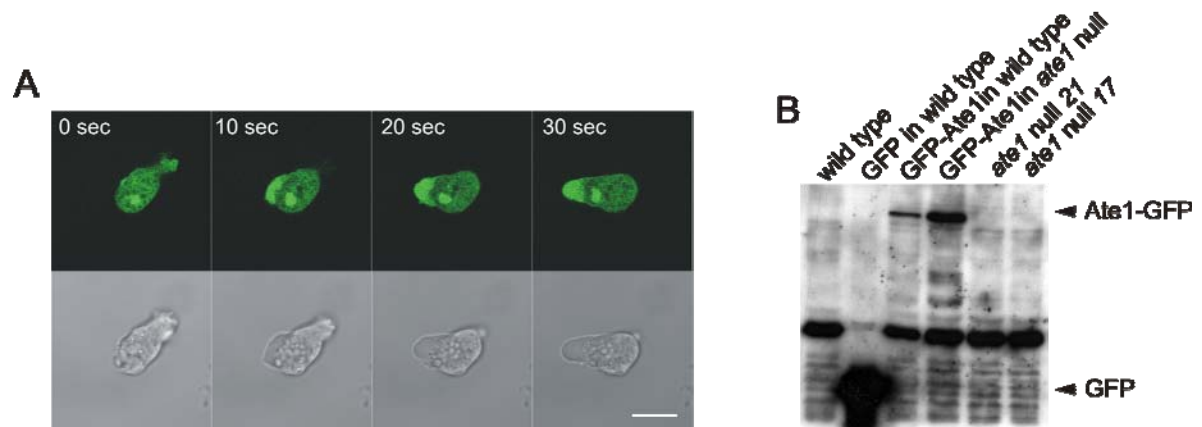


Figure 49. Subcellular localization of Ate1-GFP.

(A) Subcellular localization of Ate1-GFP in *ate1* null cells. Time lapse movies were recorded with the confocal microscope. Bar: 2  $\mu$ m. (B) Ate1-GFP expressed in *ate1* null and wild type cells. Western blots were performed with anti-GFP antibodies.

These unusual protrusions are not part of the leading front of the cell, but rather lateral protrusions which are flat and contain a dense F-actin meshwork, as judged by the characteristic appearance in the phase contrast, which also discerns them for example from membrane blebs.

### 3.2.2.3 Characterization of the *ate1* null phenotype

As previously suggested (Karakozova et al., 2006) *Ate1* might have an impact on actin polymerization, therefore *ate1* null cells were fixed and stained with TRITC-phalloidin to visualize F-actin. No significant differences in the localization or the amount of F-actin were observed in the *ate1* mutant (Figure 50 A).

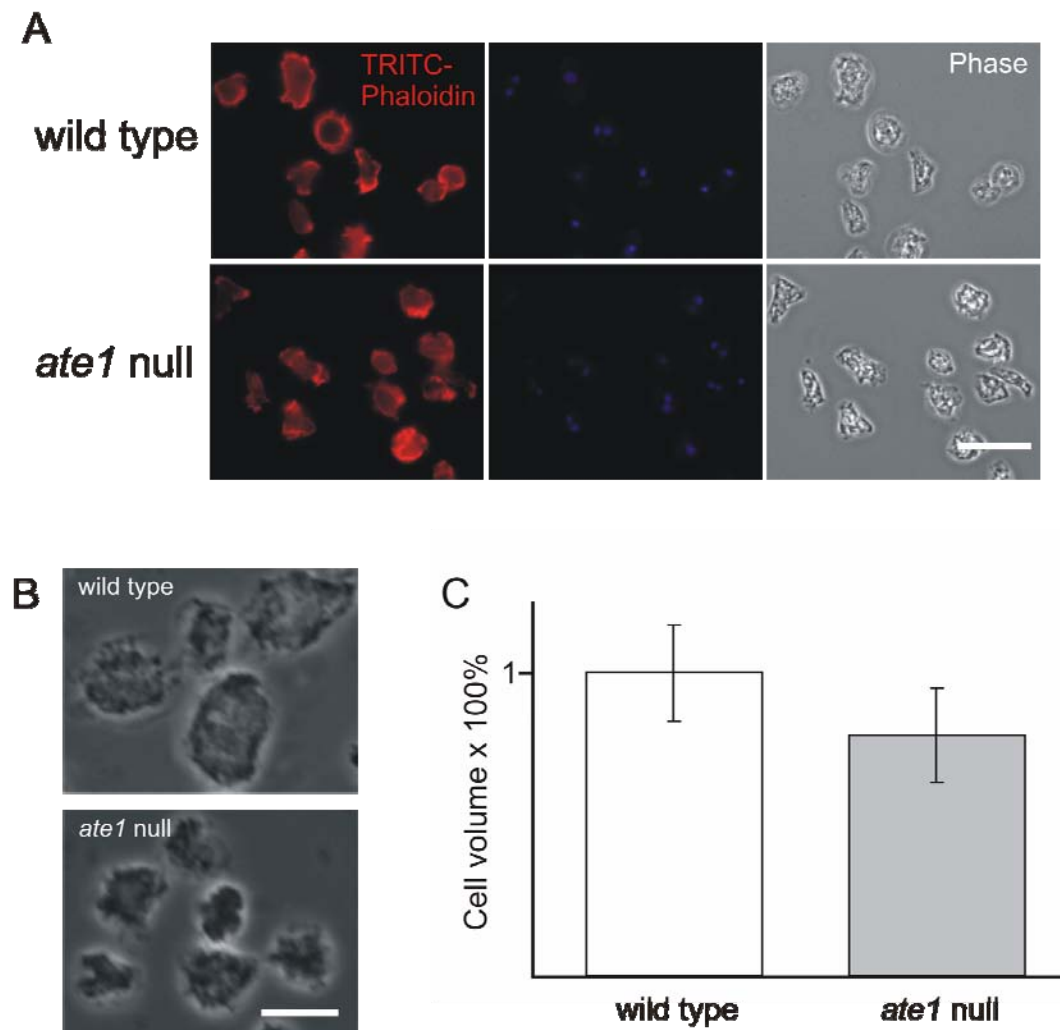


Figure 50. *Ate1* null cells are reduced in size.

(A) The F-actin content and localization in *ate1* null cells is not disturbed, as judged from fixed and TRITC-phalloidin stained cells. Bar: 8  $\mu$ m (B) The *ate1* null cells appear smaller than wild type cells when observed under the microscope. Bar: 4  $\mu$ m (C) The size of *ate1* null and wild type cells was measured in hematocrit tubes and revealed that *ate1* null cells are ~20% smaller. Error bars indicate standard deviation.

An interesting effect of the *ate1* knockout, concerns the size and the shape of the mutant cells. These cells were smaller and had a rounder appearance when compared to wild type cells (Figure 50 B). In order to quantify the decrease in size a cell volume measurement



with hematocrit tubes was performed. The results in Figure 50 C show the outcome of five measurements. *Ate1* null cells have an approximately 20% smaller volume than wild type cells. The smaller and rounded appearance was a first indication for a possible effect of *Ate1* on the cortical actin.

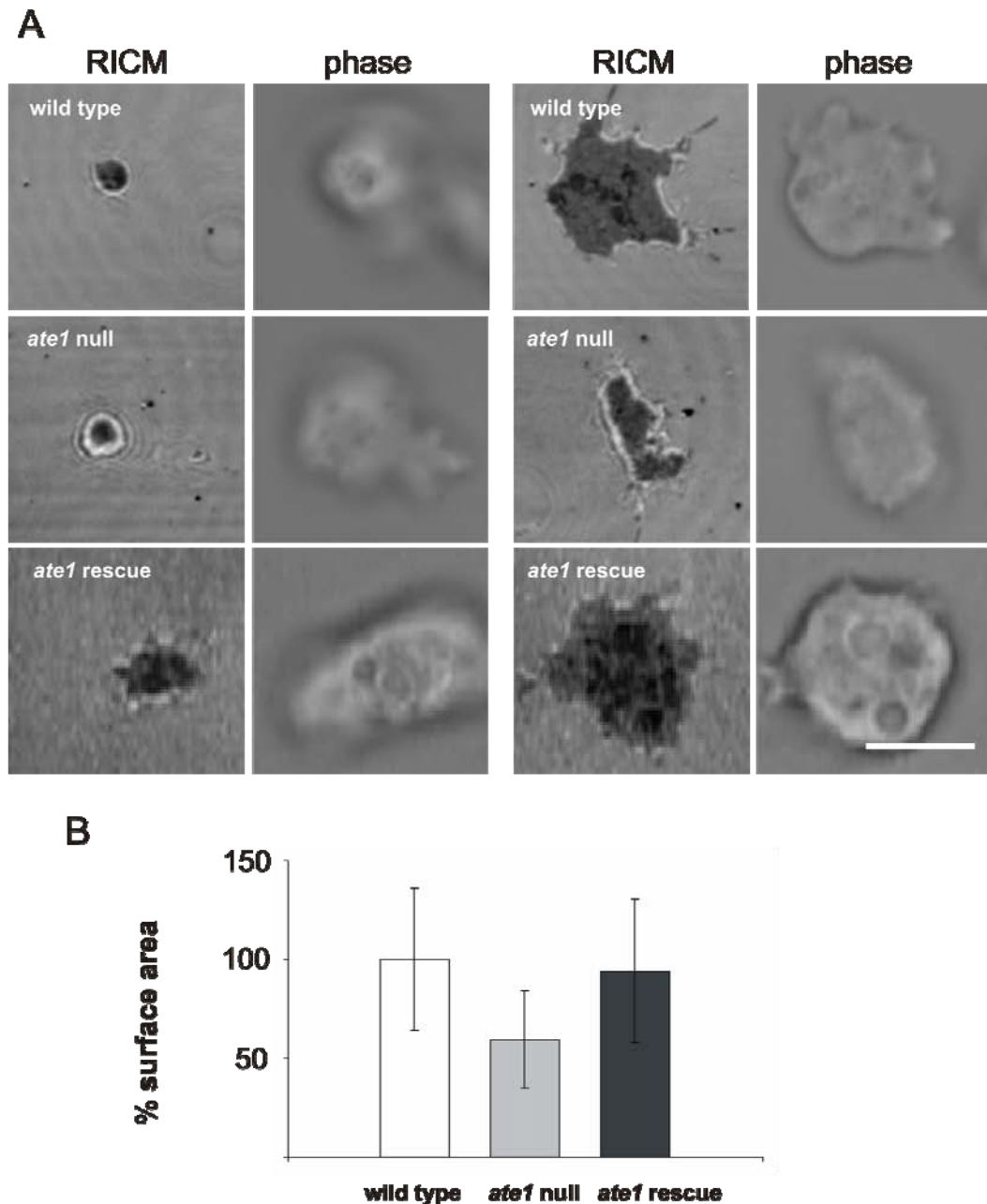


Figure 51. The *ate1* mutant makes smaller contact to the surface.

(A) The contact area of *ate1* null cells to a glass substrate is much smaller than that of wild type cells. Time lapse movies of wild type, *ate1* null and *ate1* rescue cells show the contact area to a glass cover slip, in phase (Phase) or reflection interference (RICM) contrast. Bar: 2  $\mu$ m. (B) Analysis of the mean contact area reveals that *ate1* null cells have considerably smaller cell-surface adhesion area (n = 10 cells). Error bars indicate standard deviation.



## Results

In addition to these findings, we observed, using Reflection Interference Contrast Microscopy (RICM), that the *ate1* knockout cells have a much smaller contact area with the surface. Wild type and mutant cells were plated on glass cover slips and tracked for 100 frames in 20 second intervals (Figure 51 A). The maximal and minimal contact area for every cell was measured. From these we calculated a mean contact area for *ate1* null (n=48) wild type (n=14) and rescue (n=38) cells. The *ate1* null cells show a drastic decrease (~40%) in the mean contact area (Figure 51 B). This effect is rescued by the expression of GFP-Ate1 in the *ate1* mutants.

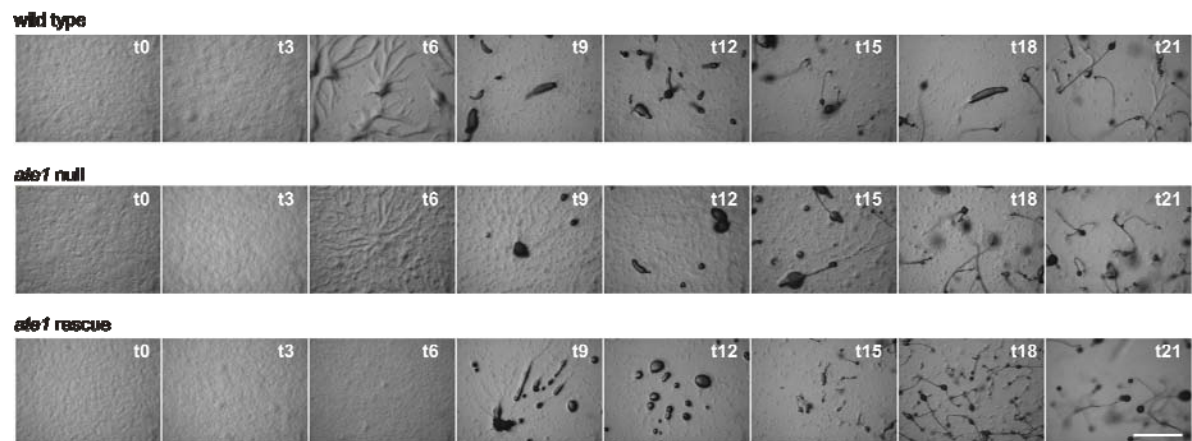


Figure 52. Development of *ate1* mutants.

No delay in the development of *ate1* null or *ate1* rescue could be observed. Bar: 5 mm

To monitor whether the observed small contact area to the surface correlates with the ability of vegetative *D. discoideum* cells to migrate, speed and persistence of random moving cells was measured (not shown). The random motility of *ate1* null cells was ~6  $\mu\text{m}/\text{min}$  which corresponds well with the speed of wild type cells, suggesting that the reduced contact area in the *ate1* null has no drastic effect on cell migration. The motility and directionality of elongated *ate1* null cells was not disturbed in a cAMP gradient during chemotaxis (not shown). Growth and development of *ate1* null cells was not affected (Figure 52).

The smaller size and round shape of the *ate1* knockout might suggest an effect of Ate1 on actin. To visualize F-actin in living *ate1* null cells we expressed the F-actin marker GFP-LimE $\Delta$ coil. In the *ate1* null the F-actin marker seems to reveal significant differences (Figure 53A). Whereas the cortical actin seems unaffected in *ate1* null cells, F-actin structures at potential cell adhesion points, clearly visible in wild type cells, are absent in

the mutant (Figure 53 A). We quantified the observed adhesion points in wild type (n=9) and *ate1* null (n=12) cells (Figure 53 C). *Ate1* null cells lack actin spots. This observation suggests that an F-actin subpopulation, which might be required for cell-substrate adhesion, is affected by the *ate1* knockout in *D. discoideum*. We expressed RFP-LimE $\Delta$ coil in *ate1* rescue cells and visualized massive actin clusters in the substrate adhesion area of *ate1* rescue cells (Figure 53 D). This overexpression phenotype indicates an involvement of Ate1 in the formation of actin clusters at the surface area of cells. When *ate1* null cells expressing GFP-LimE $\Delta$ coil were flattened under agar, they were able to form the observed spots at the surface area. This is an indication that this phenotype is a secondary effect and not the primary phenotype (Figure 53 E and F).

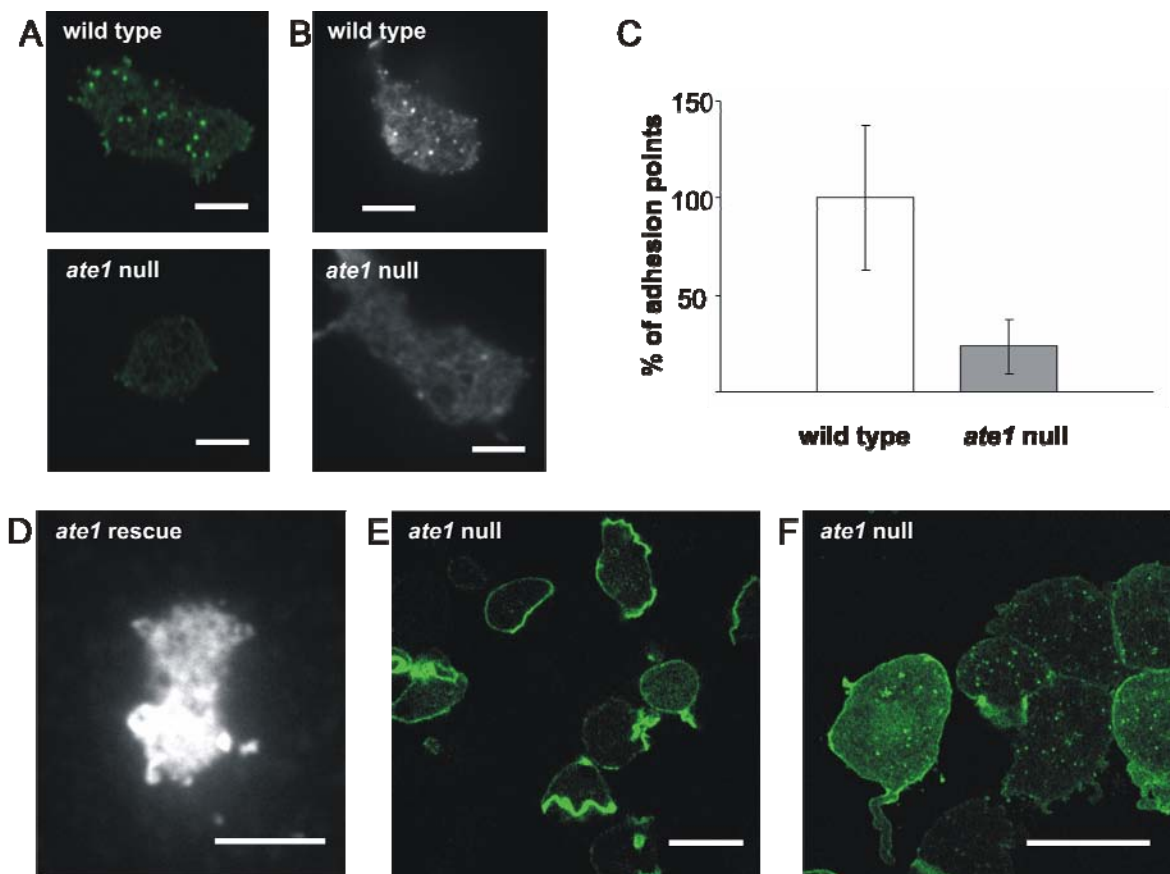


Figure 53. The *ate1* null cells lack F-actin structures at potential adhesion points.

(A) Confocal microscopy of GFP-LimE $\Delta$ coil in wild type and *ate1* null cells. (B) TIRF microscopy of GFP-LimE $\Delta$ coil in wild type and *ate1* null cells. (C) Quantification of the adhesion points in wild type (n=9) and *ate1* null (n=12) cells. Error bars indicate standard deviation. (D) TIRF microscopy of an *ate1* rescue cell expressing RFP-LimE $\Delta$ coil that forms intensive actin structures at the surface area. (E and F) *ate1* null cells expressing GFP-LimE $\Delta$ coil were overlaid (F) with agarose slides. This compressed cells form spots at the surface area. Bars: 2  $\mu$ m.

In order to see whether the observed spots, visualized with GFP-LimE $\Delta$ coil are similar to clathrin spots, points of pinocytosis, we expressed GFP-clathrin in the *ate1* null. Cells were observed in a confocal microscope (not shown). Spots that are part of clathrin-mediated endocytic vesicles were not disturbed in the *ate1* null cells.

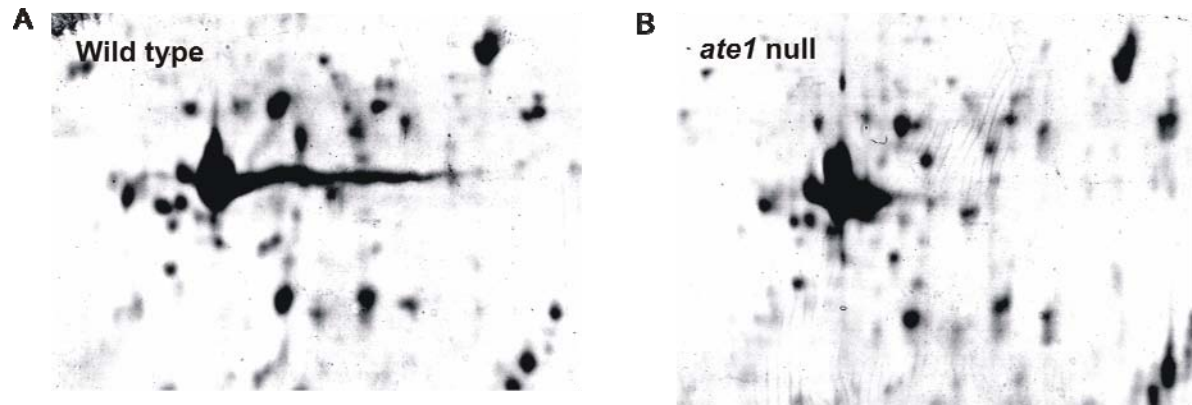
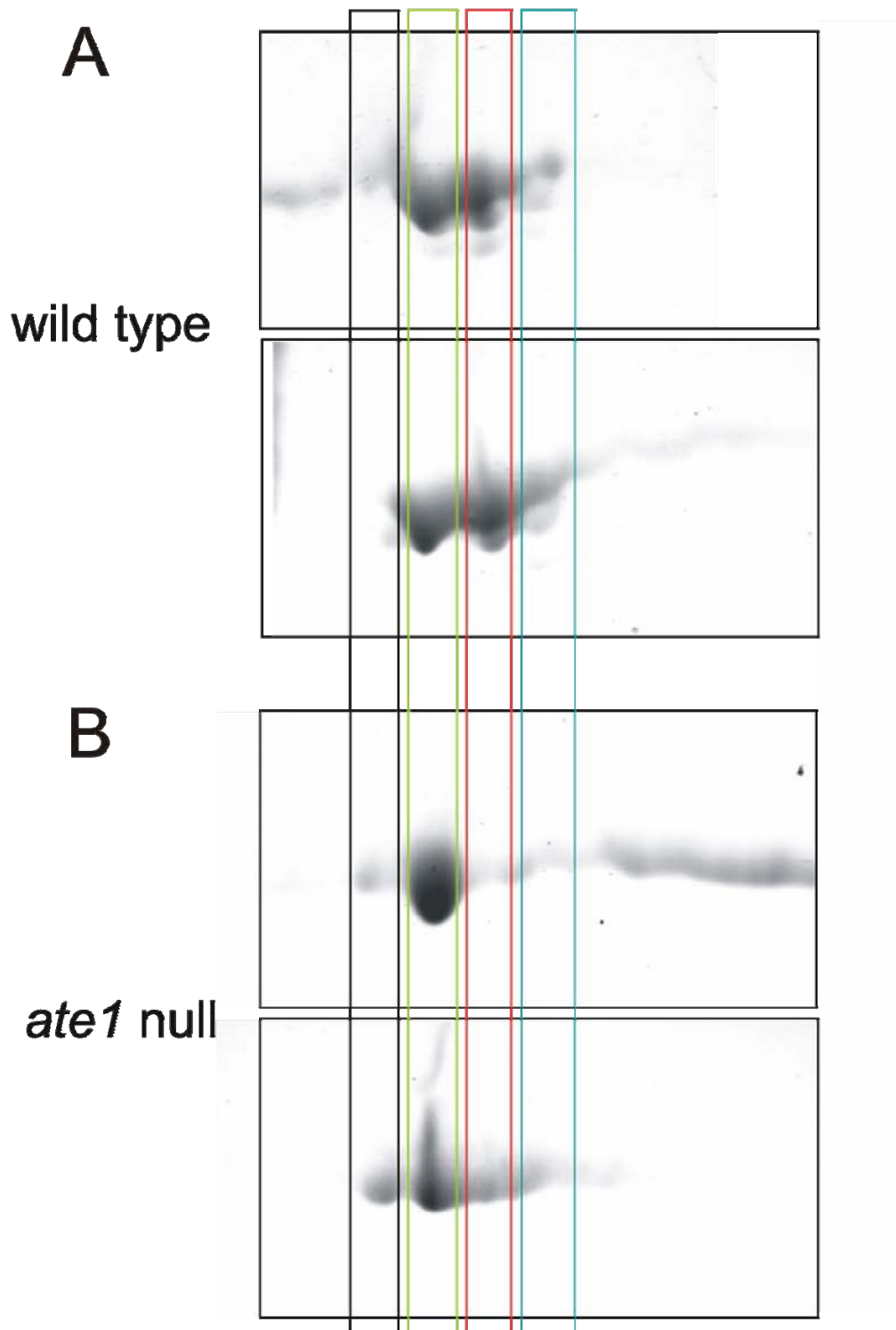


Figure 54. The proteome of *ate1* null cells lack the long basic tail of actin isoforms. (A) Wild type and (B) *ate1* null cells were lysed and separated by 2D-PAGE. The pictures highlights the different actin isoforms resolved on the 2D-PAGE, the missing comet tail of basic actin isoforms in the *ate1* null mutant is clear.

To examine differences in the biochemical properties of actin from *ate1* null cells 2D-PAGE of total *D. discoideum* lysates was performed. The pattern that is formed by the different actin isoforms on a 2D-gel shows variations in the mutant compared to the wild type (Figure 54). The *ate1* null actin spot lacks the comet tail, visible in the wild type, suggesting that positive charges are missing in the *ate1* null actins. Using MALDI/TOF we were not able to identify arginylation of actin. Actin from *D. discoideum* was purified and used the total protein samples for MALDI/TOF, to identify actin arginylation, but also in this approach we could not sequence the interesting N-terminus of the isolated actin.

Purified actin from wild type and *ate1* null cells was also compared on 2D-PAGE (Figure 55). 2D-PAGE with isolated actin allowed for a better isoelectric separation of the actin isoforms. On these gels we could observe that spots in the basic part of the gel are missing in the *ate1* null actinome. This was also noticed by Kashina et al., who separated beta-actin with similar results (Rai et al., 2008). A preliminary result of an actin polymerization assay with actin from *ate1* null cells seems to indicate that it polymerizes slower than actin from wild type cells. These different polymerization properties might be caused by the absence of post-translational modifications in *ate1* null cells.



pl 4-7, 1 mm, 12% SDS-PAGE

Figure 55. *Ate1* null actin has different properties.  
 (A) Wild type and (B) *ate1* null actin was purified and 2D-PAGE was performed in duplicates. *Ate1* null actin lacks spots at the basic side of the 2D-PAGE.

To summarize, with 2D-PAGE and MALDI/TOF several actin isoforms in *D. discoideum* that have different isoelectric properties due to post-translational modifications were identified. A knockout of the only arginyl-tRNA transferase (*ate1*) in *D. discoideum* was generated and showed to cause reduced cell size and cell-surface contact area. The only difference we observed in the actin system was the significant lacking of actin spots at the substrate area of living cells, which is probably a secondary effect. No actin arginylation could be found with MALDI/TOF, but there are indications from 2D-PAGE for changes in the post-translational modifications of *ate1* null actin. We conclude that Ate1 is an enzyme important for cell size and cell-substrate contact regulation, which also has an effect on post-translational modifications of actin.

## 4. Discussion

### 4.1 The Ste20-like kinase DstA

DstA a *Dictyostelium* specific Ste20-like kinase was characterized using several independent gene knockouts. The anti-DstA antibody we generated showed that DstA is equally expressed throughout the *D. discoideum* life cycle, which is an indication for the importance of this kinase for the amoeba development.

The localization of GFP-DstA in live cells suggests a role for this kinase in the cytosol. In fixed cells, where cytosolic staining is usually slightly depleted, we could clearly observe a localization of DstA at intracellular membrane structures. We could exclude that GFP-DstA localizes to the Golgi, but saw a partial overlap with annexin VII positive structures, a protein that is involved in endocytosis.

The *dst1* null cells are streaming in growth medium. In order to explain the observed *dst1* knockout phenotype we postulate three hypotheses: (1) The knockout cells have a defect in phago- and pinocytosis, so they starve while surrounded by abundant food and start to develop. (2) DstA could be part of a signaling pathway that normally prevents well fed cells from entering the developmental cycle, in the *dst1* knockout this switch is set to go into developmental commitment. (3) In *dst1* null cells a cell density factor is secreted that initiates the developmental cycle and aggregation.

At the moment the third hypothesis, that *dst1* null cells secrete a factor which leads to aggregation is favorite. As secondary effect DstA plays a crucial role for food uptake as is underscored by the pinocytosis and phagocytosis defects. We could not confirm that *dst1* cells entered development, because they do not seem to express contact site A (CsA) a very early developmental marker. So far there are no phagocytosis mutants reported that would lead to the initiation of development in *D. discoideum*. On contrary, it has been reported that for starving cells extracellular cAMP pulses cause developmental commitment whereas, starvation or the phagocytosis defect alone are not sufficient (Kato et al., 2007). Interestingly, *dst1* null cells, in contrast to wild type cells, react to the chemoattractant cAMP even in the presence of growth medium. The observed pinocytosis and phagocytosis defects of *dst1* null cells are most likely secondary effects as consequence of an increased cAMP stimulation. This fits well to the observation that *dst1* null cells secrete a factor that has no effect on wild type cells but triggers development in *dst1* null cells. This secretion



factor is smaller than ~10 kDa. This factor could be cAMP which is secreted and sensed by *dst1* null cells because they have already passed the initial stages of development, whereas the wild type can not sense it yet. So, DstA is a kinase that controls developmental commitment in *D. discoideum* by an increased cAMP stimulation in the vegetative stage and as a secondary consequence also inhibits phagocytosis and pinocytosis.

*The DstA signaling.* A comparison of *dst1* null and wild type cell lysates with 2D-PAGE showed that post-translational modifications of a GMF-like protein might be affected by the DstA knockout. A role of mammalian GMF-gamma for phagocytosis via regulation of the Arp2/3 complex has been reported recently (Ikeda et al., 2006; Walker, 2003). It was shown that phosphorylated GMF-gamma enhances Arp2/3 mediated actin polymerization (Ikeda et al., 2006). GMFs can be phosphorylated by PKA, and then fulfill a function by inhibiting the activity of MAP kinases ERK1/ERK2 and activating the MAP kinase p38 (Ikeda et al., 2006). In *dst1* null cells the dephosphorylated form of GMF-like is most dominant which might negatively regulate Arp2/3 mediated phagocytosis. As was shown *in vitro* GMF-like is indeed phosphorylated by PKA, but not directly by GFP-DstA. So we hypothesize that DstA is upstream of PKA.

*D. discoideum* PKA is involved in regulation of the Adenylate Cyclase A (ACA) and the cAR1 (Kriebel and Parent, 2004; Loomis, 1998). It is present at all stages of *D. discoideum* development, but upregulated during aggregation where it is important for ACA expression (Mann et al., 1997). Our hypothesis is that DstA is involved in a pathway that regulates ACA and cAR1 expression, probably upstream of PKA. Thereby DstA could regulate both phagocytosis and cAMP sensitivity. In the absence of DstA PKA might be inactive and induces the production of cAMP stimuli and the dephosphorylation of GMF and inhibition of Arp2/3 mediated phagocytosis (Figure 56). For future work this hypothesis has to be tested by investigating the expression levels of ACA, cAR1 and PKA in *dst1* null.

Another aspect of the *dst1* knockout was the secretion factor that promoted development at least in the *dst1* minus cells. The number of cells in a stream appears to be sensed by counting factor (CF), a ~450-kDa complex of proteins (Brock and Gomer, 1999). Counting factor has probably no role in *dst1* null stream formation. The secretion factor we observed in *dst1* null cells is smaller than 10 kDa, small for CF.

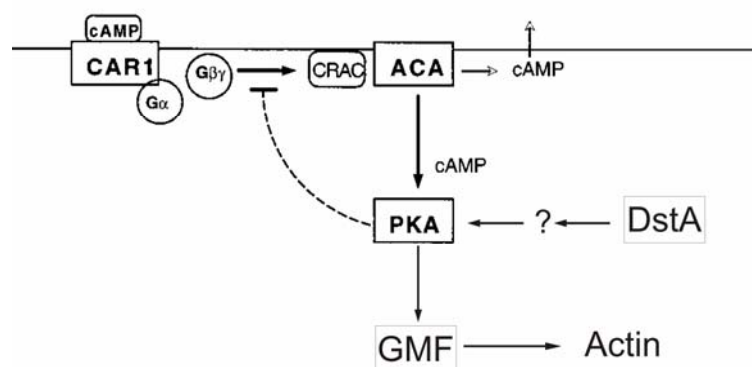


Figure 56. Postulated model of DstA function. [adapted from (Loomis, 1998)]

*Phototaxis defect.* Normally, 15 hours into the *D. discoideum* development, a slug is formed which moves towards light. DstA regulates the first stages of development as was shown. Interestingly, this kinase seems to be involved in phototaxis at the later stages of development as well. *Dst1* null cells form slugs but they do not move towards the light. This phenotype is rescued by the ectopic expression of GFP-DstA in *dst1* null cells. Phototaxis is a process which involves at least 55 genes (Fisher, 1997). The involved proteins regulate signal transduction pathways using intracellular messengers cAMP, cGMP, IP<sub>3</sub>, Ca<sup>2+</sup>, heterotrimeric and small GTP-binding proteins as well as cytoskeletal proteins such as filamin and myosin II (Bandala-Sanchez et al., 2006). Other proteins have been reported to influence phototaxis like GRP125, ErkB and PKB. Ras activates ERK in mammals via raf and MEK and in *Dictyostelium* a homologous pathway is involved in chemotaxis (Lee et al., 2005). Akt/PKB is part of the regulatory network required for sensing and responding to the chemoattractant gradient that mediates chemotaxis (Meili et al., 1999). It is not surprising that a kinase which is involved in regulation of chemotactic stimuli is important for proper phototaxis at the slug stage.

An important avenue for future research will be to identify how the DstA kinase is regulated and what its substrates are. Our finding, that DstA regulates initial phases of the development and phagocytosis in *D. discoideum* suggests a novel role for this family of kinases.

## 4.2 The Ste20-like kinase Krs2

*The Ste20-like kinase Krs2.* The Ste20-like kinase Krs2 of *D. discoideum* that is most similar to the kinases Mst1/2 in humans and Hippo in flies was characterized. A 3D model showed that an auto-phosphorylation site important for activity in Mst2, that corresponds to Thr176 is conserved in Krs2 and lies at the surface of the substrate binding pocket. Krs2 contains a unique stretch of four calpain III-like domains and it was shown that the very C-terminal domain localizes the kinase to the centrosome. Concerning the function of this kinase we found that cells lacking Krs2 have a defect in polarization and in orienting pseudopodia in a chemoattractant gradient. The newly generated anti-Krs2 antibody, showed that the kinase is slightly upregulated during early development where cells aggregate by cAMP mediated chemotaxis. These problems during early aggregation seemed the reason for the tiny fruiting bodies we observed in the *krsB* knockout.

The streams observed during chemotaxis are formed normally in the *krsB* knockout but they break often during aggregation. Analysis of the mutant cells in a chemoattractant gradient revealed the possible basis for this defect. Starved *krsB* null cells had difficulties to become polarized or correctly extend pseudopods in the direction of the gradient, which characterizes the migration of wild type cells, toward cAMP. This results in a drastic decrease in speed and directionality of aggregation competent *krsB* null cells. Ectopic expression of the GFP-Krs2 full length kinase in the knockout background rescued this phenotype and underscores the role of Krs2 on the observed defects.

To investigate which part of the polarity network is affected in the *krsB* minus cells we looked at random motility, but it was not disturbed. Interestingly, a defect in chemotaxis towards folic acid, a process that is independent of the starvation induced development pathway, was observed. This indicates that Krs2 does not have a direct role in regulating the cytoskeleton, but has a rather specialized function during chemotaxis. This defect in chemotaxis seems to be independent of the developmental program, as indicated by the ability of *krsB* null cells to initiate cAMP waves, a hallmark of early development. Our observation that *krsB* null cells move slower towards the cAMP gradient means that *krsB* null cells do not fail to sense the gradient but can not restrict pseudopod formation to the leading edge. So *krsB* null cells are not blind but limping. As PIP<sub>3</sub> production and actin

polymerization are key downstream signaling events in chemotaxis, investigation of the regulation of these pathways in *krsB* null cells would be necessary in future studies.

So how does the chemotaxis defect link to the observed localization of Krs2 at the centrosome? The human protease Calpain 6 interacts with microtubules, facilitated by its calpain domain-III. The functions of Calpain 6 do involve microtubule stabilization and cytoskeletal organization (Tonami et al., 2007). Maybe an ancient role for calpain domain III is to localize proteins to the microtubule network. Recent studies have shown that *D. discoideum* cells treated with nocodazole have defects in polarization, pseudopod persistence, and chemotaxis to both cAMP and folic acid (Satulovsky et al., 2008). The role of the centrosome for cell polarity was shown with overexpression of dominant-negative Lis1 mutants, an important component of the centrosome. The loss of cell shape in these mutants was explained with a microtubule network that detached from the cell cortex (Hestermann and Graf, 2004). In *D. discoideum*, the ability of a pseudopod to persist and generate cell locomotion depends on MTOC reorientation (Ueda et al., 1997). Recently it was shown that tsunami, a member of the fused kinase family in *D. discoideum*, is required for polarization and chemotaxis. Interestingly, this kinase shows centrosomal and microtubule localization (Tang et al., 2008). The phenotypes of tsunami and *krsB* knockouts seem quite similar. Investigation for a possible interaction of both kinases might be a good starting point to further elucidate the place of Krs2 in a signaling network.

In the future, the critical association of Krs2 with the MTOC may provide important insights. It has been shown that the role of the *krsB* homolog, *krsA*, controls cAMP relay during the early development of *D. discoideum* (Muramoto et al., 2007). A generation of a double knockout of *krsA* and *krsB* in *D. discoideum* and its investigation in the future would hopefully gain insight into the function of a Krs subfamily in *D. discoideum*. Our finding that Krs2 regulates polarity and the suppression of lateral pseudopods in *D. discoideum* suggests a support for the known role of this family of kinases.

### **4.3 Actin isoforms and post-translational modifications**

*Isoforms of actin and post-translational modifications.* A 2D-PAGE analysis combined with MALDI/TOF detection could verify the expression of different actin isoforms in *D. discoideum*. The expressed actin isoforms differ in their amino acid sequences, which causes different electrophoretic properties, that resolves the isoforms into distinct spots on a

2D-PAGE. In addition to the genetically encoded differences of actin isoforms, the electrophoretic properties are also influenced by post-translational modifications. These modifications give the spot pattern another layer of complexity, especially as post-translational modification might only affect a subpopulation of any expressed actin isoform. For the actin15 population, the obtained peptide masses might suggest that actin15 is phosphorylated on several, so far, not described residues. These potential phosphorylation sites are residues that are accessible at the surface of the actin molecule. The other possible post-translational modifications were acetylation and arginylation. Unfortunately, the MALDI/ TOF method we used was not suitable to resolve the N-terminal part of the actin molecules, where we would expect these modifications to occur. Very recently, a sensitive sequencing protocol has been described to identify especially N-terminal arginylated peptides using an Orbitrap system (Xu et al., 2009). Certainly, this new approach, combined with the now annotated 2D-gel actinome of *D. discoideum*, could, in the future, be of great importance to identify N-terminal arginylation in the different actin isoforms.

A promising aspect in this line is that the actinome of cells lacking the arginyl-transferase *ate1* looked strikingly different on 2D-gels. The main difference we could identify was that the actin comet tail, normally observed in the wild type, is drastically reduced in the *ate1* knockout. This is a possible indication that Ate1 in *D. discoideum* affects actin directly as was suggest for mouse (Wong et al., 2007). An important issue for the future will be to confirm that the lack of the actin comet tail is a direct consequence of the absent arginylation. Of course other possibilities would be that *ate1* arginylates upstream effectors of the actin cytoskeleton, that either change the phosphorylation pattern of actin or which influence the expression profiles of the different actin isoforms, that normally constitute the observed actin comet tail.

*Localization of GFP-Ate1 in D. discoideum.* GFP-Ate1 in *D. discoideum* localizes mainly in the cytosol. In addition, GFP-Ate1 was also present in the nucleus and flat protrusions, rather untypical for this amoeba. For the mouse it has been reported that the two different Ate1 splice isoforms localize differently (Kwon et al., 1999). The ATE1-2p isoform is exclusively cytosolic, whereas ATE1-1p is present in either the nucleus or the cytosol (Kwon et al., 1999). So the *D. discoideum* Ate1 ortholog seems more similar to the ATE1-2p in respect to localization. In addition the localization of GFP-Ate1 to these atypical flat protrusions, seems to indicate that in *D. discoideum* this enzyme catalyzes arginylation in

actin rich structures. The ectopic expression of Ate1 appears to affect the actin cytoskeleton in such a way that flat protusions are formed.

*Size of ate1 null cells.* The most striking phenotype of *ate1* null cells was, that their size is considerably reduced. For mouse it is known that more than 733 cellular proteins are arginylated *in vivo* (Wong et al., 2007) including cytoskeleton components and components of the house keeping machinery involved in glycolysis, nucleotide biosynthesis, chromatin remodelling/transcription etc. Whether the reduced cell size of the *ate1* knockout is due to a direct effect on actin or the result of a more global cause by the lack of arginylation is unclear. It has been reported that a knockout of clathrin, which should severely affect a multitude of vesicle traffic, increases the size of *D. discoideum* cells. Most likely Ate1 influences a large number of proteins, so that the rather unspecific phenotype of the decreased size, can not be attributed solely to changes in the cytoskeleton.

*Contact area of ate1 null.* The adhesion areas of *ate1* null cells are significantly smaller as judged by RICM. However, preliminary observations suggest that cell-surface adhesion seems not dramatically affected, as knockout cells attach to the surface and show normal cell motility. Additionally, chemotacting *ate1* null cells move normal in a cAMP gradient. The cell-surface contact in wild type cells is normally characterized by spotty structures that stain positive for the F-actin probe GFP-LimEΔcoil. In the *ate1* knockout the number of these very dynamic F-actin structures seems noticeably reduces. However, *ate1* null cells are able to form these actin structures when flattened with an agar slice. We conclude that because of the reduced contact area *ate1* null cells show less adhesion points.

Taken together, the initial characterization of an Ate1-like protein in *D. discoideum* indicates that this enzyme has an effect on the cellular actin. The knockout results in smaller cells with reduced cell-surface areas. Future work should establish if this is a direct consequence of an altered actin arginylation, or rather a response to a cell-wide change in protein arginylation. One stepping stone on this road could be the expression and purification of the recombinant DdAte1 for *in vitro* arginylations of actin. Assays for *in vitro* arginylations are already established since Ate1 was first isolated from mammals (Soffer, 1968; Takao et al., 1999). The polymerization kinetics of an arginylated actin population would help to understand the role of this interesting enzyme and the regulation of the actin cytoskeleton.



## 5. References

- Alvarez-Curto, E., Saran, S., Meima, M., Zobel, J., Scott, C. and Schaap, P. (2007) cAMP production by adenylyl cyclase G induces prespore differentiation in *Dictyostelium* slugs. *Development*, **134**, 959-966.
- Andre, E., Lottspeich, F., Schleicher, M. and Noegel, A. (1988) Severin, gelsolin, and villin share a homologous sequence in regions presumed to contain F-actin severing domains. *J Biol Chem*, **263**, 722-727.
- Arasada, R., Gloss, A., Tunggal, B., Joseph, J.M., Rieger, D., Mondal, S., Faix, J., Schleicher, M. and Noegel, A.A. (2007) Profilin isoforms in *Dictyostelium* discoideum. *Biochim Biophys Acta*, **1773**, 631-641.
- Arasada, R., Son, H., Ramalingam, N., Eichinger, L., Schleicher, M. and Rohlf, M. (2006) Characterization of the Ste20-like kinase Krs1 of *Dictyostelium* discoideum. *Eur J Cell Biol*, **85**, 1059-1068.
- Arnold, K., Bordoli, L., Kopp, J. and Schwede, T. (2006) The SWISS-MODEL workspace: a web-based environment for protein structure homology modelling. *Bioinformatics*, **22**, 195-201.
- Axelrod, D. (2003) Total internal reflection fluorescence microscopy in cell biology. *Methods Enzymol*, **361**, 1-33.
- Bakthavatsalam, D., Brazill, D., Gomer, R.H., Eichinger, L., Rivero, F. and Noegel, A.A. (2007) A G protein-coupled receptor with a lipid kinase domain is involved in cell-density sensing. *Curr Biol*, **17**, 892-897.
- Balzi, E., Choder, M., Chen, W.N., Varshavsky, A. and Goffeau, A. (1990) Cloning and functional analysis of the arginyl-tRNA-protein transferase gene ATE1 of *Saccharomyces cerevisiae*. *J Biol Chem*, **265**, 7464-7471.
- Bandala-Sanchez, E., Annesley, S.J. and Fisher, P.R. (2006) A phototaxis signalling complex in *Dictyostelium* discoideum. *Eur J Cell Biol*, **85**, 1099-1106.
- Batsios, P. (2005) Charakterisierung der Ste20-ähnlichen Kinase DST10 in *Dictyostelium* discoideum. *Diplomarbeit in Zellbiologie*. Ludwig-Maximilians-Universität, München, Vol. Diplom, p. 91.
- Boissel, J.P., Kasper, T.J. and Bunn, H.F. (1988) Cotranslational amino-terminal processing of cytosolic proteins. Cell-free expression of site-directed mutants of human hemoglobin. *J Biol Chem*, **263**, 8443-8449.
- Bradford, M.M. (1976) A rapid and sensitive method for the quantitation of microgram quantities of protein utilizing the principle of protein-dye binding. *Anal Biochem*, **72**, 248-254.

- Brock, D.A. and Gomer, R.H. (1999) A cell-counting factor regulating structure size in Dictyostelium. *Genes Dev*, **13**, 1960-1969.
- Burnett, G. and Kennedy, E.P. (1954) The enzymatic phosphorylation of proteins. *J Biol Chem*, **211**, 969-980.
- Carrascosa, J.M. and Wieland, O.H. (1986) Evidence that (a) serine specific protein kinase(s) different from protein kinase C is responsible for the insulin-stimulated actin phosphorylation by placental membrane. *FEBS Lett*, **201**, 81-86.
- Chisholm, R.L. and Firtel, R.A. (2004) Insights into morphogenesis from a simple developmental system. *Nat Rev Mol Cell Biol*, **5**, 531-541.
- Cohen, S.N., Chang, A.C. and Hsu, L. (1972) Nonchromosomal antibiotic resistance in bacteria: genetic transformation of Escherichia coli by R-factor DNA. *Proc Natl Acad Sci U S A*, **69**, 2110-2114.
- Cozzone, A.J. (1988) Protein phosphorylation in prokaryotes. *Annu Rev Microbiol*, **42**, 97-125.
- Creasy, C.L., Ambrose, D.M. and Chernoff, J. (1996) The Ste20-like protein kinase, Mst1, dimerizes and contains an inhibitory domain. *J Biol Chem*, **271**, 21049-21053.
- Czerwinski, E. (2006) Two Proteins Containing Tandem DIII Domains, Calpain 10 and Dictyostelium Cpl, are Involved in Cytoskeletal Regulation. Medical University of Ohio, Toledo, Vol. Doctor of Philosophy in Biomedical Sciences, p. 154.
- Czisch, M., Schleicher, M., Horger, S., Voelter, W. and Holak, T.A. (1993) Conformation of thymosin beta 4 in water determined by NMR spectroscopy. *Eur J Biochem*, **218**, 335-344.
- Dan, I., Watanabe, N.M. and Kusumi, A. (2001) The Ste20 group kinases as regulators of MAP kinase cascades. *Trends Cell Biol*, **11**, 220-230.
- Darcy, P.K., Wilczynska, Z. and Fisher, P.R. (1994) Genetic analysis of Dictyostelium slug phototaxis mutants. *Genetics*, **137**, 977-985.
- De Corte, V., Gettemans, J., Waelkens, E. and Vandekerckhove, J. (1996) In vivo phosphorylation of actin in Physarum polycephalum. Study of the substrate specificity of the actin-fragmin kinase. *Eur J Biochem*, **241**, 901-908.
- Deng, Y., Pang, A. and Wang, J.H. (2003) Regulation of mammalian STE20-like kinase 2 (MST2) by protein phosphorylation/dephosphorylation and proteolysis. *J Biol Chem*, **278**, 11760-11767.
- Doring, V., Veretout, F., Albrecht, R., Muhlbauer, B., Schlatterer, C., Schleicher, M. and Noegel, A.A. (1995) The in vivo role of annexin VII (synexin): characterization of an annexin VII-deficient Dictyostelium mutant indicates an involvement in Ca(2+)-regulated processes. *J Cell Sci*, **108 (Pt 5)**, 2065-2076.

- Dumontier, M., Hocht, P., Mintert, U. and Faix, J. (2000) Rac1 GTPases control filopodia formation, cell motility, endocytosis, cytokinesis and development in Dictyostelium. *J Cell Sci*, **113** (Pt 12), 2253-2265.
- Dustin, P. and Brion, J.P. (1988) [Pathology of the cytoskeleton]. *Ann Pathol*, **8**, 3-19.
- Egelman, E.H. (2003) Actin's prokaryotic homologs. *Curr Opin Struct Biol*, **13**, 244-248.
- Eichinger, L., Bahler, M., Dietz, M., Eckerskorn, C. and Schleicher, M. (1998) Characterization and cloning of a Dictyostelium Ste20-like protein kinase that phosphorylates the actin-binding protein severin. *J Biol Chem*, **273**, 12952-12959.
- Eichinger, L., Noegel, A.A. and Schleicher, M. (1991) Domain structure in actin-binding proteins: expression and functional characterization of truncated severin. *J Cell Biol*, **112**, 665-676.
- Eichinger, L., Pachebat, J.A., Glockner, G., Rajandream, M.A., Sugang, R., Berriman, M., Song, J., Olsen, R., Szafranski, K., Xu, Q., Tunggal, B., Kummerfeld, S., Madera, M., Konfortov, B.A., Rivero, F., Bankier, A.T., Lehmann, R., Hamlin, N., Davies, R., Gaudet, P., Fey, P., Pilcher, K., Chen, G., Saunders, D., Sodergren, E., Davis, P., Kerhornou, A., Nie, X., Hall, N., Anjard, C., Hemphill, L., Bason, N., Farbrother, P., Desany, B., Just, E., Morio, T., Rost, R., Churcher, C., Cooper, J., Haydock, S., van Driessche, N., Cronin, A., Goodhead, I., Muzny, D., Mourier, T., Pain, A., Lu, M., Harper, D., Lindsay, R., Hauser, H., James, K., Quiles, M., Madan Babu, M., Saito, T., Buchrieser, C., Wardroper, A., Felder, M., Thangavelu, M., Johnson, D., Knights, A., Loulseged, H., Mungall, K., Oliver, K., Price, C., Quail, M.A., Urushihara, H., Hernandez, J., Rabbinowitsch, E., Steffen, D., Sanders, M., Ma, J., Kohara, Y., Sharp, S., Simmonds, M., Spiegler, S., Tivey, A., Sugano, S., White, B., Walker, D., Woodward, J., Winckler, T., Tanaka, Y., Shaulsky, G., Schleicher, M., Weinstock, G., Rosenthal, A., Cox, E.C., Chisholm, R.L., Gibbs, R., Loomis, W.F., Platzer, M., Kay, R.R., Williams, J., Dear, P.H., Noegel, A.A., Barrell, B. and Kuspa, A. (2005) The genome of the social amoeba Dictyostelium discoideum. *Nature*, **435**, 43-57.
- Faix, J. (2002) The actin-bundling protein cortexillin is the downstream target of a Rac1-signaling pathway required for cytokinesis. *J Muscle Res Cell Motil*, **23**, 765-772.
- Faix, J., Kreppel, L., Shaulsky, G., Schleicher, M. and Kimmel, A.R. (2004) A rapid and efficient method to generate multiple gene disruptions in Dictyostelium discoideum using a single selectable marker and the Cre-loxP system. *Nucleic Acids Res*, **32**, e143.
- Faix, J., Weber, I., Mintert, U., Kohler, J., Lottspeich, F. and Marriott, G. (2001) Recruitment of cortexillin into the cleavage furrow is controlled by Rac1 and IQGAP-related proteins. *Embo J*, **20**, 3705-3715.
- Fisher, P.R. (1997) Genetics of phototaxis in a model eukaryote, Dictyostelium discoideum. *Bioessays*, **19**, 397-407.

- Fukui, Y., Yumura, S. and Yumura, T.K. (1987) Agar-overlay immunofluorescence: high-resolution studies of cytoskeletal components and their changes during chemotaxis. *Methods Cell Biol*, **28**, 347-356.
- Fukushima, N., Furuta, D., Hidaka, Y., Moriyama, R. and Tsujiuchi, T. (2009) Posttranslational modifications of tubulin in the nervous system. *J Neurochem*.
- Furuhashi, K., Ishigami, M., Suzuki, M. and Titani, K. (1998) Dry stress-induced phosphorylation of Physarum actin. *Biochem Biophys Res Commun*, **242**, 653-658.
- Gartner, A. and Dotti, C.G. (2009) Neuronal polarity: consolidation for growth, growth for consolidation. *Embo J*, **28**, 173-174.
- Gerisch, G. (1987) Cyclic AMP and other signals controlling cell development and differentiation in Dictyostelium. *Annu Rev Biochem*, **56**, 853-879.
- Gerisch, G. and Keller, H.U. (1981) Chemotactic reorientation of granulocytes stimulated with micropipettes containing fMet-Leu-Phe. *J Cell Sci*, **52**, 1-10.
- Goldberg, J.M., Manning, G., Liu, A., Fey, P., Pilcher, K.E., Xu, Y. and Smith, J.L. (2006) The dictyostelium kinome--analysis of the protein kinases from a simple model organism. *PLoS Genet*, **2**, e38.
- Goley, E.D. and Welch, M.D. (2006) The ARP2/3 complex: an actin nucleator comes of age. *Nat Rev Mol Cell Biol*, **7**, 713-726.
- Goll, D.E., Thompson, V.F., Li, H., Wei, W. and Cong, J. (2003) The calpain system. *Physiol Rev*, **83**, 731-801.
- Graf, R., Daudeker, C. and Schliwa, M. (2000) Dictyostelium DdCP224 is a microtubule-associated protein and a permanent centrosomal resident involved in centrosome duplication. *J Cell Sci*, **113** (Pt 10), 1747-1758.
- Hagedorn, M., Neuhaus, E.M. and Soldati, T. (2006) Optimized fixation and immunofluorescence staining methods for Dictyostelium cells. *Methods Mol Biol*, **346**, 327-338.
- Haus, U., Hartmann, H., Trommler, P., Noegel, A.A. and Schleicher, M. (1991) F-actin capping by cap32/34 requires heterodimeric conformation and can be inhibited with PIP2. *Biochem Biophys Res Commun*, **181**, 833-839.
- Hestermann, A. and Graf, R. (2004) The XMAP215-family protein DdCP224 is required for cortical interactions of microtubules. *BMC Cell Biol*, **5**, 24.
- Holmes, D.S. and Quigley, M. (1981) A rapid boiling method for the preparation of bacterial plasmids. *Anal Biochem*, **114**, 193-197.
- Huang, X., Czerwinski, E. and Mellgren, R.L. (2003) Purification and properties of the Dictyostelium calpain-like protein, Cpl. *Biochemistry*, **42**, 1789-1795.

- Hwang, E., Ryu, K.S., Paakkonen, K., Guntert, P., Cheong, H.K., Lim, D.S., Lee, J.O., Jeon, Y.H. and Cheong, C. (2007) Structural insight into dimeric interaction of the SARAH domains from Mst1 and RASSF family proteins in the apoptosis pathway. *Proc Natl Acad Sci U S A*, **104**, 9236-9241.
- Ikeda, K., Kundu, R.K., Ikeda, S., Kobara, M., Matsubara, H. and Quertermous, T. (2006) Glia maturation factor-gamma is preferentially expressed in microvascular endothelial and inflammatory cells and modulates actin cytoskeleton reorganization. *Circ Res*, **99**, 424-433.
- Jaffer, Z.M. and Chernoff, J. (2002) p21-activated kinases: three more join the Pak. *Int J Biochem Cell Biol*, **34**, 713-717.
- Joseph, J.M., Fey, P., Ramalingam, N., Liu, X.I., Rohlf, M., Noegel, A.A., Muller-Taubenberger, A., Glockner, G. and Schleicher, M. (2008) The actinome of *Dictyostelium discoideum* in comparison to actins and actin-related proteins from other organisms. *PLoS ONE*, **3**, e2654.
- Kaji, H. (1968) Further studies on the soluble amino acid incorporating system from rat liver. *Biochemistry*, **7**, 3844-3850.
- Kaji, H., Novelli, G.D. and Kaji, A. (1963) A Soluble Amino Acid-Incorporating System From Rat Liver. *Biochim Biophys Acta*, **76**, 474-477.
- Karakozova, M., Kozak, M., Wong, C.C., Bailey, A.O., Yates, J.R., 3rd, Mogilner, A., Zebroski, H. and Kashina, A. (2006) Arginylation of beta-actin regulates actin cytoskeleton and cell motility. *Science*, **313**, 192-196.
- Kashina, A.S. (2006) Differential arginylation of actin isoforms: the mystery of the actin N-terminus. *Trends Cell Biol*, **16**, 610-615.
- Katoh, M., Chen, G., Roberge, E., Shaulsky, G. and Kuspa, A. (2007) Developmental commitment in *Dictyostelium discoideum*. *Eukaryot Cell*, **6**, 2038-2045.
- Khairi, N., Muller, R., Blau-Wasser, R., Eichinger, L., Schleicher, M., Rief, M., Holak, T.A. and Noegel, A.A. (2007) Filamin-regulated F-actin assembly is essential for morphogenesis and controls phototaxis in *Dictyostelium*. *J Biol Chem*, **282**, 1948-1955.
- Kimmel, A.R. and Faix, J. (2006) Generation of multiple knockout mutants using the Cre-loxP system. *Methods Mol Biol*, **346**, 187-199.
- Kollmar, M. (2006) Thirteen is enough: the myosins of *Dictyostelium discoideum* and their light chains. *BMC Genomics*, **7**, 183.
- Kriebel, P.W. and Parent, C.A. (2004) Adenylyl cyclase expression and regulation during the differentiation of *Dictyostelium discoideum*. *IUBMB Life*, **56**, 541-546.
- Kwon, Y.T., Kashina, A.S. and Varshavsky, A. (1999) Alternative splicing results in differential expression, activity, and localization of the two forms of arginyl-tRNA-

- protein transferase, a component of the N-end rule pathway. *Mol Cell Biol*, **19**, 182-193.
- Laemmli, U.K. (1970) Cleavage of structural proteins during the assembly of the head of bacteriophage T4. *Nature*, **227**, 680-685.
- Lee, S., Comer, F.I., Sasaki, A., McLeod, I.X., Duong, Y., Okumura, K., Yates, J.R., 3rd, Parent, C.A. and Firtel, R.A. (2005) TOR complex 2 integrates cell movement during chemotaxis and signal relay in Dictyostelium. *Mol Biol Cell*, **16**, 4572-4583.
- Lee, S.J., Cobb, M.H. and Goldsmith, E.J. (2009) Crystal structure of domain-swapped STE20 OSR1 kinase domain. *Protein Sci*, **18**, 304-313.
- Li, J. and Pickart, C.M. (1995) Binding of phenylarsenoxide to Arg-tRNA protein transferase is independent of vicinal thiols. *Biochemistry*, **34**, 15829-15837.
- Linnell, L. and Raper, H.S. (1935) The chromogen of melanuria. *Biochem J*, **29**, 76-85.
- Loomis, W.F. (1996) Genetic networks that regulate development in Dictyostelium cells. *Microbiol Rev*, **60**, 135-150.
- Loomis, W.F. (1998) Role of PKA in the timing of developmental events in Dictyostelium cells. *Microbiol Mol Biol Rev*, **62**, 684-694.
- Lu, T.J., Lai, W.Y., Huang, C.Y., Hsieh, W.J., Yu, J.S., Hsieh, Y.J., Chang, W.T., Leu, T.H., Chang, W.C., Chuang, W.J., Tang, M.J., Chen, T.Y., Lu, T.L. and Lai, M.D. (2006) Inhibition of cell migration by autophosphorylated mammalian sterile 20-like kinase 3 (MST3) involves paxillin and protein-tyrosine phosphatase-PEST. *J Biol Chem*, **281**, 38405-38417.
- Lupas, A., Van Dyke, M. and Stock, J. (1991) Predicting coiled coils from protein sequences. *Science*, **252**, 1162-1164.
- Maciver, S.K. and Hussey, P.J. (2002) The ADF/cofilin family: actin-remodeling proteins. *Genome Biol*, **3**, reviews3007.
- Malchow, D., Nagele, B., Schwarz, H. and Gerisch, G. (1972) Membrane-bound cyclic AMP phosphodiesterase in chemotactically responding cells of Dictyostelium discoideum. *Eur J Biochem*, **28**, 136-142.
- Mandel, M. and Higa, A. (1970) Calcium-dependent bacteriophage DNA infection. *J Mol Biol*, **53**, 159-162.
- Mann, S.K., Brown, J.M., Briscoe, C., Parent, C., Pitt, G., Devreotes, P.N. and Firtel, R.A. (1997) Role of cAMP-dependent protein kinase in controlling aggregation and postaggregative development in Dictyostelium. *Dev Biol*, **183**, 208-221.
- Meili, R., Ellsworth, C., Lee, S., Reddy, T.B., Ma, H. and Firtel, R.A. (1999) Chemoattractant-mediated transient activation and membrane localization of



- Akt/PKB is required for efficient chemotaxis to cAMP in Dictyostelium. *Embo J*, **18**, 2092-2105.
- Meinzel, T., Serero, A. and Giglione, C. (2006) Impact of the N-terminal amino acid on targeted protein degradation. *Biol Chem*, **387**, 839-851.
- Moore, T.M., Garg, R., Johnson, C., Coptcoat, M.J., Ridley, A.J. and Morris, J.D. (2000) PSK, a novel STE20-like kinase derived from prostatic carcinoma that activates the c-Jun N-terminal kinase mitogen-activated protein kinase pathway and regulates actin cytoskeletal organization. *J Biol Chem*, **275**, 4311-4322.
- Muramoto, T., Kuwayama, H., Kobayashi, K. and Urushihara, H. (2007) A stress response kinase, KrsA, controls cAMP relay during the early development of Dictyostelium discoideum. *Dev Biol*, **305**, 77-89.
- Noegel, A.A. and Schleicher, M. (2000) The actin cytoskeleton of Dictyostelium: a story told by mutants. *J Cell Sci*, **113 (Pt 5)**, 759-766.
- Ojala, P.J., Paavilainen, V. and Lappalainen, P. (2001) Identification of yeast cofilin residues specific for actin monomer and PIP2 binding. *Biochemistry*, **40**, 15562-15569.
- Olie, R.A., Durrieu, F., Cornillon, S., Loughran, G., Gross, J., Earnshaw, W.C. and Golstein, P. (1998) Apparent caspase independence of programmed cell death in Dictyostelium. *Curr Biol*, **8**, 955-958.
- Parent, C.A., Blacklock, B.J., Froehlich, W.M., Murphy, D.B. and Devreotes, P.N. (1998) G protein signaling events are activated at the leading edge of chemotactic cells. *Cell*, **95**, 81-91.
- Perrin, B.J. and Huttenlocher, A. (2002) Calpain. *Int J Biochem Cell Biol*, **34**, 722-725.
- Pombo, C.M., Force, T., Kyriakis, J., Nogueira, E., Fidalgo, M. and Zalvide, J. (2007) The GCK II and III subfamilies of the STE20 group kinases. *Front Biosci*, **12**, 850-859.
- Prassler, J., Stocker, S., Marriott, G., Heidecker, M., Kellermann, J. and Gerisch, G. (1997) Interaction of a Dictyostelium member of the plastin/fimbrin family with actin filaments and actin-myosin complexes. *Mol Biol Cell*, **8**, 83-95.
- Preisinger, C., Short, B., De Corte, V., Bruyneel, E., Haas, A., Kopajtich, R., Gettemans, J. and Barr, F.A. (2004) YSK1 is activated by the Golgi matrix protein GM130 and plays a role in cell migration through its substrate 14-3-3zeta. *J Cell Biol*, **164**, 1009-1020.
- Rai, R., Wong, C.C., Xu, T., Leu, N.A., Dong, D.W., Guo, C., McLaughlin, K.J., Yates, J.R., 3rd and Kashina, A. (2008) Arginyltransferase regulates alpha cardiac actin function, myofibril formation and contractility during heart development. *Development*, **135**, 3881-3889.

- Riedl, J., Crevenna, A.H., Kessenbrock, K., Yu, J.H., Neukirchen, D., Bista, M., Bradke, F., Jenne, D., Holak, T.A., Werb, Z., Sixt, M. and Wedlich-Soldner, R. (2008) Lifeact: a versatile marker to visualize F-actin. *Nat Methods*, **5**, 605-607.
- Rohlf, M., Arasada, R., Batsios, P., Janzen, J. and Schleicher, M. (2007) The Ste20-like kinase SvkA of *Dictyostelium discoideum* is essential for late stages of cytokinesis. *J Cell Sci*, **120**, 4345-4354.
- Rothbauer, U., Zolghadr, K., Muyldermans, S., Schepers, A., Cardoso, M.C. and Leonhardt, H. (2008) A versatile nanotrap for biochemical and functional studies with fluorescent fusion proteins. *Mol Cell Proteomics*, **7**, 282-289.
- Rubenstein, P., Smith, P., Deuchler, J. and Redman, K. (1981) NH<sub>2</sub>-terminal acetylation of *Dictyostelium discoideum* actin in a cell-free protein-synthesizing system. *J Biol Chem*, **256**, 8149-8155.
- Rubenstein, P.A. (1990) The functional importance of multiple actin isoforms. *Bioessays*, **12**, 309-315.
- Rubenstein, P.A. and Martin, D.J. (1983) NH<sub>2</sub>-terminal processing of *Drosophila melanogaster* actin. Sequential removal of two amino acids. *J Biol Chem*, **258**, 11354-11360.
- Sadoul, K., Boyault, C., Pabion, M. and Khochbin, S. (2008) Regulation of protein turnover by acetyltransferases and deacetylases. *Biochimie*, **90**, 306-312.
- Sambrook, J. and Gething, M.J. (1989) Protein structure. Chaperones, paperones. *Nature*, **342**, 224-225.
- Satulovsky, J., Lui, R. and Wang, Y.L. (2008) Exploring the control circuit of cell migration by mathematical modeling. *Biophys J*, **94**, 3671-3683.
- Schirenbeck, A., Arasada, R., Bretschneider, T., Stradal, T.E., Schleicher, M. and Faix, J. (2006) The bundling activity of vasodilator-stimulated phosphoprotein is required for filopodium formation. *Proc Natl Acad Sci U S A*, **103**, 7694-7699.
- Schirenbeck, A., Bretschneider, T., Arasada, R., Schleicher, M. and Faix, J. (2005) The Diaphanous-related formin dDia2 is required for the formation and maintenance of filopodia. *Nat Cell Biol*, **7**, 619-625.
- Schulz, I., Reinders, Y., Sickmann, A. and Graf, R. (2006) An improved method for *Dictyostelium* centrosome isolation. *Methods Mol Biol*, **346**, 479-489.
- Schweiger, A., Mihalache, O., Ecke, M. and Gerisch, G. (1992) Stage-specific tyrosine phosphorylation of actin in *Dictyostelium discoideum* cells. *J Cell Sci*, **102** (Pt 3), 601-609.
- Shao, H., Chou, J., Baty, C.J., Burke, N.A., Watkins, S.C., Stolz, D.B. and Wells, A. (2006) Spatial localization of m-calpain to the plasma membrane by phosphoinositide

- biphosphate binding during epidermal growth factor receptor-mediated activation. *Mol Cell Biol*, **26**, 5481-5496.
- Shiraha, H., Glading, A., Chou, J., Jia, Z. and Wells, A. (2002) Activation of m-calpain (calpain II) by epidermal growth factor is limited by protein kinase A phosphorylation of m-calpain. *Mol Cell Biol*, **22**, 2716-2727.
- Skriwan, C., Fajardo, M., Hagele, S., Horn, M., Wagner, M., Michel, R., Krohne, G., Schleicher, M., Hacker, J. and Steinert, M. (2002) Various bacterial pathogens and symbionts infect the amoeba *Dictyostelium discoideum*. *Int J Med Microbiol*, **291**, 615-624.
- Soffer, R.L. (1968) The arginine transfer reaction. *Biochim Biophys Acta*, **155**, 228-240.
- Stegert, M.R., Hergovich, A., Tamaskovic, R., Bichsel, S.J. and Hemmings, B.A. (2005) Regulation of NDR protein kinase by hydrophobic motif phosphorylation mediated by the mammalian Ste20-like kinase MST3. *Mol Cell Biol*, **25**, 11019-11029.
- Takao, K., Xu, Y.J., Samejima, K., Shirahata, A. and Nitsu, M. (1999) Preparation and usefulness of some fluorogenic substrates for assay of arginyl-tRNA-protein transferase by HPLC. *Anal Biochem*, **267**, 373-381.
- Tang, L., Franca-Koh, J., Xiong, Y., Chen, M.Y., Long, Y., Bickford, R.M., Knecht, D.A., Iglesias, P.A. and Devreotes, P.N. (2008) tsunami, the *Dictyostelium* homolog of the Fused kinase, is required for polarization and chemotaxis. *Genes Dev*, **22**, 2278-2290.
- Tonami, K., Kurihara, Y., Aburatani, H., Uchijima, Y., Asano, T. and Kurihara, H. (2007) Calpain 6 is involved in microtubule stabilization and cytoskeletal organization. *Mol Cell Biol*, **27**, 2548-2561.
- Towbin, H., Staehelin, T. and Gordon, J. (1992) Electrophoretic transfer of proteins from polyacrylamide gels to nitrocellulose sheets: procedure and some applications. 1979. *Biotechnology*, **24**, 145-149.
- Ueda, M., Graf, R., MacWilliams, H.K., Schliwa, M. and Euteneuer, U. (1997) Centrosome positioning and directionality of cell movements. *Proc Natl Acad Sci U S A*, **94**, 9674-9678.
- Van Troys, M., Huyck, L., Leyman, S., Dhaese, S., Vandekerckhove, J. and Ampe, C. (2008) Ins and outs of ADF/cofilin activity and regulation. *Eur J Cell Biol*, **87**, 649-667.
- Vandekerckhove, J. and Weber, K. (1980) Vegetative *Dictyostelium* cells containing 17 actin genes express a single major actin. *Nature*, **284**, 475-477.
- Verschueren, H. (1985) Interference reflection microscopy in cell biology: methodology and applications. *J Cell Sci*, **75**, 279-301.

- Vosler, P.S., Brennan, C.S. and Chen, J. (2008) Calpain-mediated signaling mechanisms in neuronal injury and neurodegeneration. *Mol Neurobiol*, **38**, 78-100.
- Waelkens, E., Gettemans, J., De Corte, V., De Ville, Y., Goris, J., Vandekerckhove, J. and Merlevede, W. (1995) Microfilament dynamics: regulation of actin polymerization by actin-fragmin kinase and phosphatases. *Adv Enzyme Regul*, **35**, 199-227.
- Walker, M.G. (2003) Gene expression versus sequence for predicting function: Glia Maturation Factor gamma is not a glia maturation factor. *Genomics Proteomics Bioinformatics*, **1**, 52-57.
- Watts, D.J. and Ashworth, J.M. (1970) Growth of myxameobae of the cellular slime mould *Dictyostelium discoideum* in axenic culture. *Biochem J*, **119**, 171-174.
- Williams, K.L. and Newell, P.C. (1976) A genetic study of aggregation in the cellular slime mould *Dictyostelium discoideum* using complementation analysis. *Genetics*, **82**, 287-307.
- Witke, W., Hofmann, A., Koppel, B., Schleicher, M. and Noegel, A.A. (1993) The Ca(2+)-binding domains in non-muscle type alpha-actinin: biochemical and genetic analysis. *J Cell Biol*, **121**, 599-606.
- Wong, C.C., Xu, T., Rai, R., Bailey, A.O., Yates, J.R., 3rd, Wolf, Y.I., Zebroski, H. and Kashina, A. (2007) Global analysis of posttranslational protein arginylation. *PLoS Biol*, **5**, e258.
- Wu, H.Y., Tomizawa, K. and Matsui, H. (2007) Calpain-calcineurin signaling in the pathogenesis of calcium-dependent disorder. *Acta Med Okayama*, **61**, 123-137.
- Xu, T., Wong, C.C., Kashina, A. and Yates, J.R., 3rd. (2009) Identification of N-terminally arginylated proteins and peptides by mass spectrometry. *Nat Protoc*, **4**, 325-332.
- Yan, Y. and Merlin, D. (2008) Ste20-related proline/alanine-rich kinase: a novel regulator of intestinal inflammation. *World J Gastroenterol*, **14**, 6115-6121.
- Yanisch-Perron, C., Vieira, J. and Messing, J. (1985) Improved M13 phage cloning vectors and host strains: nucleotide sequences of the M13mp18 and pUC19 vectors. *Gene*, **33**, 103-119.
- Zatz, M. and Starling, A. (2005) Calpains and disease. *N Engl J Med*, **352**, 2413-2423.
- Zhou, T., Raman, M., Gao, Y., Earnest, S., Chen, Z., Machius, M., Cobb, M.H. and Goldsmith, E.J. (2004) Crystal structure of the TAO2 kinase domain: activation and specificity of a Ste20p MAP3K. *Structure*, **12**, 1891-1900.
- Zinda, M.J. and Singleton, C.K. (1998) The hybrid histidine kinase dhkB regulates spore germination in *Dictyostelium discoideum*. *Dev Biol*, **196**, 171-183.

## List of Figures

Figure 1. Osr1 crystal structure (Lee et al., 2009). .....	7
Figure 2. Crystallographic structure of human m-calpain [from (Goll et al., 2003)]. .....	10
Figure 3. Arginylation of actin isoforms.....	14
Figure 4. Domain architecture of DstA (adapted from Batsios 2005). .....	32
Figure 5. <i>Dst1</i> cDNA generation. ....	33
Figure 6. Tertiary model for the kinase domain of DstA.....	34
Figure 7. Expression and purification of two DstA fragments. ....	35
Figure 8. The anti-DstA antibody. ....	36
Figure 9. Expression of DstA during the <i>D. discoideum</i> development. ....	37
Figure 10. Subcellular localization of GFP-DstA in migrating polarized cells.....	38
Figure 11. Subcellular localization of DstA. ....	39
Figure 12. Colocalization of GFP-DstA with cortexillin II. ....	40
Figure 13. Co-localization of GFP-DstA with F-actin, comitin and annexin VII. ....	41
Figure 14. <i>Dst1</i> gene disruption (adapted from (Batsios, 2005)). ....	42
Figure 15. Characterization of the <i>dst1</i> null phenotype. ....	43
Figure 16. <i>Dst1</i> null cells have a defect in phagocytosis.....	44
Figure 17. GFP-coronin <i>dst1</i> null cells during phagocytosis of TRITC labeled yeast.....	46
Figure 18. Expression of the developmental markers CsA and PsA in <i>dst1</i> null cells.....	47
Figure 19. Phototaxis of <i>dst1</i> null aggregates.....	48
Figure 20. Chemotaxis of vegetative cells towards cAMP.....	49
Figure 21. Identification of the ADF/Cofilin over 2D-PAGE. ....	51
Figure 22. Multiple alignment of DDB0233884 with ADF/cofilins from <i>D. discoideum</i> . ..	52
Figure 23. GMF is phosphorylated by PKA <i>in vitro</i> . ....	53
Figure 24. Domain overview of Krs2. ....	56
Figure 25. Tertiary model of the kinase domain of Krs2.....	57
Figure 26. Phylogenetic tree for calpain cystein proteases and calpain III-like domains.....	58
Figure 27. Multiple alignments of the calpain III-like domains of Krs2. ....	59
Figure 28. Predicted structures for the calpain III-like domains of Krs2. ....	61
Figure 29. Expression and purification of the GST-Krs2 C-terminal domain.....	62
Figure 30. Subcellular localization of GFP-Krs2. ....	63
Figure 31. Subcellular localization of Krs2 GFP-tagged truncations in live cells.....	64
Figure 32. Localization of Krs2 truncations in fixed cells.....	65

Figure 33. Actin localization in <i>krsB</i> mutants. ....	66
Figure 34. GFP-Krs2 CALP 1,2,3 is not co-localizing with calnexin. ....	67
Figure 35. <i>KrsB</i> knockout generation. ....	68
Figure 36. <i>KrsB</i> null development. ....	69
Figure 37. <i>KrsB</i> null cells have a chemotaxis defect. ....	70
Figure 38. Chemotaxis of vegetative wild type vs <i>krsB</i> null cells with folic acid. ....	71
Figure 39. Chemotactic responses and induced cell polarity. ....	72
Figure 40. GFP-LimEΔcoil and GFP-actin expressed in <i>krsB</i> null cells during chemotaxis. .....	73
Figure 41. Chemotaxis of <i>krsB</i> null cells expressing GFP-tubulin. ....	74
Figure 42. Nanotrap of Krs2 GFP constructs. ....	75
Figure 43. Isoactins in <i>Dictyostelium</i> . ....	77
Figure 44. Predicted phosphorylation sites for Act15 of <i>D. discoideum</i> . ....	79
Figure 45. <i>Ate1</i> does not contain an intron sequence. ....	80
Figure 46 Arg-tRNA transferase 1. ....	81
Figure 47. The phylogenetic tree of the Ate1 proteins. ....	82
Figure 48. <i>Ate1</i> gene disruption and GFP-Ate1 expression. ....	82
Figure 49. Subcellular localization of Ate1-GFP. ....	83
Figure 50. <i>Ate1</i> null cells are reduced in size. ....	84
Figure 51. The <i>ate1</i> mutant makes smaller contact to the surface. ....	85
Figure 52. Development of <i>ate1</i> mutants. ....	86
Figure 53. The <i>ate1</i> null cells lack F-actin structures at potential adhesion points. ....	87
Figure 54. The proteome of <i>ate1</i> null cells lack the long basic tail of actin isoforms. ....	88
Figure 55. <i>Ate1</i> null actin has different properties. ....	89
Figure 56. Postulated model of DstA function. [adapted from (Loomis, 1998)]. ....	93



**List of Tables**

Table 1. Number of Ste kinases in various organisms.....6  
Table 2. Characteristics of mammalian calpains. ....9  
Table 3. Function of Calpain Subdomains.....9  
Table 4. Actin isoforms and Mascot based prediction for phosphorylation.....78

## Acknowledgements

First of all I want to thank Prof. Michael Schleicher for giving me the opportunity to do the experimental part of this work in his laboratory, for the stimulating discussions and the enormous support during my PhD time.

I thank Dr. Meino Rohlf for answers to all of my questions and for his unique demonstration in real management skills. For discussions, comments and ideas on this thesis.

I want to thank Prof. Manfred Schliwa for his excellent comments about my work during progress reports and his unique demonstrations of scientific knowledge.

Dr. Annette Müller-Taubenberger for the gift of the *ate1* knockout, for stimulating discussions and ideas concerning the Ate1 project.

Daniela (Dani) Rieger, Marlis Fürbringer, Thi-Hieu Ho for help in the lab, moral support and nice stimulating discussions.

Especially, I want to thank my colleagues Nagendran Ramalingam, Peter Kastner, Rajesh Arasada and Andreas Batsios (not only for weekend help but) for sharing the same problems with me and for having so much fun together inside and outside of the lab. I want to thank Nagendran for comments on this thesis and unforgettable moments during my PhD time.

I thank the members of the Institute for Cell Biology for sharing leisure time together and having fun outside the lab.

I want to thank all the students from the International Graduate Program “Protein-dynamics in health and disease” from the Elite-Network of Bavaria, for the interesting scientific discussions and the nice activities we shared together.

Last but not least I want to thank my parents for tolerating me all these years at home and my siblings for their support.

## **Curriculum Vitae**

### **Personal Details**

Date and place of birth 24/10/1981, Munich

Nationality German and Greek

### **Education**

1987-1993 Greek primary school in Munich

1993-1996 Greek gymnasium in Munich

1996-1999 Greek lyzeum in Munich

### **Academic Education**

1999-2000 Biology studies at the National - Kapodistrian University of Athens, Greece.

2000-2005 Biology studies at the Ludwig-Maximilians-University in Munich. Diploma thesis at the Adolf-Butenandt-Institute for Cell Biology, Principal Investigator: Prof. Schleicher.

2005-2009 Ph. D. at the Institute for Cell Biology of the Ludwig-Maximilians-University in Munich, Principal Investigator: Prof. Schleicher.

### **Graduate school**

2005-2009 Bavarian State Ministry of Sciences, Research and the Arts. Member of the international doctorate program: „Protein Dynamics in Health and Disease“, Elite Network of Bavaria.

Munich, Januar 10